DETECTION AND QUANTIFICATION OF EXPANSIVE CLAY MINERALS IN GEOLOGICALLY-DIVERSE TEXAS ROAD AGGREGATE FINES

A Thesis

by

GEORGE ANDREW RUSSELL

Submitted to the Office of Graduate Studies
Texas A&M University
in partial fulfillment of the requirements for the degree of

MASTER OF SCIENCE

Approved by:

Chair of Committee,	Youjun Deng
Committee Member,	Cristine Morgan
	Anol Mukhopadhyay
Head of Department,	David Baltensperger

December 2012

Major Subect: Soil Science

ABSTRACT

Expansive clay mineral contamination of road aggregate materials in Texas is a persistent problem. Hydrous layer silicate minerals - particularly smectites - in concretes are associated with decreased strength and durability in Portland cement and asphalt concretes. The Texas Department of Transportation (TXDOT) and Texas A&M Transportation Institute (TTI) evaluated the methylene blue adsorption test for its potential to identify and estimate quantities of expansive clays in aggregate stockpiles.

Clay mineral quantification was completed for 27 geologically-diverse aggregate materials from Texas, Oklahoma, and Arkansas. X-ray diffraction analysis (XRD) of separated clays on glass was conducted, and NEWMOD was utilized to model the resulting diffraction patterns. Methylene blue adsorption (MBA) and cation exchange capacity (CEC) of clay fractions (< 2Õm) and -40 mesh screenings (< 400 Õm) were determined for most aggregates.

Many of the aggregates exhibited significant quantities of expansive clay minerals such as smectite, which are linked to deleterious performance properties in concretes. While the majority of aggregates were derived from crushed limestone or calcareous river gravel parent materials, several exhibited uncommon origins and unusual clay mineralogy. Due to the relatively low number of aggregates tested and diverse geological origins of the different aggregates, it proved difficult to formalize any conclusions about trends between the different aggregate performance properties.

ACKNOWLEDGEMENTS

I would like to thank my thesis advisors: Drs. Youjun Deng, Cristine Morgan, and Anol Mukhopadhyay. Thank you for your support, encouragement, patience and mentorship in my completing my studies and duties as a research assistant for TTI. Thank you also to the Department of Soil and Crop Science at Texas A & M University and the Materials and Pavements Divisions of the Texas Department of Transportation and Texas A&M Transportation Institute.

Dr. Pat Harris, now of SHSU, Dr. German Claros and Mr. Michael Dawidczik of TXDOT Materials and Pavements, and Dr. Andrew Wimsatt of TTI deserve mention for sponsoring the road aggregates project and funding my research over the last 2 years. This was an extraordinary experience for me, and our project is the first or among the first to fully quantify clay minerals in real aggregate materials. In addition, Brandon Pitre of TTI did extensive work determining engineering properties of the aggregates, including methylene blue testing of the -40 screenings.

Thank you to the Soil Mineralogy Research Group for your support and friendship: Dr. Joe B. Dixon, Dr. Maria Guadalupe Tenorio, Dr. Courage Bangira, Ana Barrientos, Luke Morgan, Stacy Arteaga, Lian Liu, and others. Thanks to my friends and family and foremost to my fianc®e, Roberta McClure has been a constant support and motivation for me in completing my degree. I could not have succeeded without her.

NOMENCLATURE

AAS	atomic adsorption spectroscopy
Aggregate fines	particles less than 75 Õm in diameter
CEC	cation exchange capacity
Clay fraction	particles with diameter less than 2 µm
Clay minerals	layer silicate minerals
Coarse aggregates	gravels greater than 4.75 mm in diameter
FTIR	Fourier transform infrared spectroscopy
HIMs	hydroxy-interlayered minerals
HIS	hydroxy-interlayered smectite
HIV	hydroxy-interlayered vermiculite
ICAR	International Center for Aggregates Research
ICDD	International Center for Diffraction Data
MBA	methylene blue adsorption
NEWMOD	clay mineral modeling software
SEM	scanning electron microscope
TEM	transmission electron microscope
TTI	Texas A&M Transportation Institute
TXDOT	Texas Department of Transportation
XRD	X-ray diffraction

TABLE OF CONTENTS

LIST OF FIGURES

LIST OF TABLES

CHAPTER I

INTRODUCTION

Aggregates in civil engineering terminology are “granular mineral particles used either in combination with various types of cementing material to form concretes or alone as road bases, backfill…” (Atkins, 2003). By total market value, aggregates are considered the world’s most valuable non-fuel mineral commodity. Aggregates from natural crushed stone or river gravel constitute over 90 % of the volume of asphalt concrete and over 70 % of the volume of Portland cement concrete. Coarse aggregate is the primary component of road base and sub-base, as well.

Many aggregate physical properties affect concrete performance, including: gradation of particle size, relative density and ion adsorption, hardness, durability, shape and surface texture, deleterious substances present, and crushing strength (Atkins, 2003). Expansive clay minerals may be considered a deleterious substance, and “contamination” of aggregates may affect the other physical properties.

Clay contamination has been a persistent concern for highway departments throughout the world for several decades. However, there is no universally accepted definition of clay contamination because the allowable limit of aggregate fines in concretes varies from state-to-state and nation-to-nation. It may be said to occur when the performance of an aggregate is reduced below standards by the presence of

expansive layer silicate minerals – such as smectites and interstratified clay minerals with smectite components – in aggregate fines or as coatings on coarse aggregates.

Expansive clay mineral content in aggregates is not regulated directly in Texas, perhaps due to the considerable costs of quantitative analysis. Currently, the sand equivalency (SE) test is a commonly used technique for estimation of clay quantities in Texas road aggregates. However, sand equivalency may not adequately differentiate harmful, expansive clay minerals from relatively charge neutral ones. In this study, the modified methylene blue adsorption (MBA) test was evaluated for its capacity to detect harmful, expansive clays minerals in aggregate screening and stockpile materials.

The Texas Department of Transportation (TXDOT) regulates concrete performance of all aggregates used for new road and highway construction in Texas. TXDOT and the Texas A&M Transportation Institute (TTI) entered into a joint research project to investigate new methods for estimating expansive clay minerals - e.g. smectites and interstratified clay minerals with smectite components - in aggregate screenings and stockpile materials. Currently, clays with deleterious shrink-swell properties are detected indirectly and only later in the production cycle, during engineering performance tests.

In 2009, the Texas A&M Transportation Institute (TTI) and Texas Department of Transportation (TXDOT) entered into a research project entitled, “Treatment for Clays in Aggregates Used to Produce Cement Concrete, Bituminous Materials, and Chip Seals.” The project’s main objective were: to determine which clay minerals “are

responsible for deterioration of pavement structures" in contaminated aggregates and ultimately "to quickly identify clay minerals in a stockpile, determine what type and concentration of clay mineral will result in poor pavement performance and suggest ways to lower the clay contamination and make the aggregate acceptable for use," (RTI Project Agreement, 2009).

The primary objective of this study for researchers in the Soil Mineralogy Research Group at Texas A&M University was to identify and quantify all clay minerals – including expansive clay minerals - in the fines of aggregates sampled by TXDOT and TTI engineers, by traditional clay mineralogy laboratory methods.

Over 30 different quarries in Texas, Oklahoma, and Arkansas were selected for the study. Of these, 27 aggregates were selected for analysis by TXDOT and TTI, based primarily on known past aggregate performance problems. X-ray diffraction (XRD) analysis of separated and cation-saturated clay fractions allowed for clay mineral identification from characteristic diffraction peak d-spacing. NEWMOD, a commercial mineral modeling program, was used to generate simulated clay mineral primary diffraction peaks for estimation of mineral quantities.

Additional test methods (e.g., FTIR-ATR, CEC, and MBA) were also employed on selected aggregates in order to aid in clay mineral identification and quantification. According to the priority given to XRD analysis and limited availability of separated clay material for some samples, not all analyses were conducted for all aggregates. Infrared absorption spectroscopy (FTIR-ATR) was performed on 11 of the 27 clays,

cation exchange capacity (CEC) and methylene blue adsorption (MBA) were conducted for 21 and 15 samples, respectively. Electron microscopy (SEM/TEM) data were generated for several aggregates' silt and clay fractions.

Concurrently, Rietveld analysis was utilized in total-samples to quantify minerals in aggregates without separation of clays. A spray-dryer was constructed, and a modified spray-drying treatment with artist's air brush was implemented to attempt to reduce orientation effects during powder diffraction. It was observed earlier in the project that small quantities of clay minerals were difficult to detect and quantify by powder diffraction in the presence of pure quartz. Full-pattern simulations of total-sample mineralogy for 15 aggregates with a standard addition were generated, and the suitability of the Rietveld method for clay mineral quantification was evaluated.

CHAPTER II

LITERATURE REVIEW

Clay Contamination in Aggregate Fines

Clay mineral contamination of aggregates occurs when sufficient quantities of expansive clay minerals occur within ASTM fines (-200 mesh or < 75 μm fraction) limit recommendations - 3 % in sands, 1.5 % in coarse aggregates (> 4.75 mm fraction) - to produce concrete and pavements with acceptable performance (ASTM, 2003). Deleterious rock and mineral composition of road aggregates has been studied in the United States at least since the 1920's. At the time, widespread use of porous, water-absorbing chert rock as coarse aggregate in road base and concretes was found to contribute to road failure across the lower Midwest (Schuster, 1957).

Walker and Proudley (1932) were among the first to study the effects of clay-bearing rocks in concrete when they observed the effects of weathering cycles on concretes containing significant quantities of shale rocks. It was concluded that soft, friable, clay-bearing rocks were detrimental to concrete durability. However, these early studies focused primarily on the geologic composition of coarse aggregates and did not attempt to establish specification limits for deleterious minerals.

The first mineralogical studies of aggregate fines were conducted in the early 1930's. Lang (1931) focused on fine particles occurring as coatings on coarse aggregates. Goldbeck (1933) observed the effects of stone dust, clay minerals, and calcium

carbonate fines in the cement powder, as in coarse aggregate coatings. Clay minerals were found to be the most difficult aggregate coatings to remove through normal washing. Those clays that adhered to the aggregates after concrete mixing interfered with aggregate – cement paste bond. However, limits for clay minerals or fines in concrete were not established in these early studies.

Much of the aggregate research between the 1930's and 1980's focused on establishing which rock types and degrees of weathering were deleterious to concretes utilizing them as coarse aggregates. In the 1950's and 1960's the Scottish Laboratory of the Building Research Station (SLBRE) compared drying shrinkage of concretes made from diverse rock types from throughout that country. The study found concretes consisting of dolerites and basalts – mafic rocks – and greywackes and mudstones – which contain significant quantities of clay-sized particles and clay minerals –exhibited the highest drying shrinkages (Brown, B.V. et. al., 1990).

Moore and Gribble (1980) observed that the degree of weathering in different crushed stone aggregates samples from the same quarry influenced concrete performance. The study found that more weathered granites contained higher contents of hydrous, layered silicates – clay minerals -- than less weathered ones. Calcium and sodium were leached from the feldspar minerals, which then altered to kaolinites and illites. Concretes containing more weathered granites with greater clay mineral content exhibited higher drying shrinkage and lower compressive strength than those with unweathered granites.

A series of studies completed in the mid 2000's directly addressed the problem of clay mineral contamination in coarse and fine aggregates. Quiroga et al (2006) highlighted the distinction between clay-sized particles and expansive clay minerals through the observation that concretes incorporating manufactured fine aggregate (MFA) or "manufactured sands" could utilize fine-sized particles above the regulatory limits - up to 15 % volume of concrete sand composition – without a drop in performance. The manufactured sands in the study contained no quantities of clay minerals detectable by x-ray diffraction. MFA, in fact, is created by crushing only those natural stone and aggregate sources that have been screened for expansive clay minerals such as smectite.

The American Society for Testing and Materials (ASTM) recommends aggregate fines limits of 3 % in aggregate fines for high-friction surfaces such as highway asphalts, while the Texas Department of Transportation (TXDOT) limits fines (<75 µm) to 6 % in lower grade concretes - precisely to address the issue of clay mineral contamination. The Quiroga study therefore suggested that allowing higher content of fine-sized particles would not lower concrete performance so long as expansive clays were excluded and a common dosage of high-range water reducing admixture (HRWRA) was added to keep water demand constant and maintain constant concrete slump.

Conversely, Katz and Baum (2006) found that concrete with elevated quantities of fine-sized particles sourced from natural crushed stones not screened for expansive clay mineral content exhibited decreased performance by increased water demand, decreased workability, and increased drying shrinkage and cracking.

Varying amounts of crushed stone fines (<75 µm) - up to approximately 10 % by mass - were added to normal strength concrete mixes, less than the 15 % replacement of fines in the Quiroga study. HRWRA were added to concrete mixes, decreasing water demand and improving slump values, but cracking due to increased drying shrinkage was evident in all concretes treated with unscreened natural aggregate fines.

From X-ray diffraction (XRD) analysis of bulk materials, little to no clay mineral quantities were detected in the various fine treatments (Quiroga et. al., 2006). However, the methods of this XRD analysis were not made clear, and it did not appear that clay fractions were separated from sand and silt-sized particles in the fines. Poorly-crystalline minerals such as layer silicates present in relatively low quantities are difficult to detect in the presence of highly crystalline minerals such as quartz and feldspars. In the absence of clay fraction separation and cation saturations, identification and quantification of clay minerals is extremely difficult.

A 2006 study by the International Center for Aggregates Research (ICAR) reported the effects of 14 different manufactured fine aggregates (MFA) - from sources located throughout United States and Canada - on concrete properties. Twelve aggregates exhibited high performance and low variability between aggregates. Two additional aggregates were chosen for containing high known or suspected quantities of clay minerals. However, only one of these two aggregates, a clay-rich limestone, exhibited a high methylene blue adsorption value (MBA) that approached the limits.

In the ICAR manufactured sands study, clay-sized fractions (< 2 μm) of all 12 aggregates were separated, and minerals were identified by x-ray diffraction analysis (XRD). However, no cation saturation treatments were utilized, which would make clay mineral identification less reliable. Magnesium and potassium ion saturation would have fixed layer thickness of any expandable clay minerals present, facilitating clay mineral identification. Quantification of clay minerals in the manufactured fine aggregates was not attempted in the ICAR study.

Another study from the ICAR project measured the effects of known quantities of pure clay minerals – including montmorillonite (smectite), mica, and kaolinite - on concrete performance. Norvell, et. al. (2007) replaced fine sands in concrete mix with 1 % and 4 % treatments of kaolinite, illite, and montmorillonite. Concretes with montmorillonite - a smectite mineral – treatments exhibited increased drying shrinkage, decreased compressive strength, and heightened methylene blue adsorption (MBA) values. Effects of sand replacement were most dramatic in the 4 % montmorillonite treatments. Kaolinite and illite 1 % and 4 % treatments exhibited slight increases in methylene blue adsorption, drying shrinkage, and compressive strength over the control.

Finally, a University of Wisconsin study (Munoz et. al., 2010) measured the effects on concrete performance of fine particle coatings on coarse aggregates. Standard fine coatings of different rock type – stone dust, clays, and calcium carbonates - were added to coarse aggregate at approximately 1.5 % concentration, the allowable limit in

Wisconsin concretes. The effects of fine additions on concrete slump, dry shrinkage, and tensile strength values were measured.

The Wisconsin study concluded that the quantity of fine particle coatings in coarse aggregate alone - without considering the coatings' mineralogy - is not a good predictor of concrete performance. When the mineralogy of coatings was considered, however, notable patterns emerged. Treatments with carbonate mineral coatings showed no change in slump or dry shrinkage values. Mixed carbonate and clay coating treatments (clay coating consisted of an anorthite, amphibole, and chlorite mixture, noteworthy that none were expansive clay minerals) exhibited no change in drying shrinkage but showed reduced slump. Mixed dust and clay coatings showed decreased slump and increased drying shrinkage. Clay coating treatments experienced both significant decreases in slump and significant increases in drying shrinkage. Tensile strength and freeze-thaw durability also decreased dramatically in the clay treatments.

Identification and estimation of clay mineral quantities in aggregate fines is a global problem. A study by Land Transport New Zealand (Bartley, et. al. 2007) sampled progressively-weathered rocks from 4 quarries to observe the performance properties of marginal aggregates. Expandable clay minerals were tested for by methylene blue adsorption and semiquantitative x-ray diffraction analyses.

X-ray diffraction of clay fractions was conducted on untreated, ethylene glycol-treated, and 350 ° C and 550 ° C-heated specimens. Semi-quantitative clay mineral analysis was conducted, with individual minerals or mixed-layer assemblages

categorized as abundant (> 60 % mass), common (20-60 %), minor (5-20 %), or trace (< 5 %) in the clay fractions.

The authors concluded that the methylene blue adsorption (MBA) test "was the most useful and cost-effective test for assessing the swelling properties of the treated samples." While methylene blue values showed a strong correlation with degree of weathering in rocks from the same quarry, however, the study did not establish direct correlation between quantities of expandable layer silicates and MBA. Overall, weathered rocks from the same quarry produced higher MB values than unweathered, attributable to the higher quantities of secondary minerals, including expansive clays.

X-ray Diffraction Analysis (XRD) of Mineral Samples

X-ray diffraction (XRD) analysis was first used to determine minerals' crystal structure in the early 20th century. By 1912, Max von Laue had envisioned the regular spacing in crystal structure as a 3-dimensional diffraction grating for electromagnetic waves. At approximately the same time, W.L. Bragg formulated a simplified mathematical relationship for diffraction of waves in a 2-dimensional plane containing successive, parallel rows of atoms. In the mid-1920's, the earliest studies of clay minerals by x-ray diffraction were conducted, and in the early 1930's, soil minerals were determined to consist of crystalline materials (Moore and Reynolds, 1989).

Diffraction occurs when photons from the x-ray source or beam strike adjacent scattering centers in successive layers of the target material's crystal structure. A scattering center is an atom or cluster of atoms and may be conceptualized as a single, discrete lattice point in the crystal. The x-ray photon beam interacts primarily with electrons surrounding atomic nuclei, and the reflected beam is the sum of the interactions with all electrons at each atom or scattering center.

When reflected waves from different scattering centers are in phase or close to it, their wavelets combine to form a combined wave of greater amplitude. This occurrence is diffraction, the result of constructive interference between scattered x-ray wavelets. This may occur when the component of x-ray wavelength normal to the crystal lattice plane is approximately equal to unit cell thickness of the crystal. This satisfies the Bragg condition, where λ is wavelength, d is vertical lattice spacing in the crystal unit cell, and Θ is diffractometer beam angle to the lattice plane:

$$n\lambda = 2d\sin\Theta$$

To construct a continuous diffraction pattern for a real sample, diffraction intensity is calculated at each 2θ angle. A series of calculations is made to account for variable crystal structure within mineral specimens and x-ray beam parameters. Some of the major corrections for diffracted beam intensity calculation are mentioned briefly below.

The Structure Factor accounts for differences in electron distribution, atomic positioning, and thermal motion of different kinds of atoms in a crystal - and how those differences affect scattering intensity of a material (Jenkins and Snyder, 1996). For instance, crystals with larger atoms of relatively low electron density tend to scatter x-rays less efficiently than those with smaller atoms of higher electron density.

The Multiplicity Factor is a correction for the effects of differences in crystal habits of diverse minerals on diffraction intensity. Specifically, it corrects for the effects on diffraction intensity caused by diverse minerals' crystallites having different number of faces - and different numbers and distribution of lattice planes cutting through their unit cells. In general, a greater number of parallel lattice planes in a unit cell correlates with higher atomic density, which leads to greater diffraction intensity with an x-ray beam component normal to direction of lattice planes.

During scattering, beam photons become partially polarized, causing decrease of wave amplitude in directions not in the plane of polarization (Moore and Reynolds, 1989). This phenomenon, known as the Polarization Factor, is corrected for in calculating the diffraction pattern. The Lorentz Factor accounts for the greater diffraction intensity of beams at high 2θ angles compared to lower angles. At higher angles, more primary beam radiation penetrates the crystal lattice planes, and a greater component of the beam wavelength is oriented perpendicular to the lattice planes, increasing diffraction intensity disproportionately. These two factors are often treated as one correction, the Lorentz-Polarization Factor or Lp factor.

Mineral Quantification in Aggregate Fines

Individual minerals in a geological sample can be identified from the calculated diffraction pattern by their d-spacings, represented on the diffractogram by 2θ angle or diffraction peak position. Reference libraries such as the Mineral Powder Diffraction File Data book have published mineral diffraction data from pure mineral specimens and are widely available. In addition, Bruker's DIFFRAC^{plus} EVA software contains an automated mineral search function that connects to the International Center for Diffraction Data (ICDD) online crystallographic database.

Quantification of minerals in a real sample requires precise mineral identification and the selection of appropriate crystal models to base the simulation calculations on. It is the choosing of standard minerals with "identical diffraction characteristics" to the sample that is the single most important consideration in obtaining accurate quantification results (Moore and Reynolds, 1989). There is little margin for error in setting the crystallographic, chemical, and machine modeling parameters for a simulation to obtain accurate results.

Similarly, Kleeburg (2009) concluded that user-friendly computer programs for mineral quantitative analysis - such as RockJock - did not often achieve accurate quantification results without the input of a user with working knowledge of crystallography and XRD methods. In fact, Kleeburg found that the majority of mineral laboratories surveyed showed significant error in identifying clay minerals in real geological samples or other complex mixtures. Only a handful of labs throughout the

world regularly achieved highly accurate quantitative analysis of minerals in complex samples – considered to be below 1 % error by weight for each mineral in the sample.

Hillier (1999) emphasizes the importance of sample preparation in accurate quantification - and specifically reduction of preferred orientation of powder XRD specimens through a spray drying procedure. In a study comparing the traditional reference-intensity-ratio method (RIR) with the Rietveld method for full-pattern simulation, the two methods yielded similar accuracy in quantification from a mixture of standard minerals when utilized by an experienced researcher. It should be stressed that both methods were preceded by a careful study of the mineral species in the samples – including consideration of interstratifications and other compositional variations – to yield the appropriate intensity ratios or crystal structures.

NEWMOD Method for Mineral Quantification

NEWMOD is a commercial software program that simulates one-dimensional diffraction patterns for pure clay minerals phases and mixed phases. The program was developed as a teaching and research tool to simulate diffraction patterns of real mineral samples having varied chemical and physical characteristics. Originally, the program was developed to model diffraction patterns of interstratified clay minerals (Reynolds, 1985), whose layer structures and composition may be quite complex and difficult to characterize. The current version has the capability to simulate pure phases as well.

Researchers input data obtained from x-ray diffraction analysis of real samples, such as d-spacing of the mineral being simulated and average number of repeating layers in each crystallite. Other user important user inputs include diffractometer settings such as beam current, path length, and 2-θ angle range. NEWMOD calculates diffraction peak intensity of clay minerals from equation 4 expressed in a general form, from Reynolds and Moore (1989). Imaginary terms cancel out in the calculations.

$$I = Lp \, \Sigma_S \, G_j G_k \sigma_s \, (\cos \phi S + i \sin \phi S)$$

Lp = Lorentz-polarization factor, $[(1 + \cos^2 2\theta) \, \Psi / \sin \theta]$
Ψ = powder ring distribution factor, describes orientation of crystallites and accounts for differences in diffraction intensity
S = layer thickness value in Angstroms, varies with layer-type, e.g. 2:1 vs 1:1 minerals
G_j = complex conjugate of Fourier transform of basal reflections, any layer type, A or B
G_k = Fourier transform of basal reflections for any layer type, A or B
σ_S = frequency of occurrence of any repeating layer thickness type, S
ϕ = phase shift of radiation during scattering, $(4\pi \sin\theta) / \lambda$

For clay minerals, diffraction peaks broaden with smaller crystallite size. Discontinuities in mineral structure between layers along the z-axis are known as stacking faults. Defect broadening due to stacking faults may be accounted for in NEWMOD, as the user may choose a range for average thickness, or coherent scattering zone δ, of each clay mineral phase simulated. A higher average number of contiguous layers modeled, N, for each clay mineral yields sharper simulated diffraction peaks in NEWMOD, all other inputs remaining constant. Clay minerals typically have δ values between 6 and 10 unit cells thick, but corresponding NEWMOD N values may be

greater by a factor of 7 or more, with higher-crystallinity minerals such as kaolinites (Moore and Reynolds, 1989).

Reference-Intensity-Ratio (RIR) Method

Mineral quantities in soils and geologic samples from x-ray diffraction data may be calculated in several ways. The Reference-Intensity-Ratio method (RIR) utilizes an internal standard of known mass, commonly corundum or zincite. The ratios of diffraction peak intensities for a 50 %-50 % mass mixture of standard reference minerals is then used to calculate the uknown quantities of real minerals in samples, according to equation Z below (Snyder and Bish, 1989).

$$X_i = X_c/k_i * I_i/I_c$$

X_i is the weight fraction of the mineral of interest, X_c is the known weight fraction of the internal standard, k_i is the diffraction intensity ratio of a 50 %-50 % mixture of the internal standard and mineral of interest, I_i is the diffraction intensity of the mineral of interest in the sample, and I_c is the diffraction intensity of the internal standard in the sample. RIR was in use before the advent of personal computers, and one advantage to this method is its simplicity - it can be performed with a ruler and pencil if necessary. However, major limitations of RIR are its focus on primary diffraction peaks and the lack of entirely quantitative tools for resolving peak overlap effects.

Rietveld Method with Standard Additions

In contrast to the reference-intensity-ratio method - which measures primary diffraction peaks - the Rietveld refinement method is a full-pattern simulation. Diffraction peaks of all major minerals in a sample are simulated, e.g. all *hkl* planes, simultaneously. This powerful capability is only feasible with programs run on modern personal computers. The Rietveld method effectively resolves the problem of peak overlap encountered in the RIR method by rapidly calculating all major components of diffraction intensity for each XRD peak in a specimen.

A general form of the equation for calculated diffraction intensity is given below, with term definitions (Jenkins and Snyder, 1996):

$$I_{(hkl)\alpha} = [(I_0\lambda^3/64\lambda r)*(e^2/m_ec^2)^2]\ [(M_{hkl}/V_\alpha^2)*\mid F_{(hkl)\alpha}\mid^2(1+\cos^2 2\theta\cos^2 2\theta_m)/(\sin^2\theta\cos\theta)]\ [X_\alpha/\rho_\alpha(\mu/\rho)_s]$$

I_0 = incident-beam intensity
r = distance from specimen to detector
λ = wavelength of X-radiation
$(e^2/m_ec^2)^2$ = the square of the classical electron radius

The first term, $[(I_0\lambda^3/64\lambda r)*(e^2/m_ec^2)^2]$ is a constant for each set of diffractometer parameters with experimental conditions and does not vary during recording of a single diffraction pattern. It is sometimes represented by the term K_e. The term $[(M_{hkl}/V_\alpha^2)*\mid F_{(hkl)\alpha}\mid^2(1+\cos^2 2\theta\cos^2 2\theta_m)/(\sin^2\theta\cos\theta)]$ is also constant for each phase

undergoing diffraction and each diffraction reflection from specimen crystals. It is sometimes represented by the term, $K_{(hkl)\alpha}$. Variables are defined below:

M_{hkl} = the multiplicity for reflection *hkl* of phase α
V_α = the volume of the unit cell of phase α
$(1+\cos^2 2\theta \cos^2 2\theta_m)/(\sin^2\theta\cos\theta)$ = the Lorentz polarization for the diffractometer
$2\theta_m$ = the diffraction angle of the monochromator
$F_{(hkl)\alpha}$= structure factor of reflection *hkl,* includes scattering temperature effects

With the substitution of constants $K_{(hkl)\alpha}$.and K_e into the equation above, it is possible to simplify its form, with the following variables:

$I_{(hkl)\alpha} = [K_{(hkl)\alpha} K_e.X_\alpha]/[\rho_\alpha(\mu/\rho)_s]$
$K_{(hkl)\alpha}$. = crystal structure constant
K_e = experimental setup constant
X_α = weight fraction of phase α in the polyphase mixture
ρ_α = density of phase α
$(\mu/\rho)_s$ = mass attenuation coefficient of the polyphase specimen

Without knowing a specimen's mass attenuation coefficient $(\mu/\rho)_s$, equation 2 contains two unknown variables, $(\mu/\rho)_s$ and weight fraction of phase α, X_α. This problem can be overcome with addition of an internal standard and substitution of a known scale factor ratio for any phase α with the internal standard. In the ratio of scale factors for the two materials, the mass attenuation coefficient is in the denominator of both terms and is cancelled out. The scale factors may act as reference-intensity-ratios for the Rietveld refinement, as expressed below:

$X_\alpha = (\rho_\alpha S_\alpha / \rho_\beta S_\beta) * X_\beta$

$S_{\alpha/\beta}$ = scale factor of any phase α or internal standard β

Methylene Blue Adsorption (MBA) Test

Methylene blue (MB) is a cationic dye with formula $C_{16}H_{18}N_3ClS^+$, rectangular shape, and approximate dimension of 17 x 6.6 x 3.25 Angstroms, or 130 Angstroms-squared. MB adsorbs to surfaces of negatively-charged clay surfaces primarily by cation exchange mechanisms but also by van der Waals forces or hydrogen bonding with silicon and aluminum hydroxide surfaces in layer silicates' crystal lattice. According to Yukselen and Kaya (2008), MB adsorption values accurately predict swelling index and swell potentials of soils with diverse mineralogy.

Clay minerals' capacity to adsorb methylene blue dye disproportionately to non-clays' has been recorded 1940 or earlier (Bensted, 1985). Hang and Brindley (1970) determined that methylene blue adsorption (MBA) could be used to determine both cation exchange capacity (CEC) and specific surface area (SSA) of clay minerals. Because expansive clay minerals such as smectite characteristically have high CEC and SSA, the MBA test has been used to test for the presence of active or expansive clay minerals in geological samples.

CHAPTER III

MATERIALS AND METHODS

Sampling of Road Aggregates

Twenty-seven distinct natural crushed stone aggregate materials were sampled from quarry stockpiles and screening piles by Texas Transportation Institute (TTI) researchers and Texas Department of Transportation (TXDOT) field personnel. Twenty-two of the quarries sampled were located in Texas, 2 were in Oklahoma, and 3 were in Arkansas. Geologically and mineralogically-diverse materials were surveyed, and aggregate parent materials included: crushed limestones and dolomites of different eras, siliceous and limestone fluvial deposits, a crushed sandstone, a crushed red granite, a crushed hornfels, and a crushed basalt, or "trap rock."

Sites were selected by TXDOT project researchers for unique engineering properties and mineralogy, observed high clay content, and known performance of the aggregate materials in asphalt and Portland cement concrete. Primarily, aggregates were selected for poor performance in structures or during engineering tests. For the clay mineralogy identification and quantification, aggregate samples were delivered unwashed and unsorted – from the "pit runs."

Aggregate Pretreatment for Removal of Cementing Agents

Cementing agents such as carbonate minerals were removed from aggregates in order to separate all clay-sized particles – even those bound in the matrix of limestones. Carbonate minerals, manganese oxides, and organic matter were removed by successive treatments in a pH 5 buffer and 30% hydrogen peroxide solutions. One hundred grams of less than 4.75 mm diameter (-4 mesh) unwashed aggregate – "pit run" - was measured and weight recorded to 4 decimal places. The fraction passing a 10 mesh sieve (< 2 mm) were treated and analyzed.

For the calcareous materials, the -2 mm materials were ground to less than 105 μm diameter (passing a 140 mesh sieve) before carbonate dissolution with a pH 5 sodium acetate-acetic acid ($Na_2C_2H_3O_2$ - $HC_2H_3O_2$) buffer solution. In aggregates lacking carbonate minerals, this treatment was complete within hours or days. In crushed limestone and other carbonate-rich materials, however, complete dissolution of carbonate minerals in pH 5 buffer solution may require months or years.

To speed up the reaction of carbonate minerals, starting materials were crushed to -140 mesh size. Reaction rate was accelerated further by heating solution and sample to 90 ° C in a water bath. For samples with higher quantities of carbonate minerals and those containing less reactive minerals such as dolomite, concentrated acetic acid was added to the pH 5 buffer in a ratio approximately 1 part acetic acid to 10 parts pH 5 buffer solution. The buffering system and monitoring of solution pH was necessary to prevent alteration of the clay minerals present as would occur in a strong acid such as

hydrochloric acid < HCl >. None of the treatments' buffer solutions were observed to have pH below 4, and a pH 3 environment is the threshold for decomposition of clay minerals to quartz.

Carbonate dissolution was judged to be complete when reaction with buffer solution at 90 ° C and with minor agitation visibly ceased – that is, there was no appearance of carbon dioxide gas bubbles from the sample as occurs with the reaction of hydrogen ions with calcium carbonate. Buffer solutions were replaced every 2-3 days. For several aggregate materials, carbonate removal was suspended after months of treatment without waiting for complete disappearance of the reaction in order to expedite the mineralogical analysis. This suspension of treatment was judged not to significantly impact quantification results, as calcite was not detected in the clay fractions of those aggregates. Organic matter, sulfide minerals, and manganese oxides were removed by addition of a 10 mL 30% hydrogen peroxide (H_2O_2) solution in 50 mL of pH 5 sodium acetate – acetic acid buffer and heated to 70° C in a water bath until reaction ceased.

Size-Fractionation

After cementing agents were removed from specimens, the aggregates were treated with pH 10 sodium carbonate solution < Na_2CO_3 > to suspend silt (2 – 53) and clay (< 2 μm) sized particles in solution. Sand fractions (>53 μm) were separated by wet-sieving silts and clays through a 270-mesh sieve. Clay was separated from the silt fraction by further dispersion in pH 10 solution, and siphoning off of the upper portion

of the suspension. Necessary centrifugation speed and time to flocculate silt-sized particles to the container's bottom were calculated from Stoke's Law below:

$$t = [6.299 \times 10^{9}\ \eta * \log (R/S)] / [d^{2}N^{2}(\rho_p - \rho_f)]$$

t = centrifuging time (minutes)
η = viscosity of fluid [g $(cm*sec)^{-1}$]
S = distance of the fluid top to rotation axis
R = distance from top of sediment to rotation axis
N = centrifuging speed (rpm)
d = diameter of particle (μm)
ρ_p and ρ_f = densities of particle and fluid, respectively (g cm^{-3})

Centrifuging at 750 rpm for 5 minutes accumulated silt-sized particles to the bottom of the treatment containers, while more buoyant clay-sized particles remained in suspension in the pH 10 buffer fluid and were siphoned off and collected in a 4 liter beaker. Thirteen of the aggregates underwent further separation to coarse clay (0.2-2 μm) and fine clay (< 0.2 μm) fractions because this was called for in the original project plan. This separation into coarse and fine clay fractions, however, was ultimately deemed unnecessary due to improvements in X-ray diffractometer technology that have increased precision of diffraction detection. This step was discontinued when the project was extended to double the number of aggregates analyzed. Figure 3.1 below summarizes sample pretreatment and size fractionation (Deng et. al., 2010).

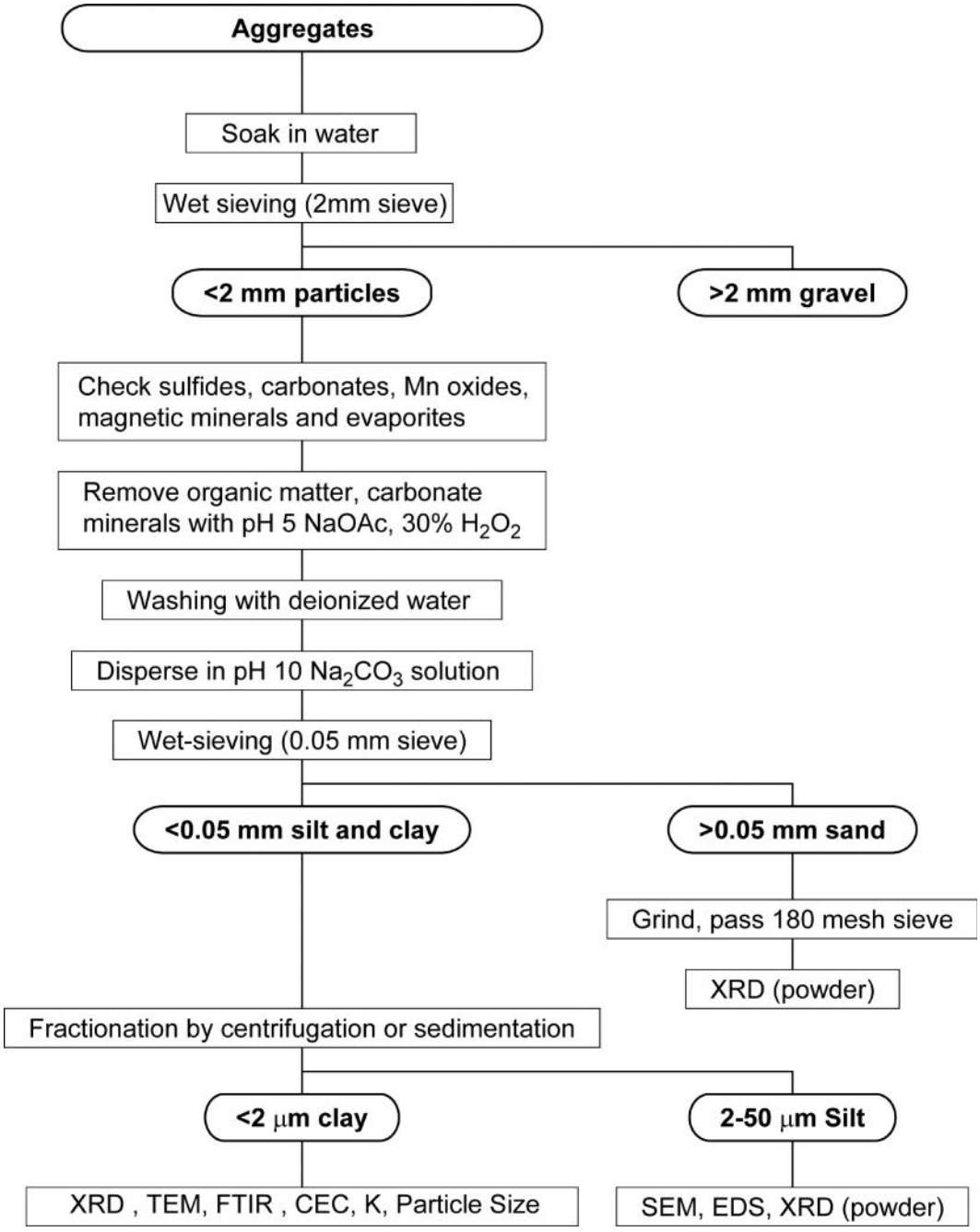

Fig. 3.1. Pretreatment of aggregates and separation of clay fractions

Dialysis of Clays

After multiple repetitions of dispersion, centrifugation, and siphoning steps, suspension volume of the separated clay fraction was sufficiently high to inconvenience further treatments – volume often exceeds 4 liters. To reduce clay suspension volume, 50 g <NaCl> were added to the collection beakers containing clay fractions. After the clay flocculated, a clear supernatant above the reduced-volume clay suspension transparent layer was suctioned off.

However, because <NaCl> was added to the clay to reduce volume - and this compound may hinder identification of clay minerals - excess electrolytes were removed by dialysis (Deng et. al., 2010). Clay suspension was transferred to dialysis tubing and placed in deionized water for several hours in order for electrolytes to diffuse out. Water in the beakers was replaced twice per day until measurable electroconductivity of water in each beaker was lower than 5 $mScm^{-1}$ at equilibrium. Quantity of clay was determined by oven-drying and weighing 1-mL of suspension and multiplying concentration determined by the total mass of clay suspension recovered.

Cation Saturation of Clays

Cation saturation of clays requires further chemical treatment of the aggregate clay fractions (< 2 μm) to enable clay mineral identification by x-ray diffraction. Cation saturation treatment of clay fractions is necessary to distinguish individual clay minerals – for example, smectite from vermiculite and clay-sized chlorite minerals -- in the XRD patterns. Cation saturation aids in identification by fixing layer thickness of expansive clay minerals such as smectite.

As smectite expands with water adsorbed between layers, it has variable layer thickness with hydration energy of the particular interlayer cations in a specimen. By establishing magnesium as the dominant cation in the clay suspensions, if smectite is present in a specimen, it can be identified by the known 2-Θ diffraction angle for magnesium-saturated (Deng et. al., 2010).

Magnesium and potassium-saturated suspensions were deposited on 25.4 mm by 1 mm glass discs and left to air-dry, overnight. The samples with magnesium treatments were tested by XRD at room temperature and again after solvation by misting with a 20 % glycerol solution onto the clay films. The samples with potassium treatments were analyzed by XRD at room temperature and again after 1 hour heating at 330 ° C and 550 ° C. A total of five XRD patterns were collected for each clay fraction separated from the 27 bulk aggregate materials.

In separate Mg or K saturation treatments, approximately 50 mg clay was saturated 3 times with 15 mL of 0.5 M magnesium chloride < $MgCl_2$ > or 0.5 M potassium chloride < KCl > solution. Clay was dispersed in the solution and shaken for 15 minutes on a reciprocated shaker. The suspensions were centrifuged for 10 minutes at 1500 rpm to flocculate clays, and clear supernatant solutions were pipetted off and discarded. After three cation saturation treatments, two identical rinsing treatments in 10-mL and 5-mL deionized water were conducted, and 1-mL of DI water was added to the clays to form concentrated suspensions.

X-ray Diffraction Analysis (XRD) of Clays

The Bruker D8 Advance X-ray diffractometer was used to record the diffraction patterns. Diffraction parameters included: Cu Kα source, 35 kV and 45 mA beam energy, variable divergence and antiscatter slit widths, 0.05° step size, 3 second dwell time, 30 rpm disc rotation, and SolX energy-dispersive, solid-state radiation detector. . The diffractometer is automated, with Bruker software capable of running 90 samples in succession via a robotic sample loader.

After generating the diffractions patterns for all 27 aggregate samples, XRD analysis was performed to identify and quantify the clay minerals present. The identification of clay minerals was performed after stacking the 5 patterns into a single figure, as in Figure 3.2. Smectite is identifiable by layer thickness of 14 to 15 Å (Angstroms) in the magnesium saturation treatment that expands to approximately 18 Å in the magnesium

glycerol treatment. This is observable in Figure 3.2 in the prominent peak at 14.6 Å in the bottom pattern that moves to 17.9 Å in the second pattern from the bottom.

Vermiculite, however, does not undergo peak shift in the glycerol treatment, and it is identifiable from the glycerol treatment's 14.4 Å peak. Furthermore, vermiculite layer thickness collapses to 10 Å upon expulsion of water during the heating treatments to 550 °C. Therefore, by process of elimination, the 14.4 Å peak in the potassium 550 °C treatment was attributable to chlorite minerals.

Kaolinite is identifiable from a peak in the 7 Å region visible in the lower four patterns that disappears in the 550 °C treatment. Illite is visible as a shoulder of the smectite peak at approximately 10 Å in the magnesium and potassium treatments. Because smectite, vermiculite, and chlorite all have peaks in the 14 Å region with no saturations or magnesium treatment, all 5 treatments are necessary.

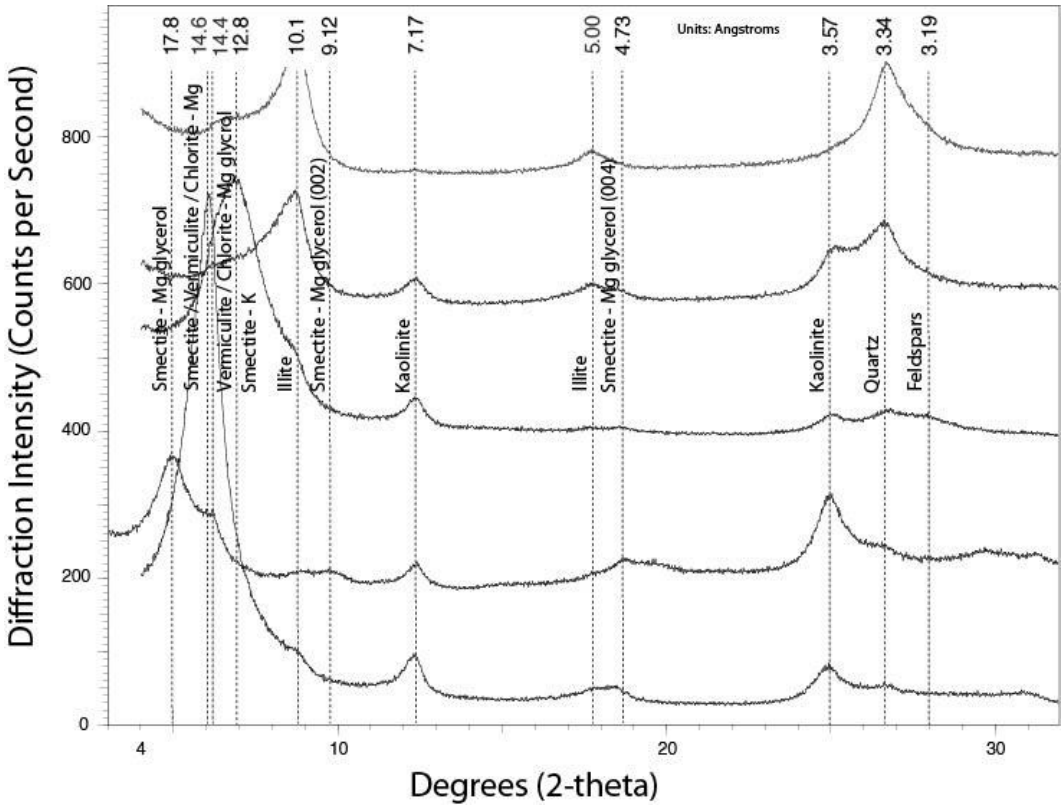

Fig. 3.2. Clay minerals identified from XRD pattern of Jones Mill fine clay

Quantification of Clay Minerals in NEWMOD

NEWMOD is a self-contained software program that allows users to simulate x-ray diffraction peaks of individual clay minerals. NEWMOD has been the benchmark of clay mineral analysis and quantification for 25 years. One major limitation is that NEWMOD does not model non-clay, crystalline minerals such as quartz and calcite.

A least-squares refinement approach was utilized to attain the best match between simulated x-ray diffraction patterns and actual diffraction patterns recorded for each aggregate's clay fraction. Raw XRD data for each clay fraction's magnesium or magnesium-glycerol treatment was imported into a Microsoft Excel spreadsheet – only one of the 5 patterns is necessary to model in the quantification stage. If a significant quantity of vermiculite was identified in the aggregate, the magnesium-glycerol XRD pattern was modeled because the smectite peak shift allows smectite and vermiculite peaks to be distinguished and modeled in NEWMOD (Moore and Reynolds, 1989).

Each primary (001) peak evident in the aggregate diffraction patterns was modeled in NEWMOD and fitted by manipulating peak intensity manually in Microsoft Excel, exhibited in Figure 3.3. Once parameters were set in NEWMOD for the lab's Bruker D8 XRD, layer thickness - or d-spacing – and average number of layers per clay mineral crystallite was the major variables manipulated in the program (Deng et. al., 2010).

Optimal pattern fitting required the creation and importing of many simulated patterns from NEWMOD into Excel. After the primary diffraction peaks were fitted for all clay minerals in the sample, relative mineral quantities in the clay fractions and in the overall -2 mm fractions were calculated.

Crystalline phases such as quartz and feldspars were identified in some samples. As NEWMOD doesn't provide models for non-clay highly crystalline minerals, these highly-crystalline minerals were not accounted for in these calculations. Aggregates with intense quartz peaks in clay fractions may overestimate clay mineral quantities

slightly. The greatest possibility of quartz in the clay fractions came from the carbonate-rich aggregates that were ground to -140 mesh sieve prior to pretreatment.

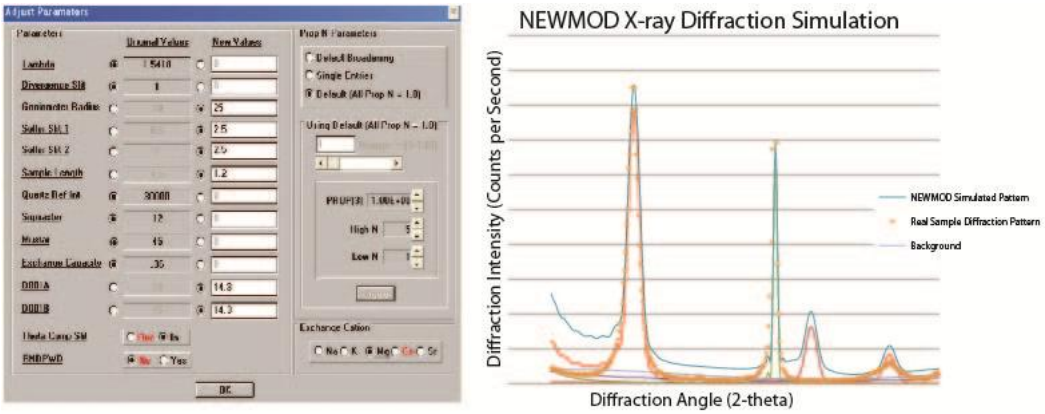

Fig. 3.3. NEWMOD graphical interface and pattern-fitting in Excel

Separation of clay fractions, identification of clay minerals after saturation with cationic solutions, and quantification by NEWMOD simulation is a time-consuming but established and reliable method for clay mineral identification and quantification. Without the separation of clay fractions (< 2 μm) and fixing of layer thickness with magnesium and potassium cationic solutions, correct identification of clay minerals is not possible using current methods.

Correction for Quartz in Clay Fractions

One problem of quantifying quartz and clay minerals occurring in the same specimen is difference in their particle morphology and habit. While clay minerals such as smectites are platy, with repeating structure along the x and y-axes, quartz is highly crystalline - exhibiting repeating atomic arrangement in 3 dimensions. The greater crystallinity of quartz results in higher diffraction intensity, disproportionate to actual mineral quantities. Quartz' presence in a specimen's clay fraction, as is represented in the XRD pattern in Figure 3.4 below, was corrected for in order to prevent the overestimation of clay mineral quantities.

The reference-intensity-ratio method (RIR) was used to correct for the presence of non-clay minerals and clay minerals for which NEWMOD has no models. The Armor aggregate clay fraction, for instance, had strong diffraction peaks at 10.6 and 12.2 Angstroms, suggesting presence of palygorskite and sepiolite. NEWMOD does not have the capability to model these clay minerals or crystalline materials such as quartz and feldspars. Standard, pure mineral mixtures of 50 % palygorskite - 50 % smectite, 50 % sepiolite - 50 % smectite, and 50 % palgorskite – 50 % sepiolite were prepared and analyzed by XRD to determine the reference-intensity-ratios of these mineral phases.

Quartz was accounted for in clay fractions first by creating a 50 percent mixture of pure kaolinite and fine-sized quartz (< 53 μm quartz crushed further) mineral standards. Kaolinite exhibits relatively high crystallinity and low orientation effects for a clay mineral and is present with quartz in the majority of affected clay fractions. Water was

added to the mixture to create a suspension, and the particles were dispersed by microsonication. An x-ray diffraction pattern of the mixture was recorded, and peak intensities of quartz and kaolinite measured. Reference-intensity-ratio of quartz and kaolinite was used to determine proportion of quartz in the clay fractions.

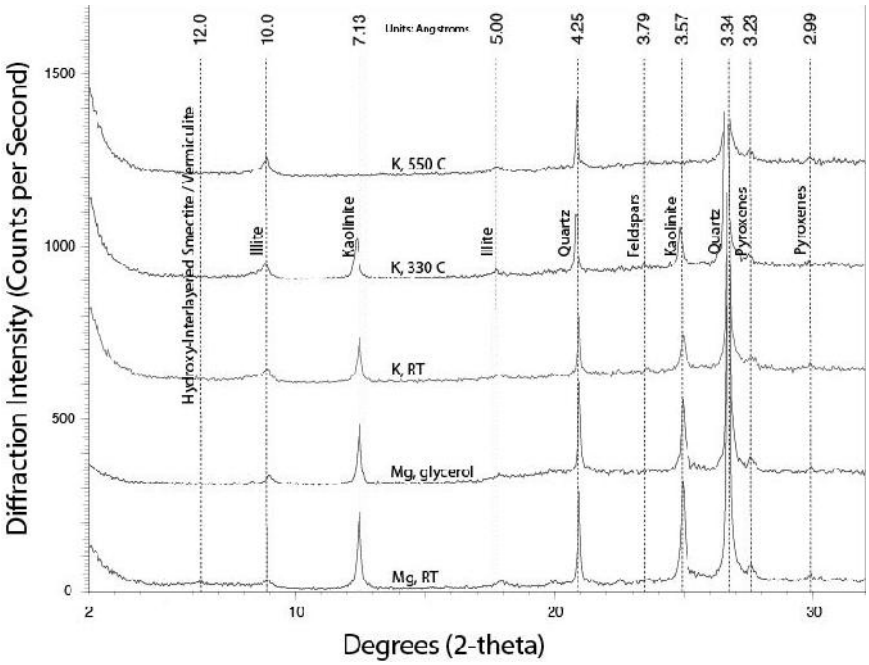

Fig. 3.4. XRD of North Troy clay fraction, with quartz peak at 3.34 Angstroms

Validation of NEWMOD Method

Three artificial mixtures were prepared with recorded quantities of standard kaolinite and smectite minerals. Mixtures underwent a 0.5 M magnesium chloride saturation treatment identical to the treatment performed on all aggregate clay specimens. X-ray diffractometer parameters were identical to the aggregate clay analysis. According to Moore and Reynolds (1989) +/- 10 % accuracy for quantification of each major clay mineral phase and +/- 20 % accuracy for each minor clay mineral phase present – components that make up less than 20 % weight fraction of the specimen - is a good result. Three percent accuracy for clay mineral phases is considered a very good result.

Spray-Drying Procedure for Powder Diffraction

Quantification of crystalline minerals in road aggregates was completed from a whole-sample starting material (<2 mm). Approximately 15 grams of aggregate was crushed with mortar and pestle until all material passed through a 60-mesh sieve (< 250 μm). Four and one-half grams of ground sample was weighed to three decimal places precision. One-half grams of zinc oxide standard was weighed out separately.

Sample and standard were mixed and added to a cylinder containing aggregate grinding elements. Approximately 10 milliliters of 0.5 % polyvinyl alcohol (PVA) in deionized water solution was added to the mixture. The sample was slurry-ground in a McCrone micronizing mill for 5 - 10 minutes at 3500 rpm. The slurry was transferred to

a 50 mL glass beaker through the pouring cap. Grinding elements were rinsed with added PVA solution until the final solution was relatively clear after cleaning. Slurry suspension volume was minimized, as dilute suspensions lost too much sample from evaporation. Range of optimal suspension volume was 20 - 30 mL for 5 g of sample.

A custom-fabricated, 90 x 44 cm aluminum spray-dryer equipped with 2, 1500 watt heating coils – pictured in Figure 3.5, inset (a) below - was heated to 130 ° C chamber temperature. Slurry solution was sprayed into the chamber through an opening in its conical lid. A Badger artist's air brush was connected to a vacuum pump and to the sample slurry by PVC tubing. Slurry was sprayed downward slowly, in as fine a mist as the air brush and vacuum pressured allowed. Dried spherical particles were collected from the chamber floor on a sheet of Post-It® white easel pad paper. Particle size and morphology of spray-dried specimens was observed at 6 X magnification under a light microscope and at higher magnification with scanning electron microscope (SEM).

Fig. 3.5. Spray-drying procedure for reducing orientation effects during powder diffraction

Rietveld Method for Total-Sample Quantification

Each spray-dried specimen was side-mounted into an XRD powder holder enclosed by a frosted-glass cover. Unique diffractometer parameters for Rietveld analysis included: 3 – 80° 2Θ angle, 0.02° step size, 15 second dwell time per step, variable divergence and anti-scattering slit widths, and 0 rpm stage rotation. XRD analysis required approximately 16 hours per specimen.

The Rietveld method utilizes a full-pattern simulation to model diffraction patterns of real samples. It incorporates a least difference of squares statistical analysis to minimize the difference between real and simulated patterns. Online databases of crystal structures such as the International Center for Diffraction Data (ICDD) library are contributed to by researchers around the world, and models are easily downloadable. In addition, many mineralogy labs catalog standard mineral diffraction patterns and use the crystal structure data in modeling diffraction patterns.

Quantification by the Rietveld method works by minimizing the difference between actual and modeled diffraction patterns. Researchers work to identify the minerals and select the appropriate crystal models from an online database or their own lab's mineral reference library. A software program, such as Bruker DIFFRAC^{plus} TOPAS, then runs a full pattern simulation, modeling all major diffraction peaks (Young, 1993). In modeling all peaks -even the lesser peaks in a diffraction pattern - the Rietveld approach resolves the significant issue of peak overlap that complicates quantification by other methods, such as the Reference-Intensity-Ratio method (RIR).

The major limitation of the Rietveld method is that it calculates diffraction patterns assuming 3-dimensional periodicity in sample crystal structure. This condition, however, is only true for highly crystalline materials or minerals -- such as quartz and calcite. Clay mineral structure exhibits ordered arrangement of atoms in 2 dimensions along the X and Y axes, but between layers there is disordered stacking. In addition, crystallite size is much smaller in clay minerals than in more crystalline minerals, and chemical variation by isomorphic substitution is common in clay minerals as well.

The lack of 3-dimensional diffraction characteristics and variability in structure and chemical composition of clay minerals means that the development of crystal structure models for Rietveld analysis of clays is an area of ongoing research among clay researchers. Clay mineral structure is less definable due to the variable layer thickness, interstratification of clay minerals, and difference angles of layer sheet stacking.

Furthermore, in a total-sample Rietveld refinement, clay minerals may not be easily identifiable because of their lower intensities. It was determined in a previous experiment that smectite diffraction peaks weren't detectable in a quartz-bentonite powder mix when bentonite was present in quantities below than 5 % mass of mixture. Definitive identification of clay minerals without fixing layer thickness of any expansive clay minerals present is further complicated by peak overlap of different phases near 14 Angstroms d-spacing.

Cation Exchange Capacity (CEC) Procedures

Cation exchange capacity (CEC) is a measurement of the chemical reactivity of materials and may be an important property in concrete design. Expandable layer silicate minerals such as smectite and vermiculite have relatively high CEC – exceeding 100 meq / 100 g. CEC is a useful test for identifying and quantifying clay minerals in aggregate fines. However, CEC is not exactly proportional to expandable clays such as smectite, as non-expandable clays, non-clay minerals, and other materials have CEC as well. In this procedure, the CEC of treated and separated clay fractions (< 2 μm) was determined.

Two identical treatments were completed for each aggregate clay fraction – one repetition or duplicate is typically completed for each sample to reduce experimental error. For each treatment, 100 mg clay each was saturated 3 times successively in a 0.5 M calcium chloride and 3 times in a 0.005 M calcium chloride solution ($CaCl_2$) to fix Ca^{2+} as the saturation cation. 4 ensuing saturations of 0.5 M magnesium chloride <$MgCl_2$> solution followed to replace Mg^{2+} for Ca^{2+} on the cation exchange sites in the clay interlayer and particle edge sites.

After each washing with magnesium chloride solution, supernatant containing the displaced calcium ions was collected and set aside. Calcium concentration in the magnesium solution was determined by atomic absorption spectroscopy (AAS) analysis with an acetylene flame. CEC was calculated in units of milli-equivalents charge per 100 grams sample, per the following equation (Deng et. al., 2010):

CEC = [(A-B)/(200.4 mg/cmol)*OD]*[1000 g/kg]

A = weight of exchangeable and interstitial Ca (mg)

B = weight of interstitial Ca (mg)

OD = oven-dried sample weight (mg)

For the CEC determination of -40 screenings (< 400 μm), sodium and ammonium were used as the saturation and exchange cations, respectively, in place of calcium and magnesium. Two treatments for each aggregate of 2.5 grams per specimen was weighed into extraction tubes – shown in Figure 3.6, inset (a), below - and treated with sequential 20-mL and 40-mL of a pH 8.2 sodium acetate <NaOAc> solution. The first treatment was extracted rapidly and the second slowly, over 2 hours. Next, 2 treatments of 40-mL ethanol were extracted over 45 minutes each treatment.

Finally, 20-mL and 40-mL of pH 7.0 ammonium acetate <NH_4OAc> were extracted from each specimen, the 20-mL treatment rapidly and the 40-mL treatment for 2 hours. Ammonium extract was collected, diluted in ammonium acetate, and sodium concentration determined by flame emission on a Varian SpectrAA atomic absorption spectrometer (AAS). CEC was calculated according to the equation:

CEC (meq/100g) = [(extract weight)(mg/1 mol Na^+)(dilution factor)] /
[(sample weight)(230)]

Fig. 3.6. Cation exchange determination for clays (b) and -40 screenings (a and c)

Methylene Blue Adsorption (MBA) Procedures

The methylene blue adsorption (MBA) test was used to estimate both CEC and expansive clay mineral content of soils and aggregates. The methylene blue molecule is a cationic dye that adsorbs to exchange sites in the interlayer and edges of layer silicates. Maximum absorption of ultraviolet radiation by a pure solution of 5 ppm methylene blue was measured by ultraviolet visible spectroscopy (UV-VIS) at approximately 660 nm wavelength. Some specimens exhibited changes in color from blue to violet and shift in maximum absorption to lower wavelengths, indicating probable dimerization at the clay surface, influenced by the layer charge (Cenens and Schoonheydt, 1988).

For all aggregate clay fractions tested, approximately 0.325 milligrams suspension was transferred to 10 mL test tubes. Five mL of 10 parts per million methylene blue solution was added to clay suspensions, and water was added to make final suspension volume of 10 mL. The mixture was agitated overnight by reciprocal shaker. Specimens were centrifuged to flocculate clays, and ultraviolet absorption of the supernatant was measured between 350 to 800 nanometers wavelengths. Adsorption of MB by clays was calculated in units of grams methylene blue per kilogram clay. MB was conducted on 15 of the 27 aggregate clays.

In a separate procedure for aggregate -40 screenings, 20 grams of sample was placed in a 45-mL test tube with 30 grams of 0.5 weight percent methylene blue solution. Materials were shaken by hand for 1 minute, allowed to rest for 3 minutes, and shaken for 1 additional minute. One hundred thirty microliters of filtered supernatant was

diluted to 45 grams, and methylene blue (MB) concentration was determined in a portable calorimeter. Concentration of MB in a 130 μL aliquot diluted to 45 grams was determined by the same method, and methylene blue adsorption calculated according to the equation below, in units of milligrams MB adsorbed per gram sample:

$$MB = [(C_{0,measured} - C_{0,theoretical}) + (MB_{measured})(20\ g)/(30\ mL)(1000)](30\ mL) / (20\ g)(1000)$$

Infrared Spectroscopy Analysis (FTIR-ATR)

Infrared absorption analysis (FTIR-ATR) measures absorbance of infrared radiation of different wavenumbers – the inverse of wavelength – through diverse materials of organic and mineral origin. A plot of absorbance vs. wavenumber may be generated, and the resulting graph is used to identify what minerals are present in a specimen.

Many minerals may be identified by their characteristic absorption of infrared radiation – peaks – but not all clay minerals are able to be identified definitively by this method. In particular, there is no unique IR peak for the class of expandable layer minerals known as smectites, which are indistinguishable from illites and other water-adsorbing minerals in the infrared spectrum.

A small specimen of separated and dried clay was oven-dried and analyzed by an attenuated total reflectance infrared absorption (FTIR-ATR) technique between 670 and 2000 cm^{-1} wavenumber under ambient condition - without heat or nitrogen gas

treatments. An example of an infrared absorption spectra from Blum pit's clay fraction is exhibited in Figure 3.7 below.

Data collection time for ATR was a few minutes for each sample, and the stage was cleaned with methanol after each specimen run. Identification of minerals was undertaken with pertinent reference materials containing standard absorption data for clay minerals. Infrared absorption patterns were recorded for the original aggregate fines received from the Texas Department of Transportation (TXDOT), 11 of the 27 total aggregate clay fractions.

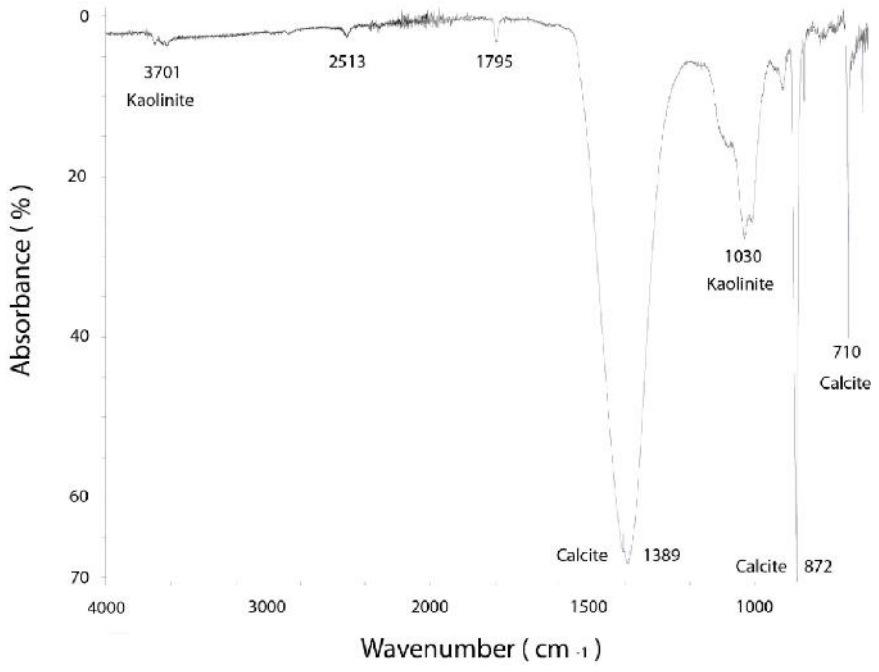

Fig. 3.7. Infrared absorption spectra (FTIR-ATR) of Blum clay fraction

Electron Microscopy with Chemical Analysis (EDS)

Electron microscopy makes visible size and morphology of silt and clay-sized particles. In addition, electron microscopes are equipped with X-ray energy dispersive spectrometers that allow chemical analysis of individual particles. Scanning electron microscopy (SEM) differ from light microscopes and transmission electron microscopy (TEM) by its conversion of secondary electrons reflected from specimen surfaces to an electrical signal that is then converted back to an image by cathode ray tube or digital device. In light microscopy and TEM, the beam passes through a specimen and 2-dimensional image is magnified and projected (Deng et al., 2010).

Specimens for SEM analysis were collected from separated aggregate silt fractions (2-53 μm particle diameter) or from total samples (< 2 mm diameter). Specimens for TEM analysis were diluted from aggregate clay suspensions (< 2 μm particle diameter). Dilute suspensions were deposited on carbon tape and coated with platinum or carbon "sputtered" at extreme temperatures to reduce charging of specimen surfaces. An FEI Quanta 600 FE-SEM with Oxford EDS system was used for SEM analysis, while a JEOL JEM-2010 with Oxford ATW EDS detector was used for TEM analysis. Backscattered electron detector and imaging was utilized to observe heavy element distribution in several specimens in the FE-SEM.

CHAPTER IV

RESULTS AND DISCUSSION

Clay Mineral Identification by X-ray Diffraction Analysis

After generating the diffractions patterns for all 27 aggregate samples, XRD analysis was performed to identify and quantify the clay minerals present. The identification of clay minerals was performed after stacking the 5 patterns into a single figure, as in Figure 4.1 below. Smectite is identifiable by layer thickness of 14 to 15 Angstroms (Å) in the magnesium saturation treatment that expands to approximately 18 Å in the magnesium glycerol treatment. This is observable in Figure 4.1 in the prominent peak at 14.6 Å in the bottom pattern that moves to 17.9 Å in the second pattern from the bottom. Vermiculite, however, does not undergo peak shift in the glycerol treatment, and it is identifiable from the glycerol treatment's 14.4 Å peak.

However, vermiculite layer thickness collapses to 10 A upon heating to 550 °C. Therefore, the 14.4 Å peak in the potassium 550 °C treatment is attributable to chlorite minerals. Kaolinite is identifiable from a peak in the 7 Å region visible in the lower 4 patterns that disappears in the 550 °C treatment. Illite is visible as a shoulder of the smectite peak at approximately 10 Å in the magnesium and potassium treatments. Because smectite, vermiculite, and chlorite all have peaks in the 14 Å region with no saturations or heat treatments, all 5 treatments are necessary.

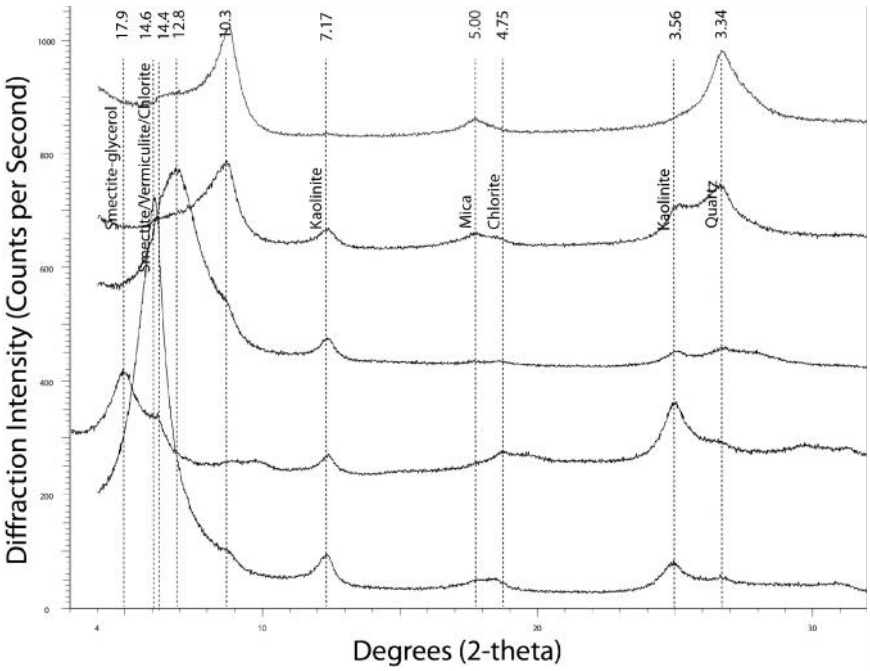

Fig.4.1. Clay minerals identified from XRD pattern of Jones Mill clay

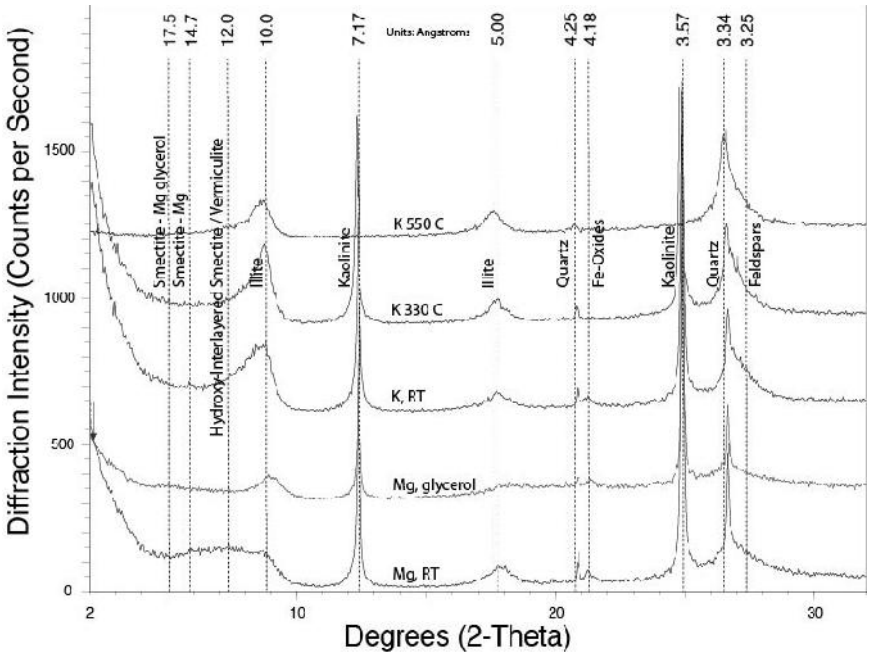

Fig. 4.2. Rankin clay with HIM plateau at 12 Å of ‘Mg, RT’ treatment

Rankin aggregate's clay fractions in Figure 4.2 above exhibited two important phases characteristic to several of the aggregate materials: hydroxyl-interlayered minerals (HIMs) and highly-crystalline kaolinite. HIMs, e.g. hydroxy-interlayered smectites and vermiculites, were evidenced in the broad and irregular diffraction plateau centered at 12 Angstroms in the magnesium-room temperature pattern. The plateau disappears with glycerol solvation. High-crystallinity kaolinite was identified by SEM (see Figure 4.3) and the distinct, sharp diffraction peaks in the 7 Å region that disappear at 550 °C.

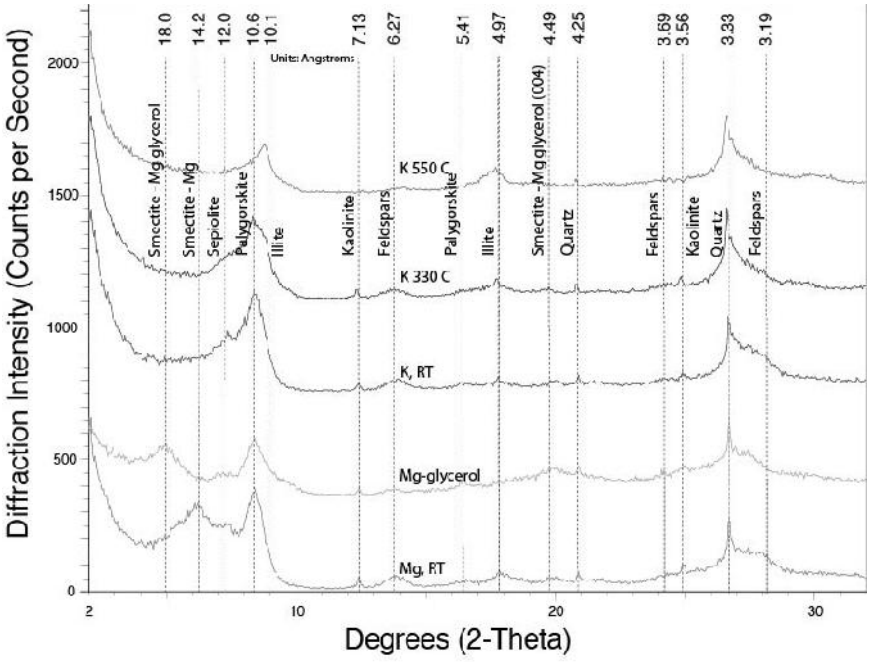

Fig. 4.3. Armor aggregate with palygorskite (10.6 Å) and sepiolite (12.2 Å)

Palygorskite is exhibited in Armor clay's XRD pattern fraction in Figure 4.3 above by the prominent peak at 10.6 Å that reduced at 550 °C - with removal of water and hydroxyl groups (Hayashi, et. al. 1969). The sepiolite peak at 12.2 Å did not shift to 10 Å with glycerol treatment, as interstratified illite-smectite would (Deng, et. al. 2010). Both phases have d-spacing of approximately 12 Å. In addition, the 12.2 Å peak diminishes with heat treatment as sepiolite would be expected to do. Figure 4.4 is a transmission electron micrograph fibrous or needle-like morphology of palygorskite and sepiolite particles in Armor aggregate.

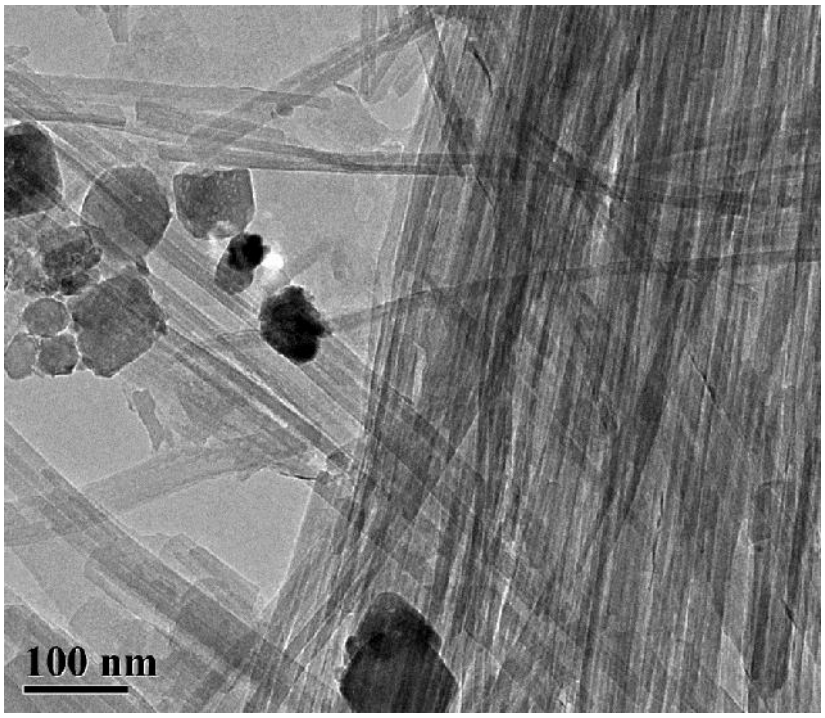

Fig. 4.4. Fibrous palygorskite and sepiolite minerals in Armor clay (29000X)

Clay Mineral Quantification by NEWMOD Method

Table 4.1 gives estimated clay mineral quantities in the 27 aggregates from the NEWMOD diffraction peak simulations. Clay mineral quantity in each aggregate starting material (< 2 mm fraction) was estimated by separating clay fractions (< 2 μm) chemically and measuring total amount of clay recovered to back-calculate percentages of clay minerals in bulk starting materials, similar to Lynch's procedure (1997).

This method assumed no clay mineral occurrence in separated silt or sand fractions, which seemed reasonable with the removal of cementing agents during pretreatment - larger aggregates containing clay minerals should release the smaller particles as carbonate minerals and iron oxides dissolve. Srodon, et. al. (2001) critiques this normalization technique as introducing a potential source of error. Accurately identifying clay mineral phases present without prior separation of clay fractions and fixation of layer thickness, however, is infeasible for non-expert clay researchers.

The most expedient and reliable method for clay mineral quantification for inexperienced researchers appears to be size-fractionation, cation saturation with heat treatments, and mineral identification in conjunction with NEWMOD simulations. Encountering a diversity of real samples and creating a library of diffraction patterns may require many years of experience (Moore and Reynolds, 1989). Selecting appropriate structure models for diffraction simulation of clay minerals during Rietveld analysis poses special challenges to accurate quantification. This remains an area of

ongoing research; there is no widely-used “black box” or automated solution to clay mineral quantification in total-sample analysis, currently.

All values in Table 4.1 were calculated as quantities of clay minerals in the starting fraction treated (passing 10 mesh sieve or less than 2 mm particle diameter), expressed as weight percent. ‘Clay’ refers to total quantity of clay-sized particles recovered as a percentage of the starting materials. For the sake of fitting all data onto a single page, clay mineral names are abbreviated, as follows: ‘Sm’ for smectites, ‘Vc’ for vermiculite, ‘Kaol’ for kaolinite, ‘Chl’ for chlorites, ‘HIM’ for hydroxy-interlayered minerals (HIS/HIV), ‘I-S’ for interstratified clay minerals, and ‘P/S’ for palygorskite and sepiolite. The ‘M’ abbreviation in two of the samples indicates the McKelligon locality.

Aggregate	Clay	Sm	Vc	Ill	Kaol	Chl	HIM	I-S	P/S
Blum	1.26	0.96	-	0.14	0.16	-	-		
Hoot	0.71	0.34		0.07	0.29	-	-		
Jarrell 1	0.37	0.27		0.01	0.09	-	-		
Jarrell 2	0.89	0.65	0.0	0.01	0.06	-	-		
Jones Mill	5.98	1.70	2.5	0.47	1.10	0.1	-		
Little River	1.52	0.58	0.1	0.35	0.47	-	-		
M Granite	3.86	2.70	0.1	0.57	0.44	-	-		
Pit 365	28.0	18.2	-	4.3	5.6	-	-		
Scarmado	0.21	0.16	-	0.03	0.03	-	-		
South Noodle	16.6	6.94	-	5.94	1.00	-	-		
Tolar	8.01	0.17	-	4.32	0.26	-	3.20		
Whitney	5.2	3.2	-	1.1	0.9		--		
Woods	4.8	4.5	-	1.1	0.9	-	-		
Yarrington	7.5	4.2	-	1.4	1.7	-	-		
Armor	3.02	1.02							2.0
Black	1.82	0.35	-	0.25	0.89	-	-	0.2	
TX Crushed	0.86	0.53	-	0.10	0.24	-	-		
L. Bridgeport	1.16	0.55	-	0.13	0.12	-	-		
Buster/Bird	3.3	-	-	0.17	0.80	-	0.12		
M Dolomite	13.5	-	-	13.5	-	-	-		
Bird Hill	6.6	-	-	1.00	3.63	-	1.97		
Huebner	3.1	1.29	-	0.34	1.24	-	-		
Rankin	6.9	0.23	-	1.9	1.9	-	2.59		
Helotes	3.3	1.62	-	0.30	1.18	-	-		
Cemex South	3.1	-	-	0.62	0.16	-	-	0.5	
North Troy	3.5	0.04	-	0.15	0.79	-	0.08		
F Murphy	9.8	7.2	-	0.72	1.3	-	-		

Table 4.1. Clay and clay mineral quantities in 27 aggregate (< 2 mm) materials

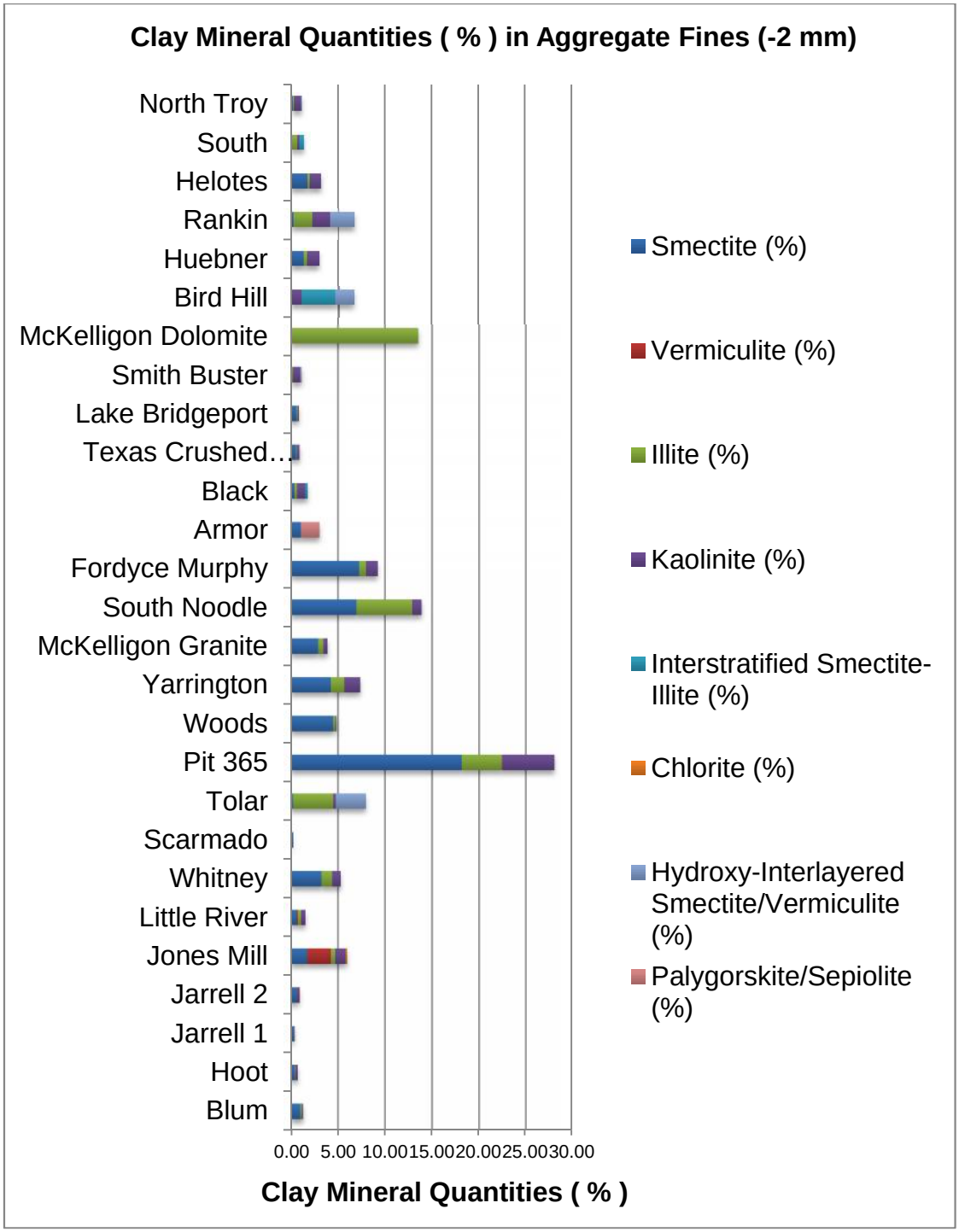

Fig. 4.5. Clay mineral quantities in aggregate fines (- 2 mm starting material)

Both volume of clay fraction and concentration of expansive clay minerals in the clay suspensions are exhibited in Figure 4.5 above. The dark blue bar represents smectites, the class of clay minerals with the greatest shrink-swell properties and most important for the Texas Department of Transportation (TXDOT) to be able to detect.

A recent study by the International Center for Aggregates Research (Norvell, et al, 2007) substituted pure smectite and illite into aggregate microfines (< 75 μm). Concretes with substitutions of 1 % and 4 % smectite exhibited elevated methylene blue values, and the 4 % smectite mixes showed high linear shrinkage and low compressive strength. Five aggregates in this study - Fordyce Murphy, South Noodle, Yarrington, Woods, and Pit 365 - showed smectite content higher than 4 % in < 2 mm starting material. Of these 5 materials, only Yarrington did not have river gravel for parent material – it was a crushed limestone with interbedding of shale.

An additional 6 aggregate specimens demonstrated smectite quantities greater than 1 % calculated for -2 mm starting materials: Armor, Helotes, Huebner, Jones Mill, McKelligon Granite, and Whitney. As evidenced in Table 4.2 on the following page, 14 of the 27 separated aggregate clay fractions contained greater than 50 % smectite mineral quantities, including 5 aggregates with less than 1 % smectites in total sample (< 2 mm starting materials): Jarrell 1, Jarrell 2 , Lake Bridgeport, Scarmado, and Texas Crushed Stone. These aggregates had high concentrations of smectite in the recovered clay fractions (< 2 μm) but relatively low overall clay content.

Aggregate	Smectite % (< 2 mm)	Smectite % (-2«m)
Armor	1.02	33.8
Blum	0.96	76.0
Fordyce Murphy	7.23	78.5
Helotes	1.62	52.4
Jarrell 1	0.27	72.1
Jarrell 2	0.65	70.5
Huebner	1.29	45.3
Jones Mill	1.70	29.3
Lake Bridgeport	0.55	69.0
McKelligon Granite	2.85	73.8
Pit 365	18.2	64.9
Scarmado	0.16	72.9
South Noodle	6.94	50.1
Texas Crushed Stone	0.53	60.5
Whitney	3.23	61.2
Woods	4.49	92.9
Yarrington	4.22	57.4

Table 4.2. Aggregates containing high smectite quantities in clay fractions and/or starting materials

It is important again to note that the aggregate specimens provided by TXDOT were screening materials that did not undergo standard washing treatments for removal of clays. Clay content therefore is elevated from what would be encountered in stockpiles or used in asphalt or Portland cement concretes as road aggregate. The unwashed or "pit run" screenings from coarse aggregates were expected to exhibit greater variation in clay mineral quantities between quarries as compared to stockpile samples that had undergone washings to remove clays.

In many of the calcareous aggregates that were crushed to pass a 140-mesh sieve - to increase rate of carbonate dissolution - sharp diffraction peaks for quartz were observed

in the magnesium saturation treatments. Clay-sized quartz particles are not desirable for quantification and usually indicate a deviation from standard sample preparation procedures. Quartz' presence in the clay fractions was an unintended consequence of the steps taken to facilitate dissolution of carbonates in the carbonate-rich samples. Several aggregate clay specimens exhibited quartz diffraction peaks sufficiently sharp that the accuracies of clay mineral quantifications were in doubt. Results of this correction by reference-intensity-ratio are given in Table 4.3.

Aggregate	**Quartz Content (% of < 2 «m fraction)**
Black	4.2
Buster	67.0
Cemex South	57.8
Fordyce Murphy	6.3
Helotes	6.7
Huebner	4.5
Lake Bridgeport	31.0
North Troy	69.3
Rankin	4.2
South Noodle	16.3

Table 4.3. Quartz quantities in clay fractions of calcareous aggregates

Validation results for the NEWMOD clay mineral quantification method are shown in Table 4.4 below. Three artificial mixtures were prepared with recorded quantities of standard kaolinite and smectite minerals. The percentage compositions of mixtures were not calculated prior to modeling. The kaolinite standard was a dried powder, while the smectite standard was in suspension in water.

According to Moore and Reynolds (1989) +/- 10 % accuracy for quantification of each major clay mineral phase and +/- 20 % accuracy for each minor clay mineral phase present – components that make up less than 20 % weight fraction of the specimen - is a good result. +/- 3 % accuracy for clay mineral phases is considered a very good result.

Specimen	Actual Smectite (%)	NEWMOD Smectite (%)	Accuracy (%)
Mixture 1	47.9	45.0	-6.1
Mixture 2	54.7	52.8	-3.5
Mixture 3	78.4	71.7	-8.5

Table 4.4. NEWMOD validation for standard smectite-kaolinite mixtures

Results for the NEWMOD quantification validation were good – all 3 results were well within 10 percent accuracy, and Mixture 2 was approaching the criterion for 'very good.' Underestimation of smectite quantities relative to kaolinite was observed for all 3 mixtures. Many of the road aggregates' clay XRD patterns exhibited unusually sharp diffraction peaks for kaolinite. This may be explained by the very perfect kaolinite crystals present, viewable by electron microscope.

An image of high-order kaolinite “books” is viewable in Figure 4.6 below. High-order kaolinite was most prevalent in crushed limestone samples from which carbonate minerals had been removed. It is believed those kaolinites occurred within the limestone matrices, as weathered materials from soils would not be pristine.

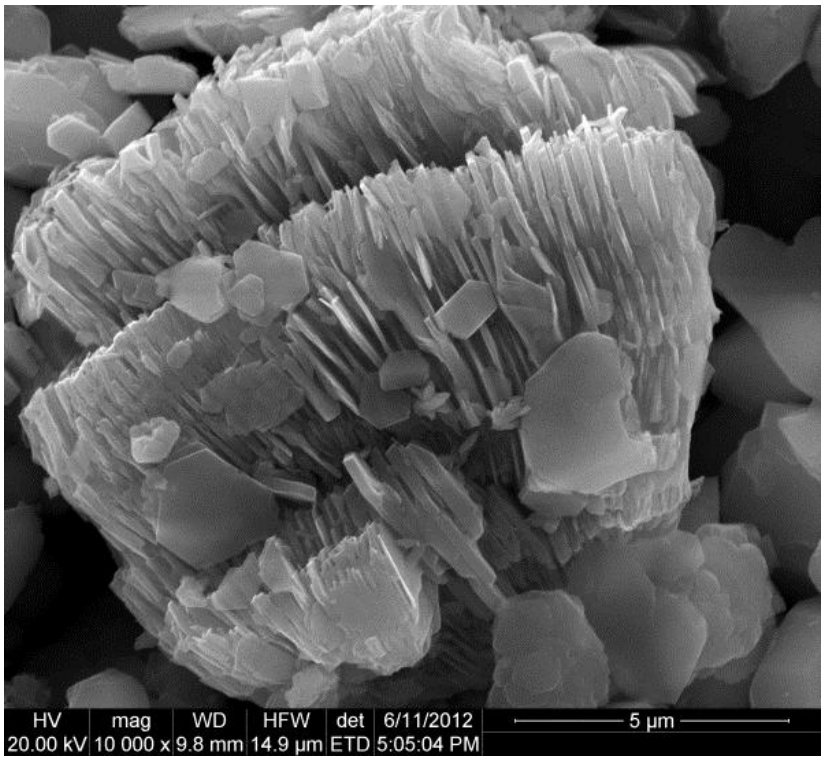

Fig. 4.6. SEM image of high-crystallinity kaolinite “books” in Rankin fines

Overestimation of kaolinite was a problem, initially, for the real aggregate specimens as well. As the kaolinite standard was a dried material, it is possible that there was aggregation of those minerals that was not dispersed, resulting in artificially-heightened

diffraction intensity. In addition, there may be some overlap of the *002* diffraction peak for smectite diffraction with the kaolinite *001* peak. If not accounted for, this would contribute to error of overestimating diffraction intensity of kaolinite peaks. A low-order kaolinite peak was modeled for the 3 mixtures and included in the analysis that appeared to address the potential issue of peak overlap.

Spray-Drying Procedure for Random Orientation in Powders

In x-ray diffraction and quantification of powder mineral samples, preferred orientation occurs when particles or crystallites tend to align in the same direction (Jenkins and Snyder, 1996). This causes distortion of diffraction peak intensities and affects accuracy of quantification calculations – which assume random orientation of crystallites in a powder (Brindley and Brown, 1980). Preferred orientation occurs when particles with similar mineralogy or habit pack into a powder sample holder along the same axes of planes. Orientation effects are a central problem in powder diffraction and leads to artificial, heightened intensity of diffraction peaks for mineral phases affected.

One strategy for minimizing orientation effects is to attempt to form aggregates of uniform particle size and shape with random orientation from smaller crystallites of diverse size, habit, and orientation effects. Hillier (1999) described a modified spray-drying procedure that utilizes a commercial artist's air brush to spray a concentration suspension of sample in water into a heated chamber at a constant pressure. The force

from movement of hot air out of the chamber drives suspension droplets upward, while the force of gravity works to bring them to the chamber floor.

It is necessary to control size and flow rate of droplets of suspension from the air brush in order to achieve good recovery of uniformly-sized, spherical particles. In general, a more viscous suspension that minimized fluid volume coupled with a slow and dispersed air brush nozzle setting achieved the best results. Chamber temperature observed below 130° C at commencement of spray-drying resulted in sample loss when suspension dropped to the chamber floor without drying.

Ideal spray-dried aggregates are spherical in morphology and approximately 50 μm in diameter. A fraction of the sample is lost during micronizing, some exits through the chamber's ceiling, another part falls to the chamber floor without drying, and a final portion is lost during transfer from the collection paper. Expected yield of spray-dried product from starting materials for experienced technicians is between 50 and 80 percent of dried starting material (Hillier, 1999).

However, due to the limited number of samples processed during this project, acceptable recovery was determined to be the minimum quantity required to fill a side-mounted powder sample holder. Starting material of 5 grams allowed some margin of error, as only 0.7 grams was needed for powder XRD analysis – or approximately 15 percent recovery. Spray-dryer yield and percent recovery are presented in Table 4.5 below, along with range in diameter of and morphology of spray-dried aggregate particles.

Sample	Recovered (g)	Yield (%)	Morphology	Diameter («m)
Blum	2.28	45.6	Spherical/perfect	30 - 80
Fordyce	1.86	37.1	Spherical/dimpled	40 - 70
Hoot	2.07	41.5	Spherical/pitted	30 - 100
Jarrell 1	2.10	42.0	Spherical/perfect	50 - 100
Jarrell 2	1.76	35.2	Spherical/dimpled	30 - 80
Jones Mill	2.89	57.9	Spherical/pitted	20 - 70
Little River	1.37	27.4	Spherical/dimpled	30 - 70
McK Granite	1.29	25.8	Ovoid/dimpled	40 - 90
Pit 365	1.67	33.3	Spherical/perfect	20 - 80
Scarmado	2.03	40.7	Irregular	10 - 50
South Noodle	1.55	31.0	Spherical/Ovoid	40 - 70
Tolar	1.91	38.1	Spherical/Perfect	30 - 70
Whitney	2.28	45.6	Spherical/Dimpled	20 - 70
Woods	2.58	51.7	Spherical/Dimpled	40 - 70
Yarrington	1.22	24.3	Spherical/Needle	20 - 50

Table 4.5. Recovery of spray-dried specimen from 5 grams starting materials

The three spray-dried samples observed under scanning electron microscope had extremely diverse clay mineral content, and the lack of sufficient clays likely diminished aggregate formation. Clay minerals act as cementing agents or binders in soil and geological aggregates, as they carry layer charge and bind to charge surfaces of larger particles. Scarmado, with 0.19 percent clay-sized particles in starting material, had the lowest clay content of the 15 aggregates spray-dried, and it formed spherical-shaped aggregate inconsistently. While the 0.5 percent polyvinyl alcohol (PVA) solution has the effect of facilitating aggregation of smaller particles generally, results for Scarmado were the poorest observed under light or electron microscope. Many small, irregular particles from Scarmado are evident in Figure 4.7 (a) and A (b) above. Some preferred-

orientation would be expected from this specimen. Micronizing this sample with a more-concentrated PVA solution and taking care to minimize suspension volume might yield more uniform, spherical aggregates.

Yarrington spray-dried results in Figure 4.7 (c) and (d) show spherical aggregate particles better formed than Scarmado's but with some imperfections stemming from high clay content in the bulk starting (< 2 mm) material. Yarrington registered 7.34 percent clay-sized particles during size-fractionation, with 4.22 percent smectite. The imperfections in insets (c) and (d) appears to be small extrusions aggregating to the surfaces of well-developed, uniformly-sized spherical aggregates. Perhaps Yarrington and other clay-rich materials do not require a coagulating agent such as PVA in suspension. Ethanol might produce superior results for smectite-rich aggregates.

On the other hand, Tolar - insets (e) and (f) - formed perfect, nearly-homogenous spherical aggregates. Clay-sized particles constituted 7.95 percent of starting material, with 0.17 percent of total material measured as smectite. Tolar was rich in total clays but relatively smectite-poor, and its aggregate fines produced the best spray-drying results in PVA solution. Some variation in results may have been caused by differences in chamber temperature and suspension volume. In general, spray-dried sample recovery and morphology improved with time, as procedure consistency improved.

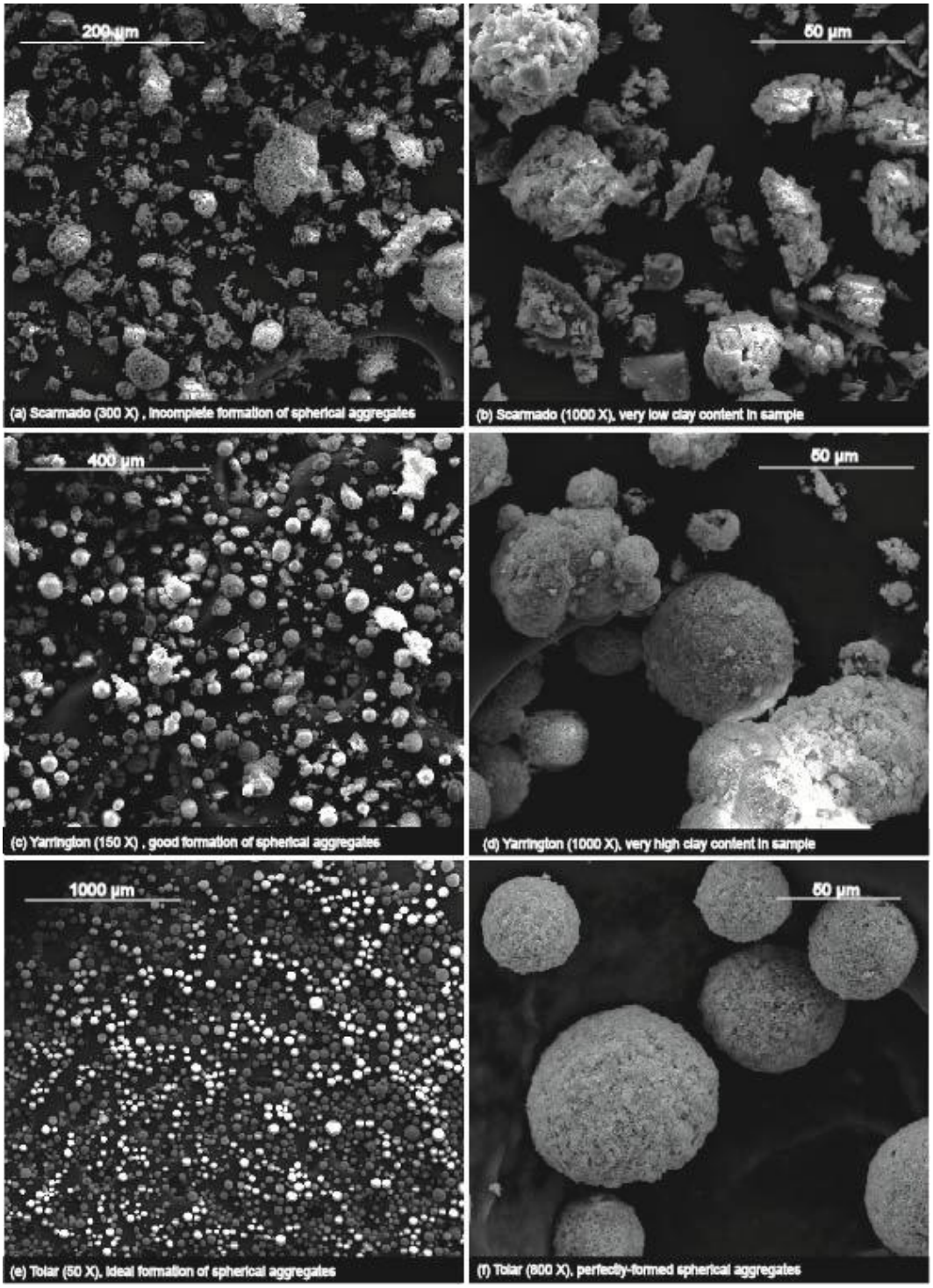

Fig. 4.7. SEM images of Scarmado, Tolar, and Yarrington spray-dried specimens

Rietveld Method Quantification Results

Quantification of clay minerals wasn't achieved from total-sample analysis via the Rietveld method in this study. Observable diffraction peaks in the region typical of clay minerals were rare – peaks attributable to chlorite and kaolinite, however, were observed in Figure 4.8 - suggesting that separation of fine fractions is necessary for clay mineral analysis. Rietveld results are shown in Table 4.6 on the following page but are not discussed in detail because the focus of the study was clay mineral quantification.

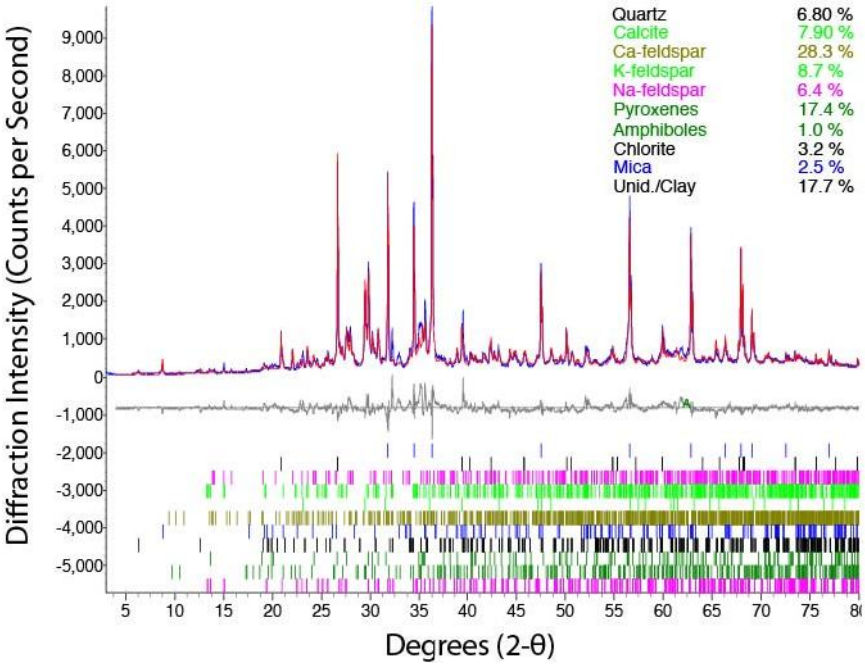

Fig. 4.8 Rietveld method quantification in Bruker DIFFRAC^{plus} TOPAS software

Figure 4.5 shows the Rietveld quantification results for the crystalline minerals in an aggregate. Each colored notch at the figure's bottom represents a simulated diffraction peak for the minerals with corresponding colors, in the upper right. The red diffraction pattern represents the actual sample, while the blue pattern is calculated. The grey pattern represents the closeness of fit, or difference between real and simulated patterns.

Aggregate	% Q	% C	% D	% F	% K	% Ch	% M	% P/A	% Un
Blum	0.5	85.5	0.1	-	-	-	-	-	13.9
Fordyce	95.9	4.1	-	-	-	-	-	-	-
Hoot	97.5	-	-	2.5	-	-	-	-	-
Jarrell 1	0.9	94.2	-	-	-	-	-	-	4.0
Jarrell 2	0.9	91.5	-	-	-	-	-	-	6.5
Jones Mill	6.8	7.9	-	15.1	-	3.2	2.5	18.4	17.7
L. River	96.4	-	-	1.3	-	-	-	-	2.3
M. Granite	18.4	6.0	0.1	46.7	-	-	4.7	-	24.2
S. Noodle	65.7	17.5	-	1.6	-	-	-	-	15.2
Pit 365	7.6	64.6	11.9	0.5	-	-	5.9	0	9.5
Scarmado	95.4	3.3	-	-	1.3	-	-	-	-
Tolar	7.6	64.6	11.9	0.5	-	-	5.9	-	9.5
Whitney	8.9	58.0	-	1.0	-	-	6.2	-	25.9
Woods	65.0	6.4	-	13.4	-	-	2.5	-	12.7
Yarrington	2.7	91.7	-	-	-	-	-	-	5.6

Table 4.6. Rietveld, total-sample quantification results

Results are expressed as mass percent of 4.5 grams starting material. Mineral abbreviations are as follows: ‘Q’ for quartz, ‘C’ for calcite, ‘D’ for dolomite, ‘F’ for feldspars, ‘K’ for kaolinite, ‘Ch’ for chlorite, ‘M’ for mica, ‘P/A’ for pyroxene and amphibole minerals, and ‘Un’ for unidentified phases and clay minerals.

Cation Exchange Capacity (CEC) Results

Cation exchange capacity (CEC) is an important indicator of surface charge and reactivity in clay minerals and more generally in all materials. CEC and methylene blue adsorption (MBA) both function by cation exchange mechanisms, and MBA values may be used to approximate CEC. CEC determination is useful in quantification of expansive layer minerals, which in pure form have high adsorption – often in excess of 100 milliequivalents charge / 100 grams.

For mineral samples composed entirely of clay-sized particles (< 2 μm), CEC approaching 30 meq / 100 g indicates presence of high-exchange minerals: smectite, vermiculite, interstratified clay minerals, or hydroxy-interlayered smectite or vermiculite (HIS/HIV). CEC ranges of clay minerals identified in the aggregate specimens are listed in Table 4.7 below, from Righi, et. al. (1993) and Dixon and Schulze (1977).

Clay Mineral	CEC (meq / 100 g)[1]	Expansiveness
Smectite	80 – 150	High
Vermiculite	130 – 210	Low
Interstratified Illite-Smectite	40 – 60	Moderate
Hydroxy-Interlayered Minerals	50 – 80	None
Primary Chlorites	25 – 45	None
Palygorskite/Sepiolite	5 – 45	None

Table 4.7. CEC of major cation-adsorbing clay mineral groups

Not all clay minerals with high cation exchange capacities are expansive – or cause the same problems in concrete performance. Because HIS/HIV, vermiculite, and possibly palygorskite/sepiolite have high CECs but do not have variable layer thickness, these minerals may falsely inidicate significant presence of smectite in the absence of other data, such as x-ray diffraction analyses. However, these minerals are less common than smectite, and it may be possible to predict their occurrence from geography or parent materials. Results of CEC analysis are provided in Table 4.8 below.

CEC values for – 40 mesh aggregate screenings (< 400 μm, dry-sieved) is more representative of total quantity of clay-sized particles in each aggregate, than CEC values of clay fractions. CEC measurement of clay fractions, however, is more sensitive to expansive clays, particularly when coarser sands have adsorbing materials. This condition is satisfied in igneous and metamorphic rocks – the highest 2 CEC values for -40 screenings were observed for Bird Hill and Jones Mill, a basalt and a hornfels.

Neither aggregate exhibited extremely high total clay content or smectite quantities in less than 2 mm or 2 μm content. However, both aggregate source materials contained significant quantities of chlorites and their weathering products, vermiculite and hydroxy-interlayered minerals (HIM). While unweathered, primary chlorite minerals have low CEC and are not expansive, minerals such as HIM, vermiculite, and iron oxides have high CEC with low expansive properties (Stapel and Voerhoff, 1988).

Of the 5 aggregates sampled that exhibited the highest CEC in – 40 fraction, 3 were igneous or metamorphic (including McKelligon Granite), while the other 2 – South Noodle and Woods Pit – showed the 2 highest smectite contents in bulk starting materials (< 2 mm). CEC determination of -40 screenings may detect high smectite quantities in clay fractions, but it also identifies non-expansive adsorbing materials, particularly in weathered rocks of igneous or metamorphic origins. Therefore, a potential problem with false positive identification of smectite must be considered with tests measuring cation exchange, including the methylene blue adsorption test. The relationship between smectite content and MBA was investigated and will be presented.

Aggregate	CEC –40 (meq / 100 g)	Clays (< 2 «m)	Fine Clays (< 0.2 «m)
Armor	4.4	31.7	-
Beckman	2.1	-	-
Bird Hill	24.7	28.0	-
C. South	2.5	14.5	-
Helotes	1.5	31.7	-
Hoot	-	15.2	-
Huebner	2.3	35.5	-
Jones Mill	14.9	28.2	-
La Burrita	4.5	-	-
Lake Bridge.	0.8	27.2	-
Little River	-	13.5	-
McK Dolomite	2.2	20.1	-
McK Granite	4.6	-	58.1
North Troy	1.1	7.5	-
Pit 365	-	15.2	-
Rankin	1.5	29.8	-
Scarmado	0.8	-	-
Smith Buster	0.6	8.9	-
South Noodle	5.7	34.0	-
Texas Crushed	1.4	-	-
Tolar	4.5	-	-
Whitney	3.4	26.8	-
Woods	5.7	-	86.9
Yarrington	2.1	20.9	-

Table 4.8. Measured CEC of aggregate clay fractions and -40 screenings

Methylene Blue Adsorption (MBA) Results

Two separate methylene blue adsorption procedures were used to the road aggregates. In the Soil Mineralogy Lab, a small quantity of separated clay fractions was shaken overnight and MB concentration in the supernatant measured by UV-VIS. At the Texas Transportation Institute, researchers analyzed up to 20 grams of -40 mesh passing material with by the Grace rapid field test. The Grace method can be completed in as little as 5 minutes with a hand-held calorimeter, and does not require lengthy sample preparation (Grace Custom Aggregate Solutions, 2010).

Methylene blue adsorption values (MBA) for clay fractions were calculated in units of cation exchange, or millimoles of equivalent charge per 100 grams of samples. MBA values for the -40 screenings were calculated in the standard units of milligrams adsorbed per gram of materials. UV-VIS readings for the MBA clay treatments were reasonable when clay was in aqueous suspension and improbably for materials that had been freeze-dried or oven dried. The poor results from air-dried starting material were discarded, and no attempt was made to revise the experimental procedure for the dried specimens, as the priority was to evaluate the Grace rapid test method.

For the clay specimens in aqueous solution, measured adsorption values plateaued at approximately 30 meq/100 g in specimens containing different quantities of smectite. It was expected that if sufficient concentration of methylene blue solution was present, MBA would correlate linearly with smectite content, and no plateau in MBA values would be seen. It was hypothesized that the 5 ppm initial MB concentration in solution

was too low and was exhausted by the smectite-rich clays, explaining the lack of sensitivity to the MBA test with higher smectite quantities. It was expected that potential follow-up experiments using higher initial concentrations of MB would support this explanation.

Methylene blue adsorption values were measured for 14 of the 27 aggregate clays and are presented in Table 4.9. Tests were not rerun for those specimens whose adsorption capacity possibly exceeded concentration of suspension. Unlike the cation exchange procedures utilizing 2 cations – a saturation and an exchange cation - the methylene blue adsorption procedure for clay fractions did not control for variation in type and concentrations of adsorbed cations present in the different aggregate clays.

Indeed, while the MB molecule has a strong adsorption affinity for charged clay surfaces other, it is uncertain if a dilute methylene blue solution (5 ppm) would displace high-valence cations already adsorbed to the specimens' charged clay surface. Hang and Bradley (1970) saturated their clays with concentrated sodium chloride solution prior to MBA testing in order to establish a uniform interlayer environment prior to replacement with the methylene blue molecule.

Aggregate	MB – 40 screenings (mg/g)	MB Clays (meq/100 g)
South Noodle	20.3	22.6
Troy	3.0	6.6
Fordyce Murphy	9.4	29.82
Lake Bridgeport	1.6	24.5
Black	-	31.5
Smith Buster	1.3	10.2
McKelligon Dolomite	2.8	9.0
Cemex South	5.5	15.2
Bird Hill	11.8	29.1
Texas Crushed Stone	4.2	31.5
Rankin	4.0	29.0
Helotes	-	31.4
Armor	13.7	31.3
Huebner	9.2	31.0
McKelligon Granite	6.7	-
Jones Mill	9.8	-
Yarrington	4.0	-
Tolar	19.5	-
Woods	14.7	-
Hoot	1.8	-
Whitney	19.4	-
Scarmado	1.5	-
Pit 365	33.6	-
Little River	10.6	-
Jarrell 1	1.7	-
Jarrell 2	4.4	-
Blum	4.6	-

Table 4.9. Measured MBA of aggregate clay fractions and -40 screenings

CHAPTER V

CONCLUSIONS

In this study, 27 geologically-diverse aggregate fines from throughout Texas, Oklahoma, and Arkansas underwent clay mineral quantification by quantitative X-ray diffraction (XRD) analysis. Texas Department of Tranpsortation (TXDOT) researchers selected and sampled aggregates that had exhibited signs of clay mineral contamination in past performance studies.

Many of the aggregates exhibited significant quantities of expansive clay minerals such as smectite, which are linked to deleterious performance properties in concretes. While the majority of aggregates were derived from crushed limestone or calcareous river gravel parent materials, several exhibited uncommon origins and unusual clay mineralogy. Due to the relatively low number of aggregates tested and diverse geological origins of the different aggregates, it was difficult to support conclusions about trends between different aggregate performance properties in these real samples.

REFERENCES

Atkins, H.N. (2003). *Highway materials, soils, and concretes, 4th ed.* Prentice Hall, New York.

ASTM Standard C33 (2003). Specification for concrete aggregates. ASTM International, West Conshohocken, PA.

Bartley, F.G., Harvey, C.C., Bignal, G., Christie, A.B., Reyes, A., Soong, R., and Faure, K. (2007). Clay mineralogy of modified marginal aggregates. *Transfer New Zealand Research Report,* **318**.

Bensted, J. (1985). Application of the methylene blue test to cement raw materials. *Journal of Chemical Technology and Biotechnology*, **35A**, 181-184.

Brindley, G.W. and Brown, G., Eds. (1980). *Crystal structures of clay minerals and their x-ray identification.* Mineralogical Society, Monograph **5**. Mineralogical Society, London.

Brown, B.V., Hobbs, D.W., and Lavers, G.R. (1990). Aggregates for Concrete. In Pike, D.C. (ed.), *Standards for Aggregates* (p. 64-125). Ellis Harwood Ltd., Chichester, UK.

Cenens, J. and Schoonheydt, R.A. (1988). Visible spectroscopy of methylene blue on hectorite, laponite B, and brasym in aqueous suspension. *Clays and Clay Minerals*, **36**, 214-224.

Deng, Y., White, G.N., and Dixon, J.B. (2010). Soil mineralogy laboratory manual, 12th ed. *Published by the authors.* Department of Soil and Crop Sciences, Texas A&M University, College Station, Texas, 77843-2474.

Goldbeck, A.T. (1933). Nature and effect of surface coatings on coarse aggregates. *American Highways/Highway Research Board Proceedings*, **12**:**3**, p. 9-13. Transportation Research Board.

Grace Custom Aggregate Solutions, (2010). *Grace rapid clay test kit: step-by-step procedure,* **AGG-003A 02/11 SPN**. W.R. Grace & Co., Camridge, MA.

Hang, P.T. and Brindley, G.W. (1970). Methylene blue absorption by clay minerals. Determination of surface areas and cation exchange capacities (Clay-Organic Studies XVIII). *Clays and Clay Minerals*, **18**, 203-212.

Hayashi, et. al. (1969). Infrared study of sepiolite and palygorskite on heating. *American Mineralogist*, **53**, 1613-1624.

Hillier, S. (1999) Use of an air brush to spray dry samples for x-ray powder diffraction. *Clay Minerals*, **34**, 127-135.

Jenkins, R. and Snyder, R.L. (1996). Introduction to X-ray powder diffractometry. Chemical Analysis, Monograph **138**. Wiley, New York, 432 pp.

Katz, A. and Baum, H. (2006). Effect of high levels of fines content on concrete properties. *ACI Materials Journal*, **103**, 474-482.

Kleeburg, R. (2009). State-of-the-art and trends in quantitative phase analysis of geological and raw materials. *Zietcraft fur Kristallographie*, Supllemental **30**, 47-52.

Lang, F.C. (1931). Deleterious substances in concrete aggregates. *National Sand and Gravel Bulletin*, **12:4**, 17-20.

Lynch, F.L. (1997). Frio shale mineralogy and the stoichiometery of the smectite-to-illite reaction: the most important reaction in clastic sedimentary diagenesis. *Clays and Clay Minerals*, **45**, 618-631.

Moore, D.M. and Reynolds, R.C., Jr. (1989). *X-ray diffraction and identification and analysis of clay minerals*. Oxford University Press, New York, 332 pp.

Moore, I.C. and Gribble, C.D. (1980). The suitability of aggregates from weathered Peterhead granites. *Quarterly Journal of Engineering Geology and Hydrology*, **13**, 305-313.

Munoz, J.F. (2010). Effect of microfines associated with aggregates on concrete performance and microstructure (Doctoral dissertation). Retrieved from UMI (**3424257**).

Norvell, J.K., Stewart, J.G., Juenger, M.C.G, and Fowler, D.W. (2007). Influence of clays and clay-sized particles on concrete performance. *Journals of Materials in Civil Engineering*, **19**, 1053-1059.

Quiroga, P.N., Ahn, N., and Fowler, D.W. (2006). Concrete mixtures with high microfines. *ACI Materials Journal*, **103**, 258-264.

Reynolds, R.C., Jr. (1985). NEWMOD a computer program for the calculation of one-dimensional X-ray diffraction patterns of mixed-layered clays. Reynolds, R.C. Jr., 8 Brook Dr., Hanover, New Hampshire.

Righi, D., Petit, S., and Bouchet, A. (1993). Characterization of hydroxy-interlayered vermiculite and illite/smectite interstratified minerals from the weathering of chlorite in a cryothod. *Clays and Clay Minerals*, **41**, 484-495.

RTI Project Agreement (2009). *Treatments for clays in aggregates used to produce cement concrete, bituminous materials, and chip seals*. Texas Department of Transporation, **Project Number 0-6444**.

Schuster, R.L. (1957). *A review of research on deleterious substances in concrete aggregates: technical paper*. Publication FHWA/IN/JHRP-57/37. Joint Highway Research Project, Indiana Department of Transportation and Purdue University **No. C-26-42E**.

Srodon, J., Drits, V.A., McCarty, D.K., Hsieh, J.C.C., and Eberl, D.D. (2001). Quantitative x-ray diffraction analysis of clay-bearing rocks from random preparations. *Clays and Clay Minerals*, **49**, 514-528.

Stapel, E.E. and Verhoef, P.N.W. (1989). The use of the methylene blue adsorption test in assessing the quality of basaltic tuff rock aggregate. *Engineering Geology*, **26**, 233-246.

Walker, S. and Proudly, C.E. (1932). Shale in concrete aggregates. *Proceedings of the Highway Research Board* **12**, 273.

Young, R.A., Ed. (1993). *The Rietveld Method*. International Union of Crystallography Monograph **5**. Oxford University Press.

APPENDIX A

X-RAY DIFFRACTION PATTERNS OF AGGREGATE CLAYS

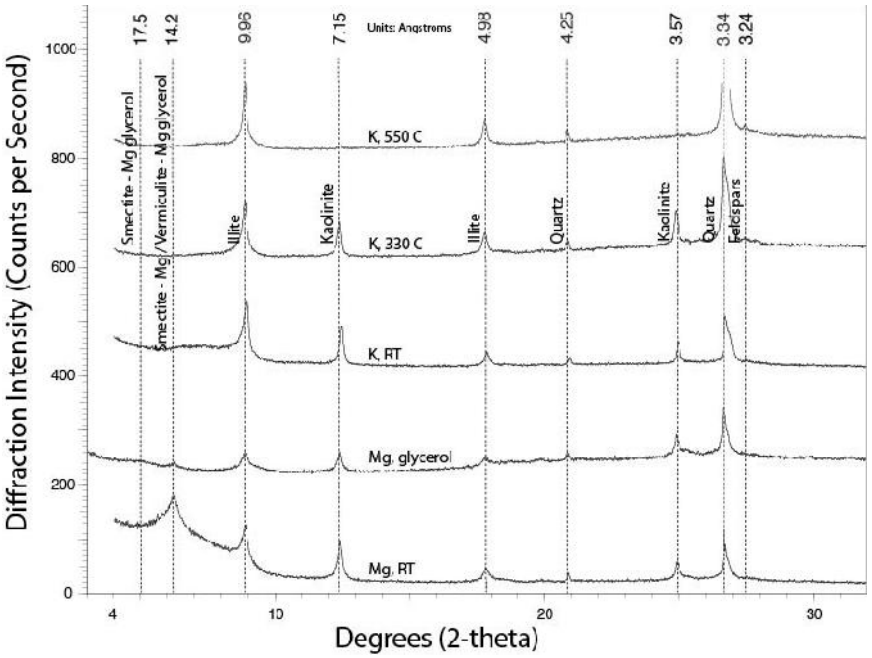

Fig. A.1. Pit 365 Coarse clay fraction mineral identification by X-ray diffraction analysis

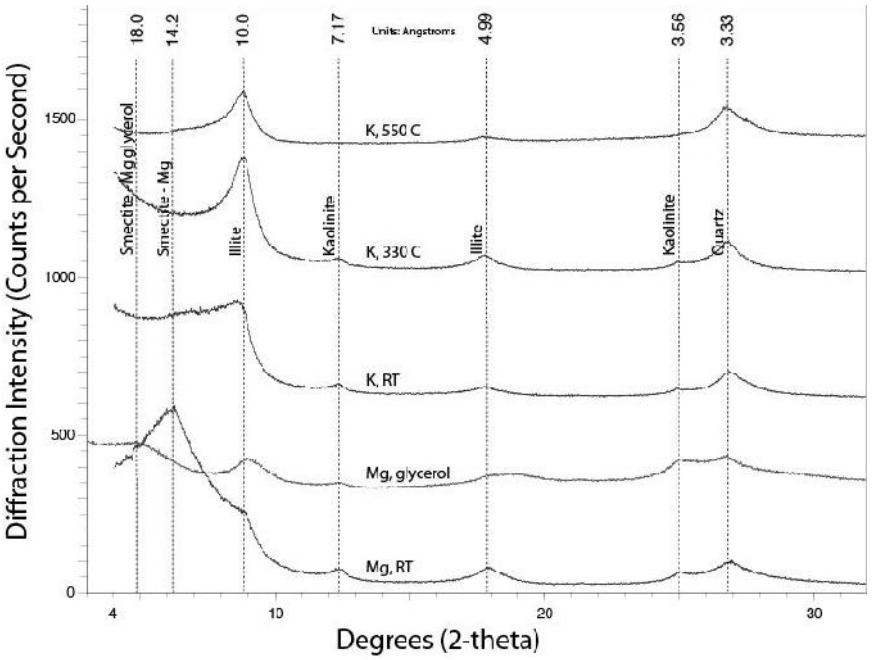

Fig. A.2. Pit 365 Fine clay fraction mineral identification by X-ray diffraction analysis

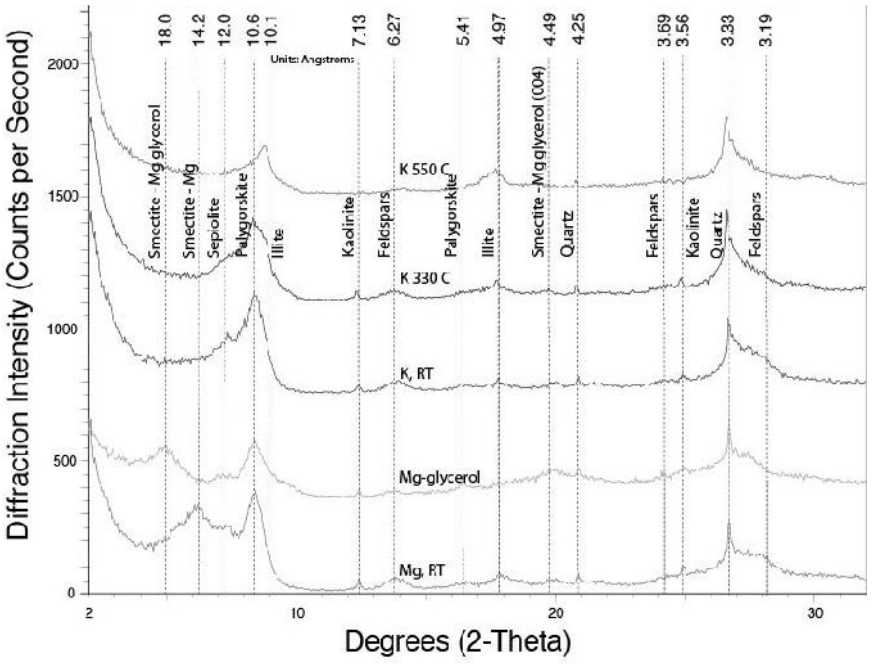

Fig. A.3. Armor clay fraction mineral identification by X-ray diffraction analysis

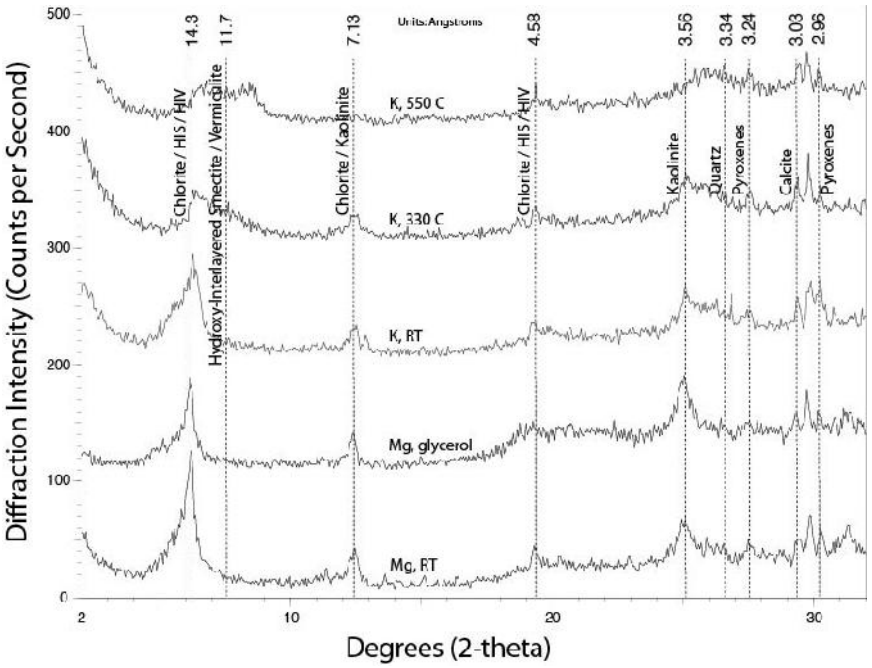

Fig. A.4. Bird Hill clay fraction mineral identification by X-ray diffraction analysis

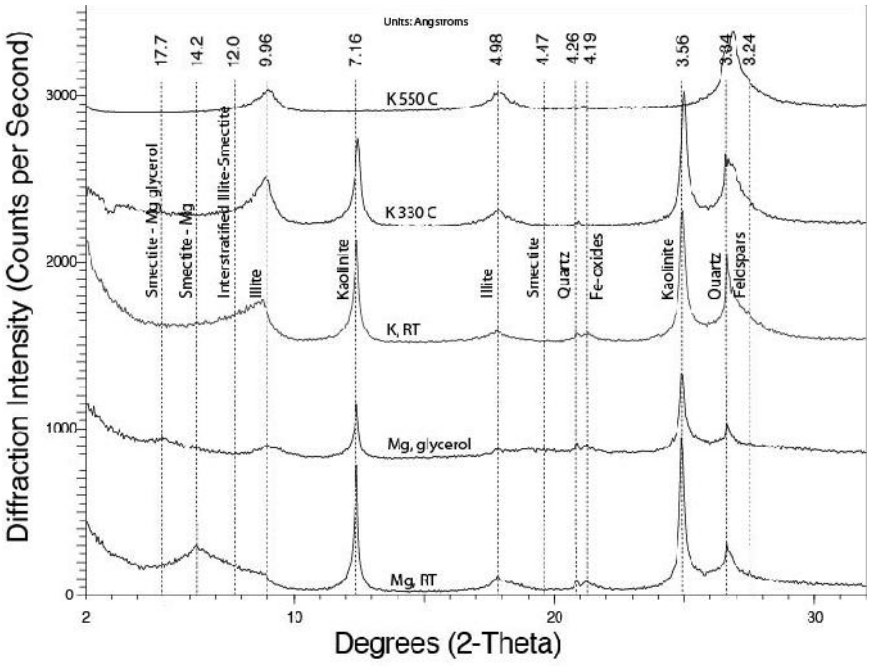

Fig. A.5. Black clay fraction mineral identification by X-ray diffraction analysis

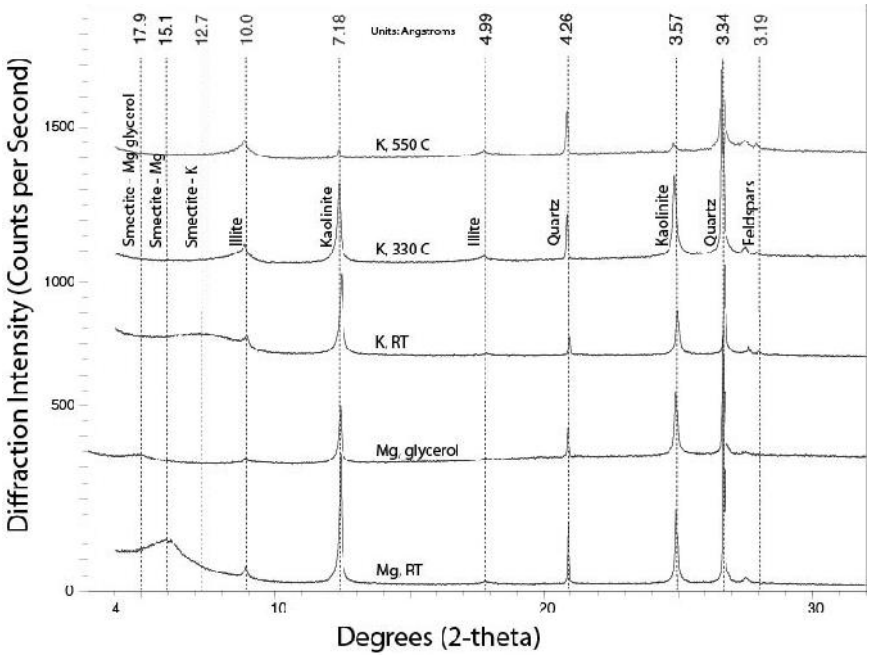

Fig. A.6. Blum Coarse clay fraction mineral identification by X-ray diffraction analysis

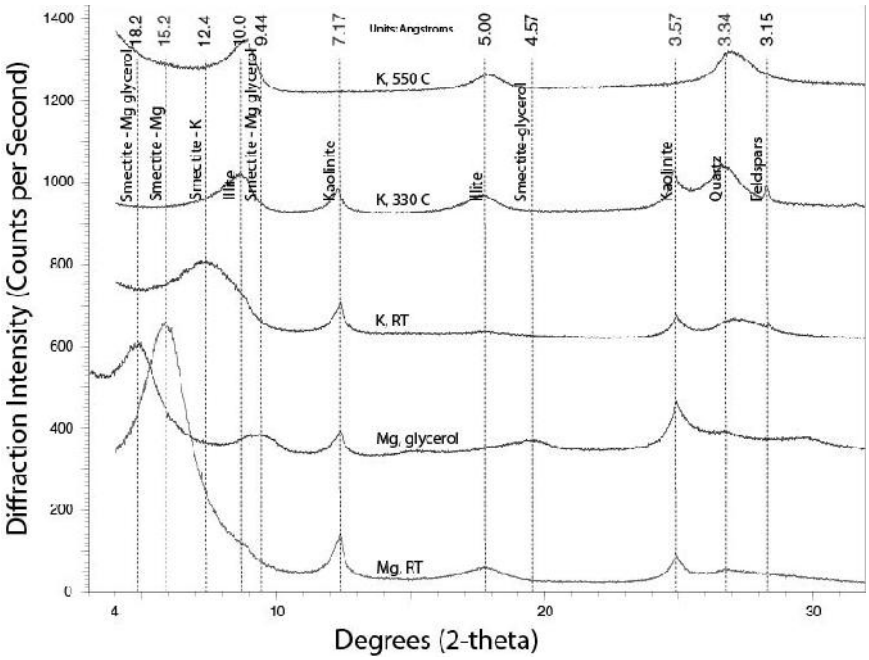

Fig. A.7. Blum Fine clay fraction mineral identification by X-ray diffraction analysis

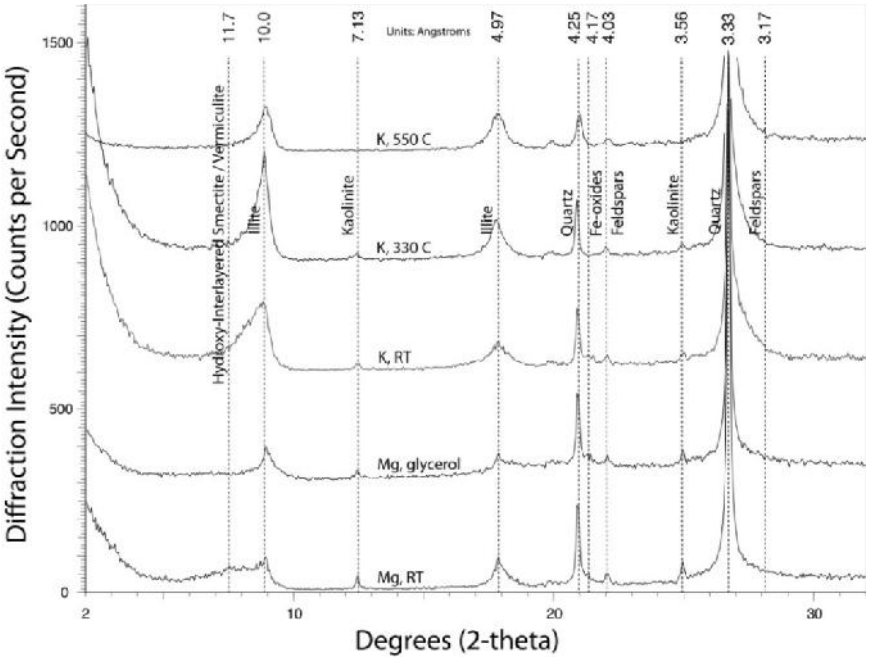

Fig. A.8. Cemex South clay fraction mineral identification by X-ray diffraction analysis

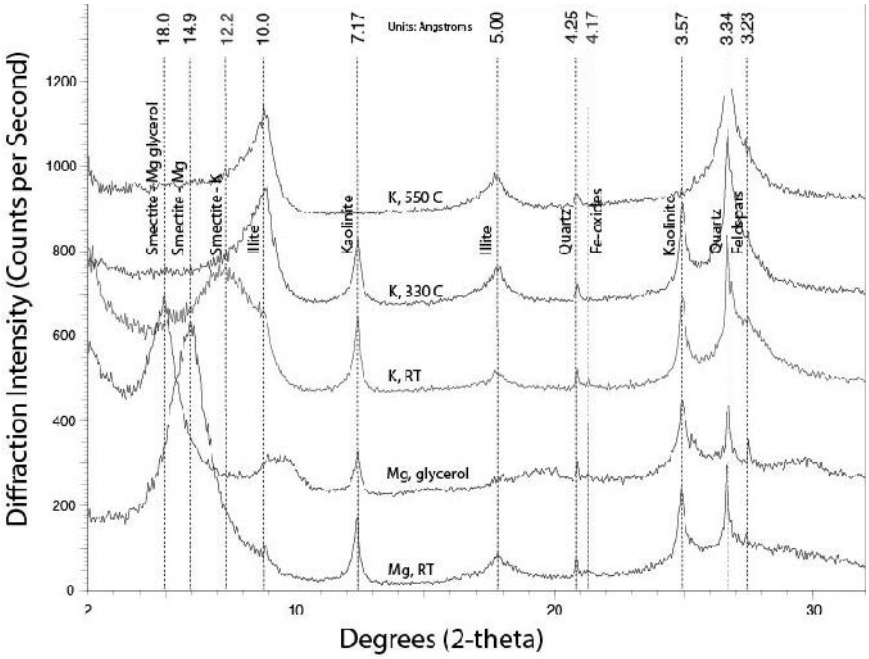

Fig. A.9. Fordyce Murphy clay fraction mineral identification by X-ray diffraction analysis

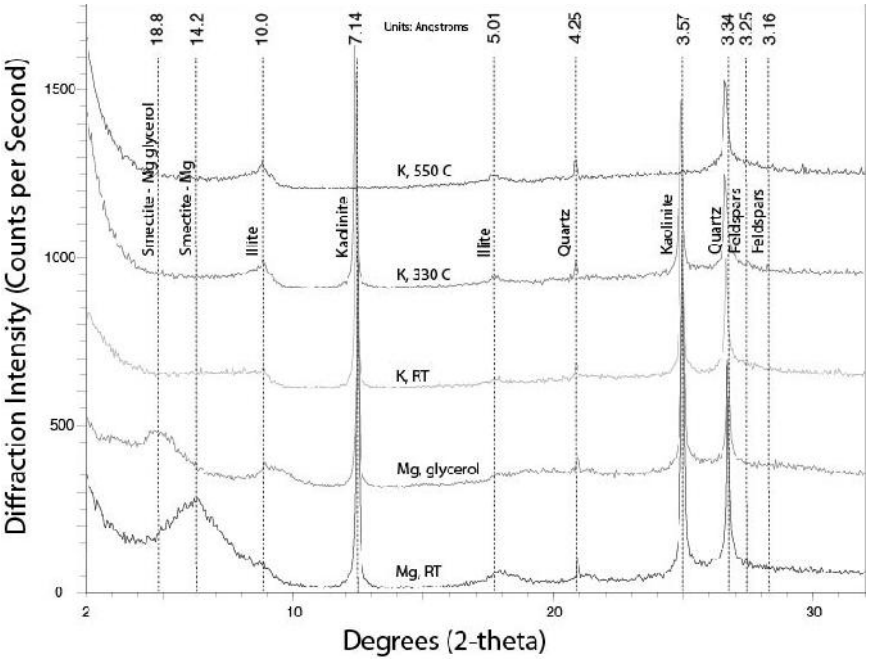

Fig. A.10. Helotes clay fraction mineral identification by X-ray diffraction analysis

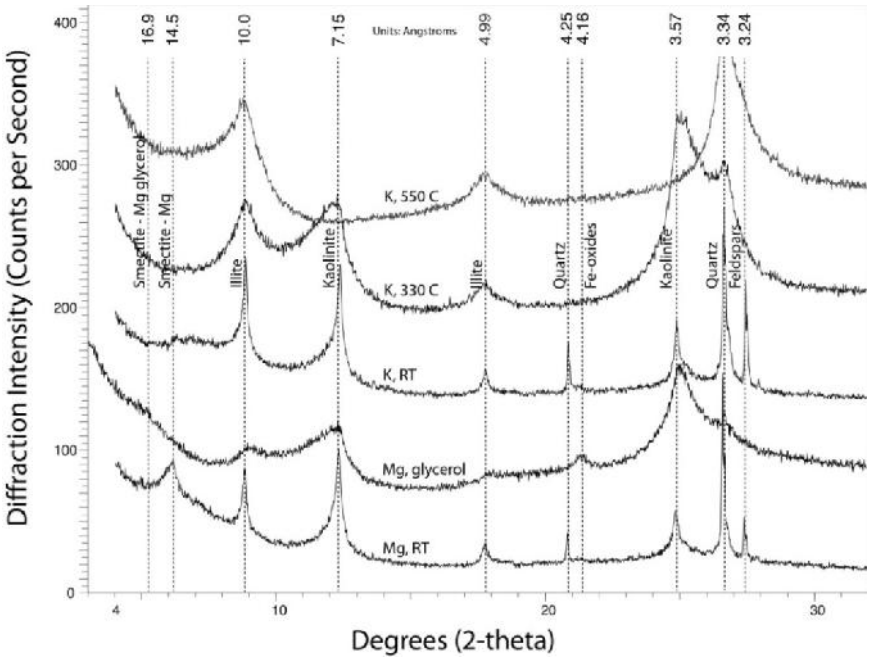

Fig. A.11. Hoot coarse clay fraction mineral identification by X-ray diffraction analysis

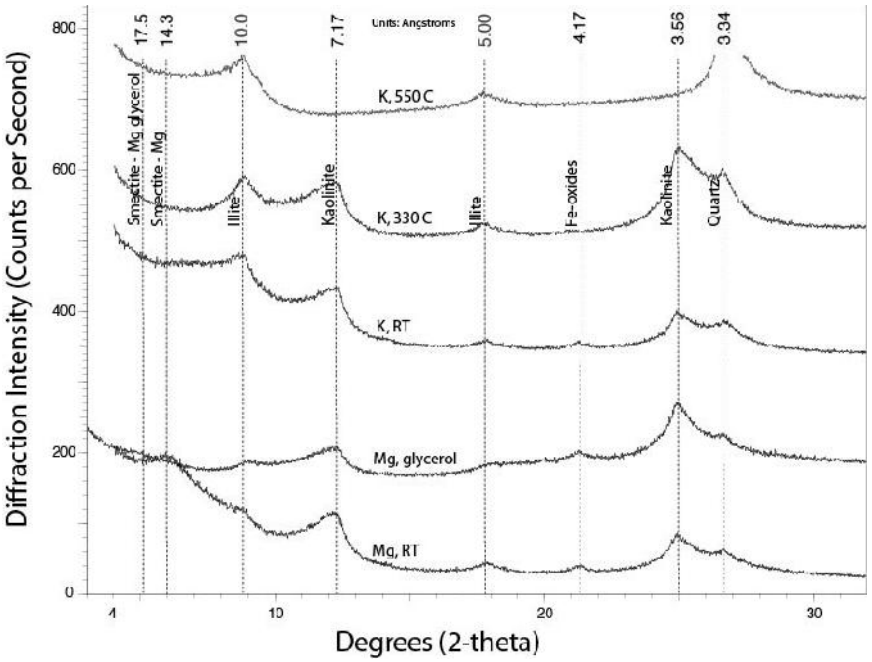

Fig. A.12. Hoot Fine clay fraction mineral identification by X-ray diffraction analysis

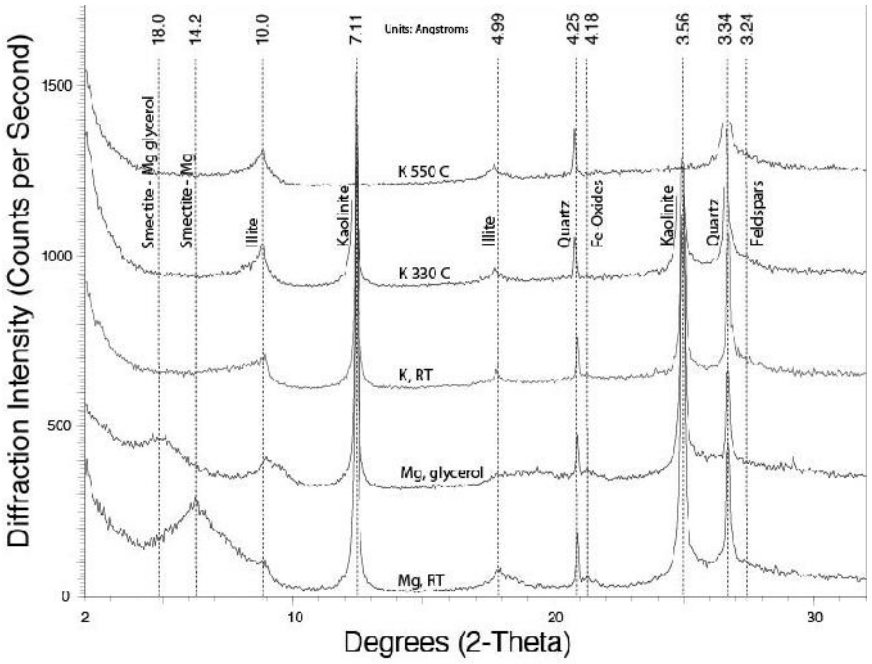

Fig. A.13. Huebner clay fraction mineral identification by X-ray diffraction analysis

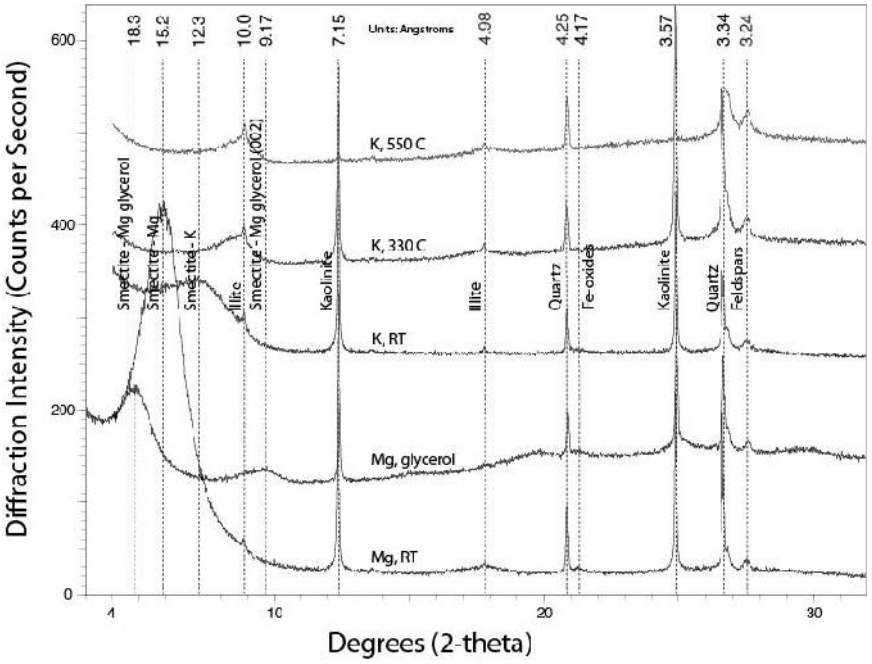

Fig. A.14. Jarrell 1 coarse clay fraction mineral identification by X-ray diffraction analysis

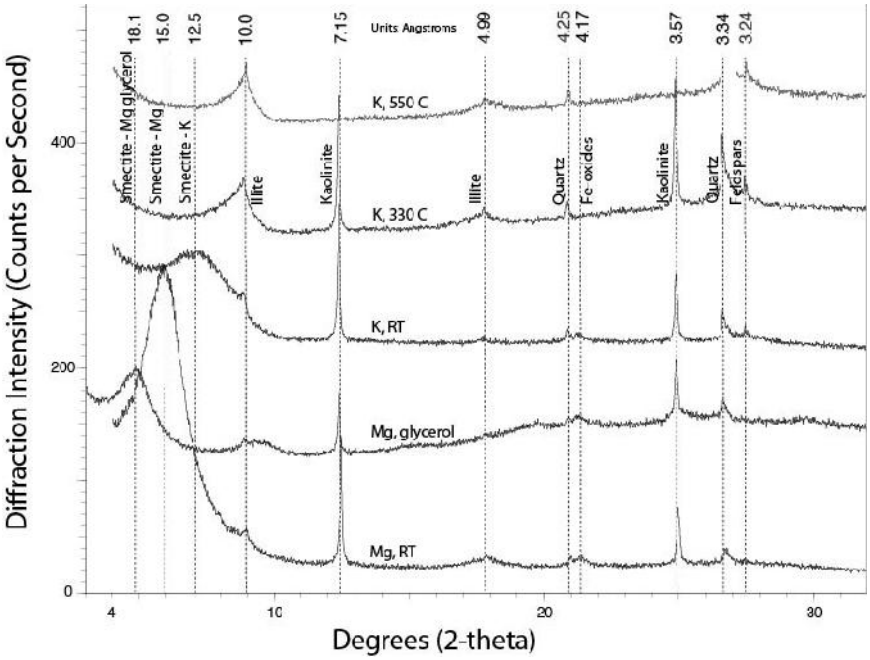

Fig. A.15. Jarrell 1 fine clay fraction mineral identification by X-ray diffraction analysis

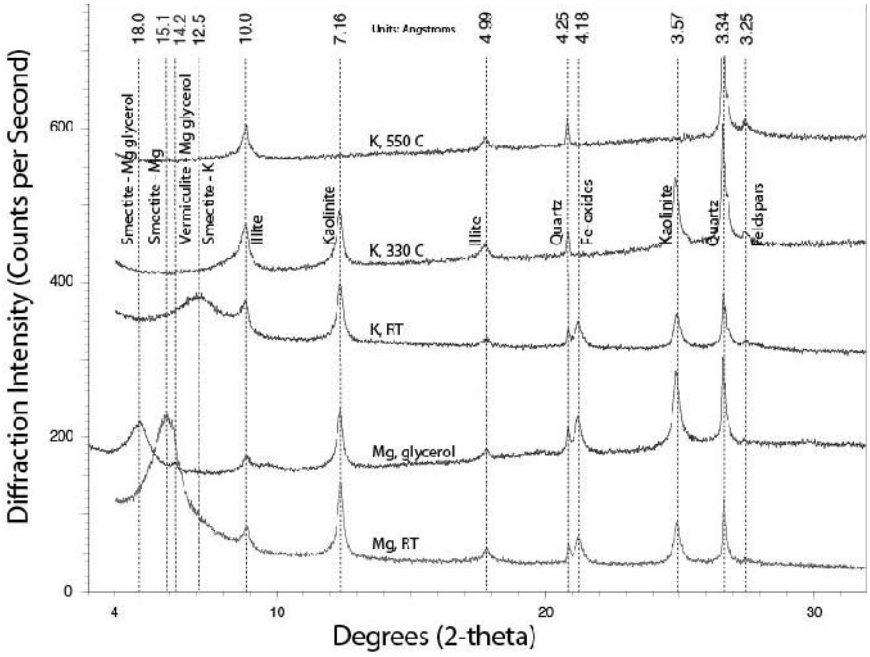

Fig. A.16. Jarrell 2 coarse clay fraction mineral identification by X-ray diffraction analysis

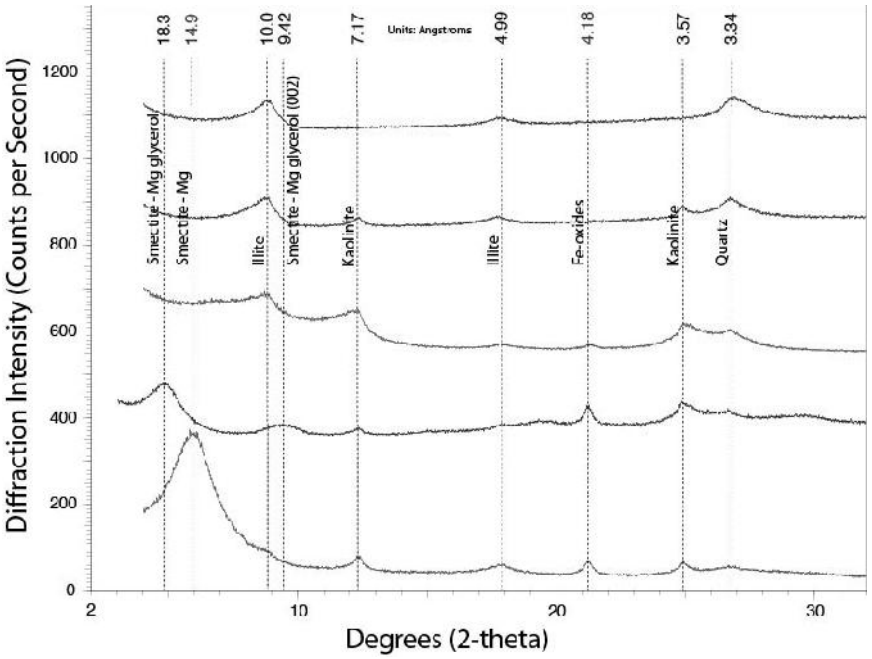

Fig. A.17. Jarrell 2 fine clay fraction mineral identification by X-ray diffraction analysis

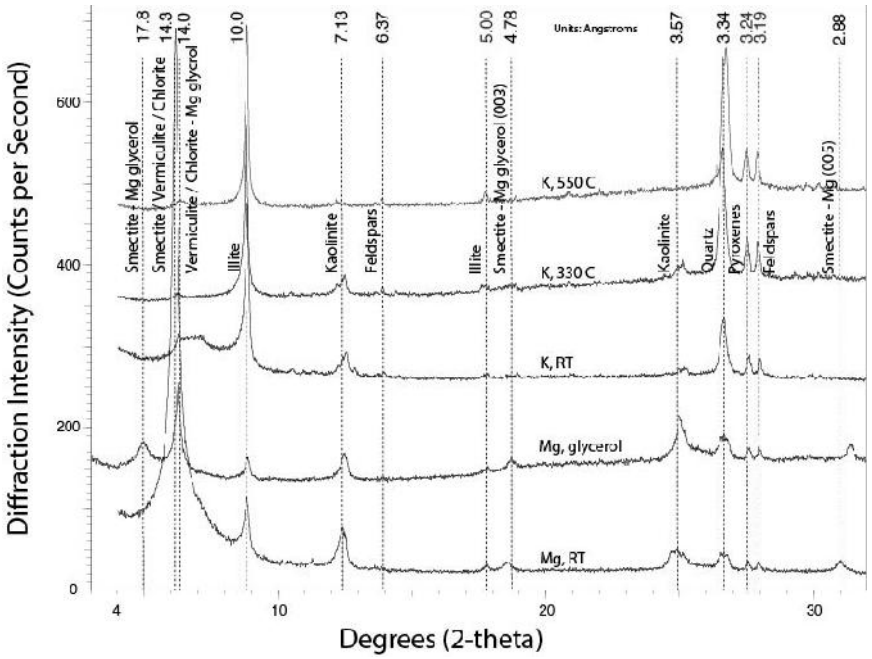

Fig. A.18. Jones Mill coarse clay fraction mineral identification by X-ray diffraction analysis

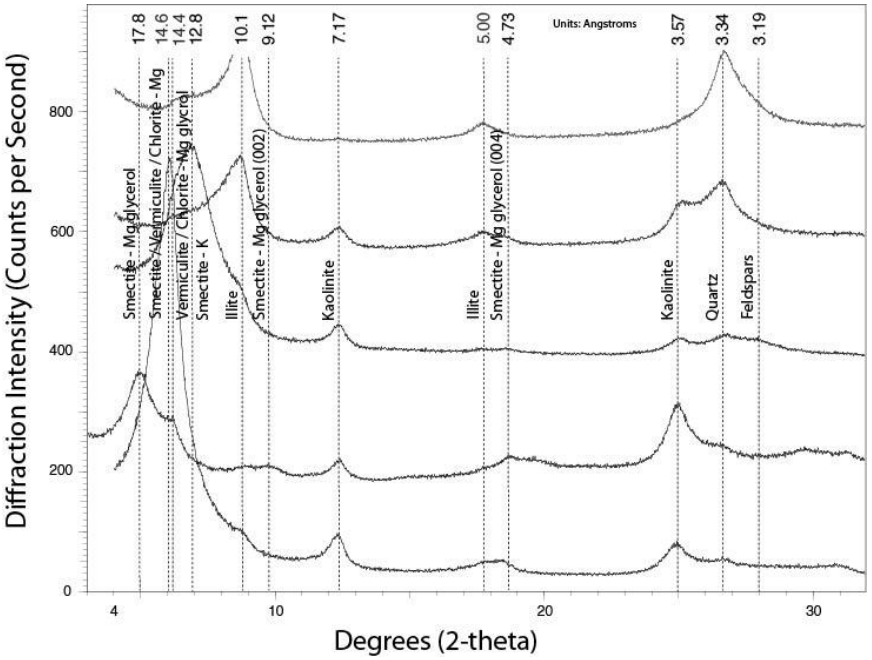

Fig. A.19. Jones Mill fine clay fraction mineral identification by X-ray diffraction analysis

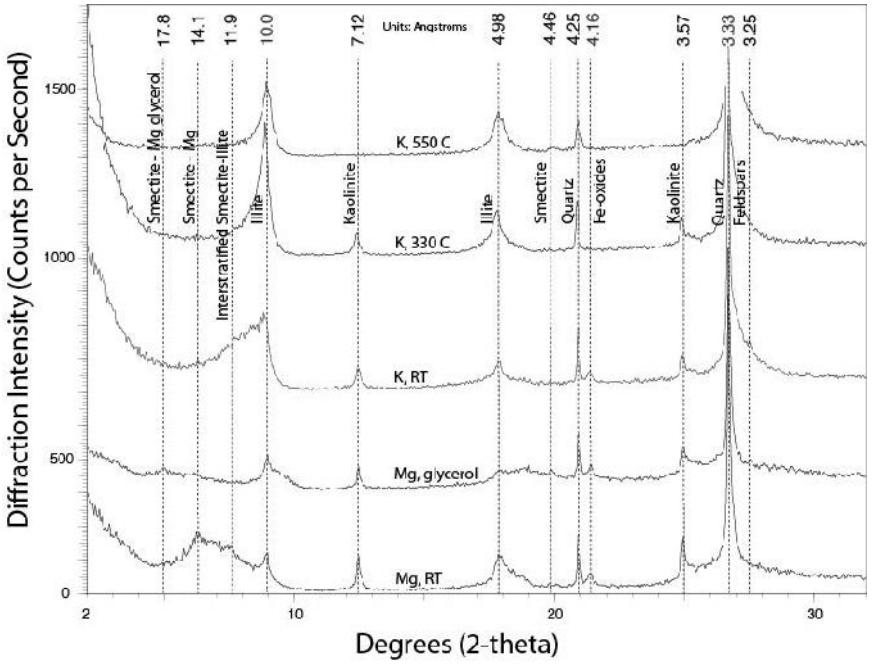

Fig. A.20. Lake Bridgeport clay fraction mineral identification by X-ray diffraction analysis

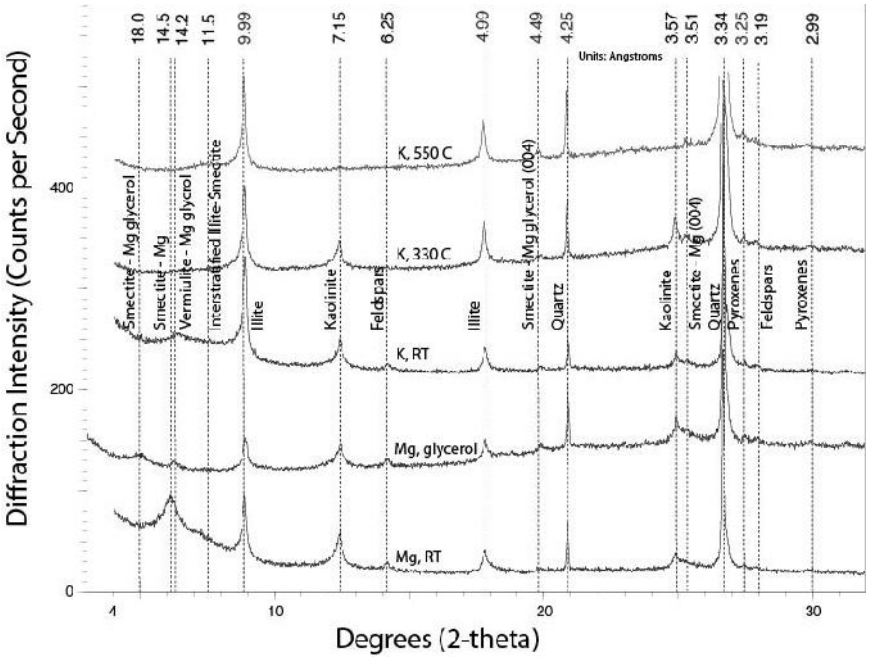

Fig. A.21. Little River coarse clay fraction mineral identification by X-ray diffraction analysis

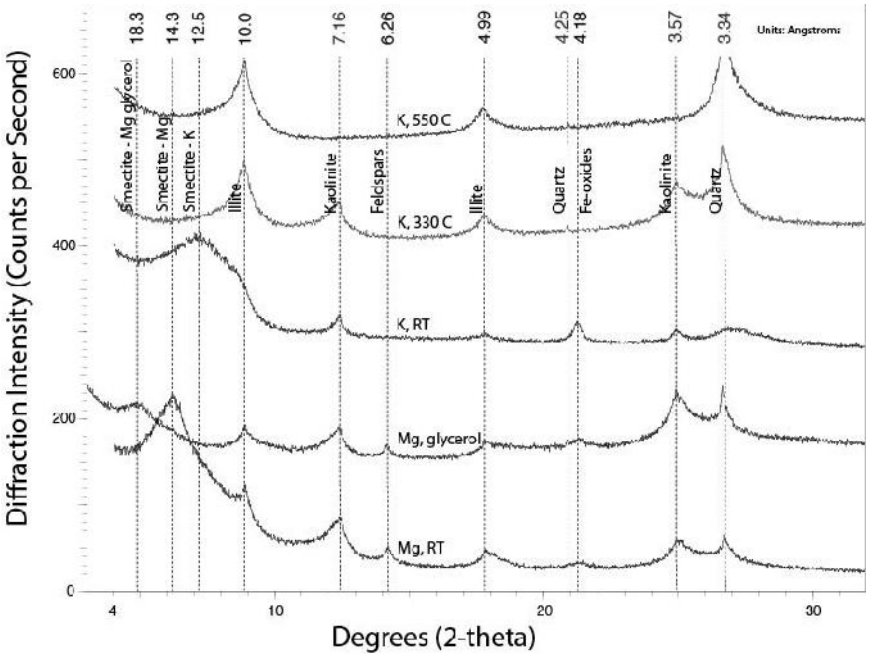

Fig. A.22. Little River fine clay fraction mineral identification by X-ray diffraction analysis

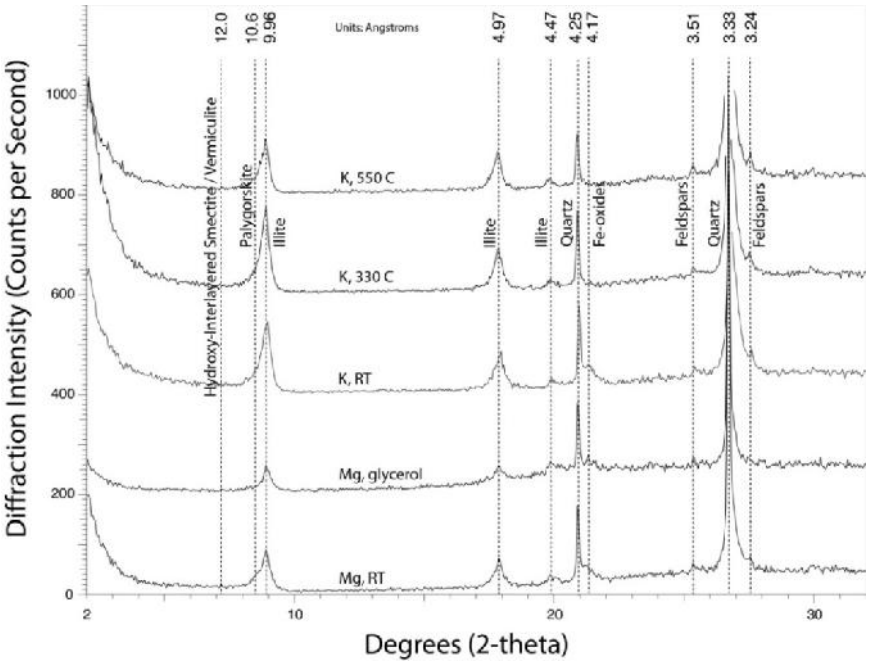

Fig. A.23. McKelligon Dolomite clay fraction mineral identification by X-ray diffraction analysis

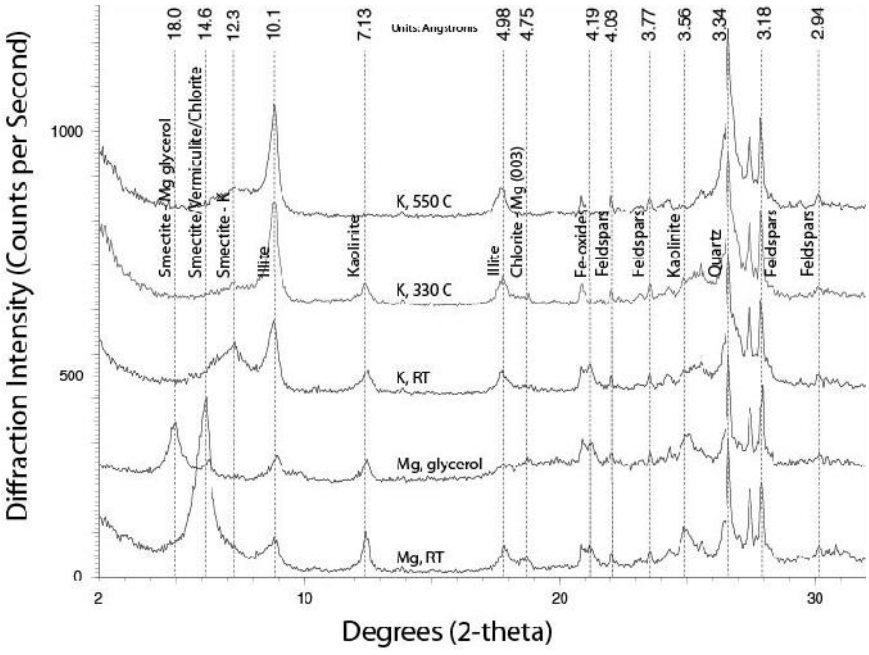

Fig. A.24. McKelligon Granite coarse clay fraction mineral identification by X-ray diffraction analysis

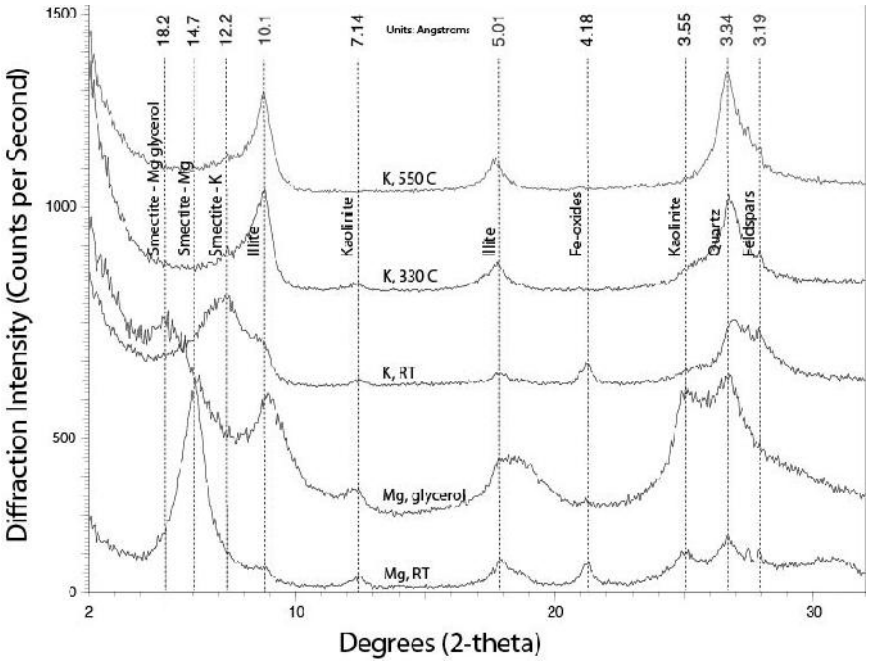

Fig. A.25. McKelligon Granite fine clay fraction mineral identification by X-ray diffraction analysis

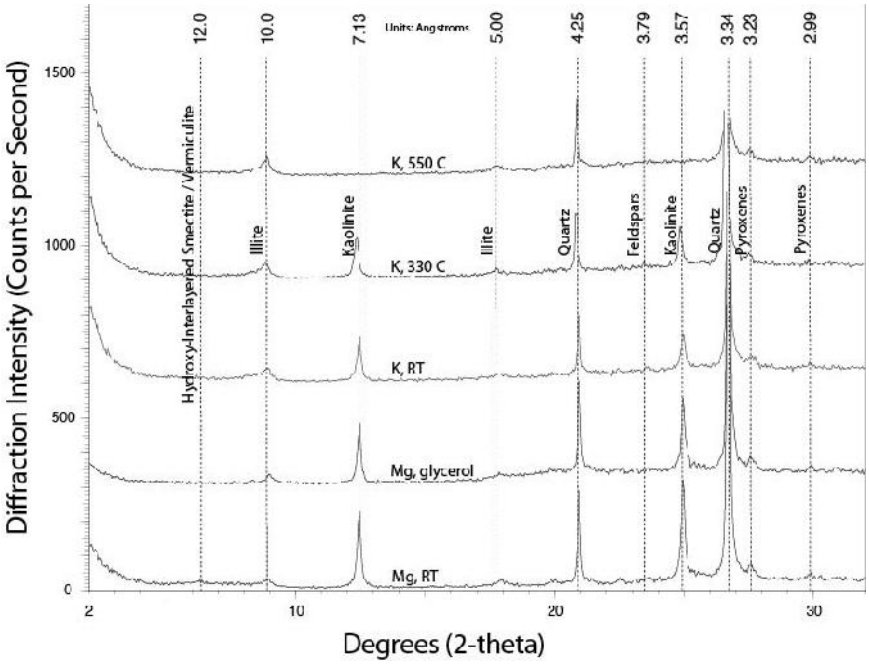

Fig. A.26. North Troy clay fraction mineral identification by X-ray diffraction analysis

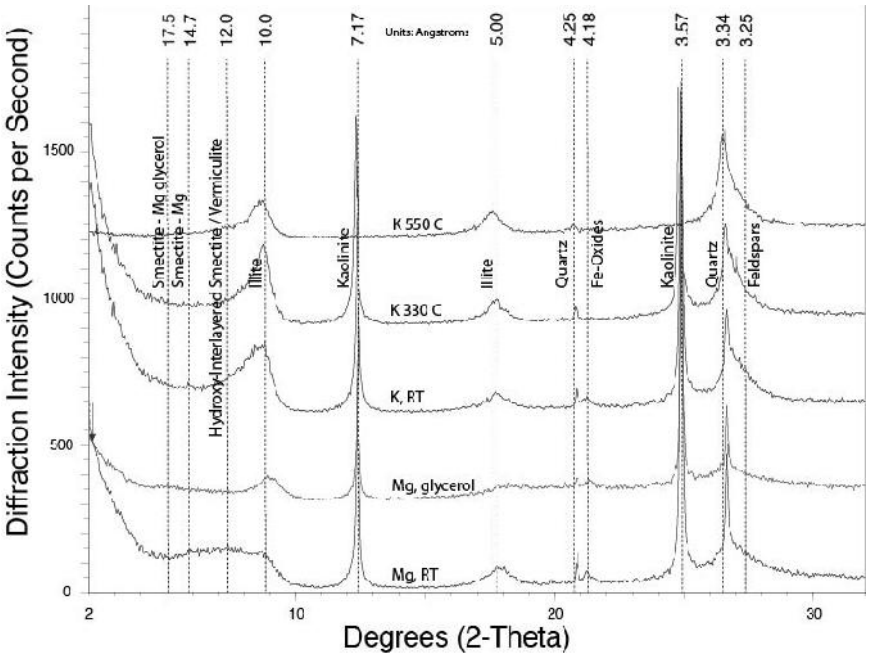

Fig. A.27. Rankin clay fraction mineral identification by X-ray diffraction analysis

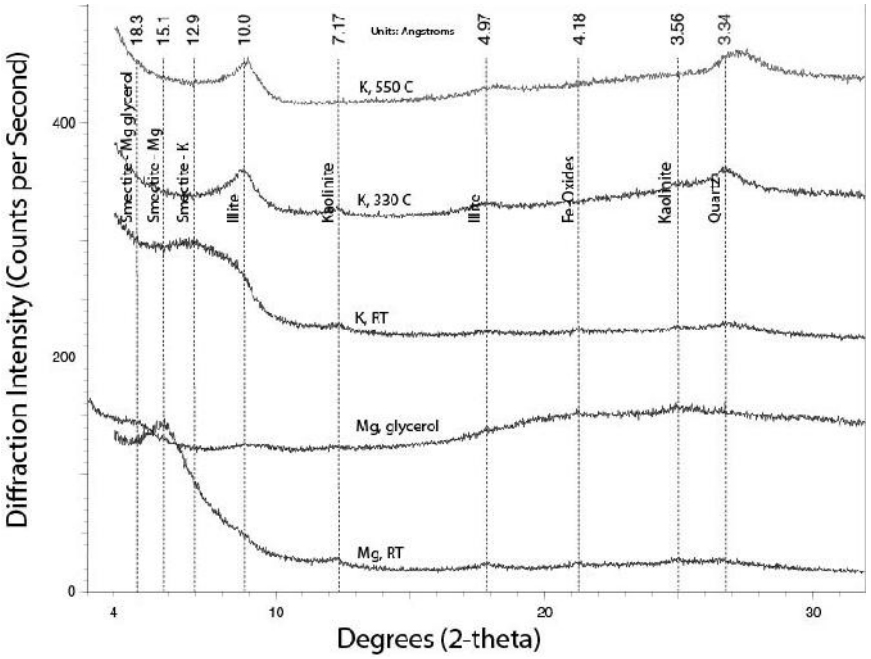

Fig. A.28. Scarmado coarse clay fraction mineral identification by X-ray diffraction analysis

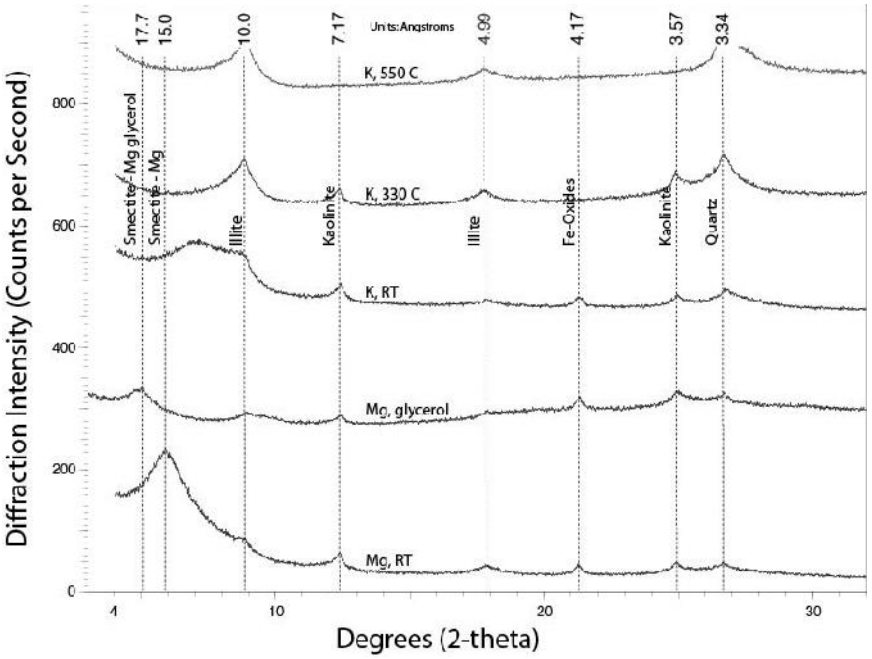

Fig. A.29. Scarmado fine clay fraction mineral identification by X-ray diffraction analysis

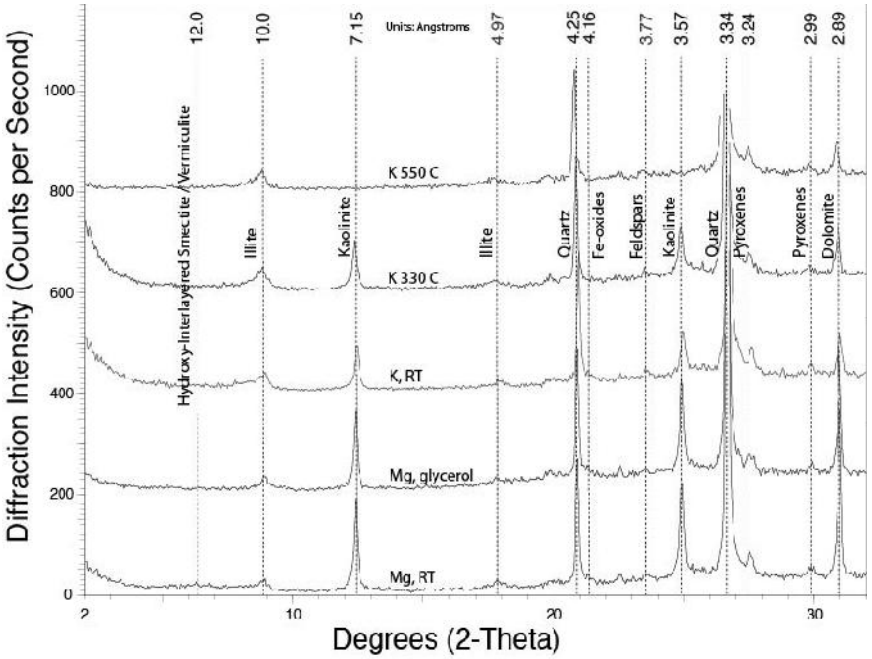

Fig. A.30. Smith Buster clay fraction mineral identification by X-ray diffraction analysis

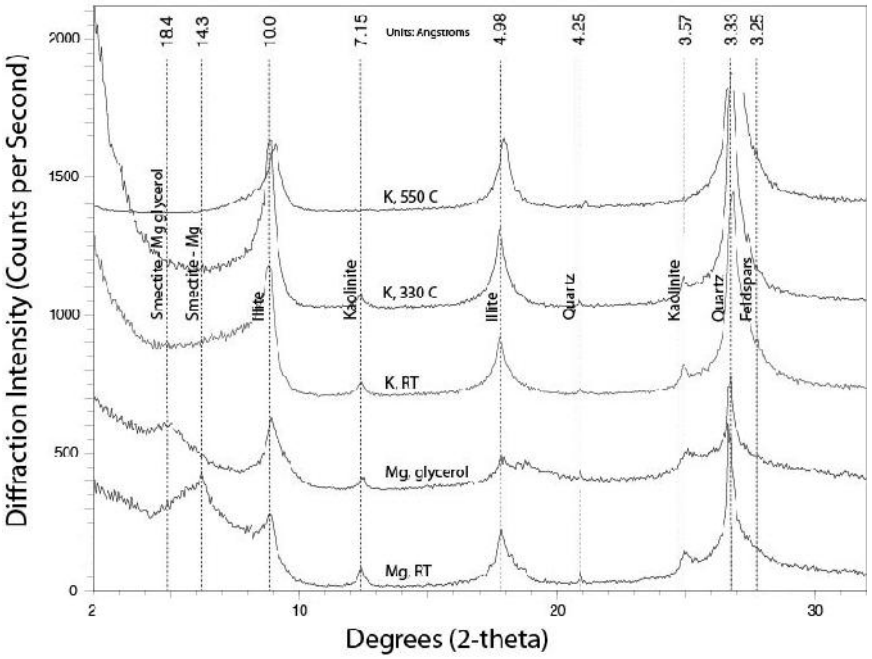

Fig. A.31. South Noodle clay fraction mineral identification by X-ray diffraction analysis

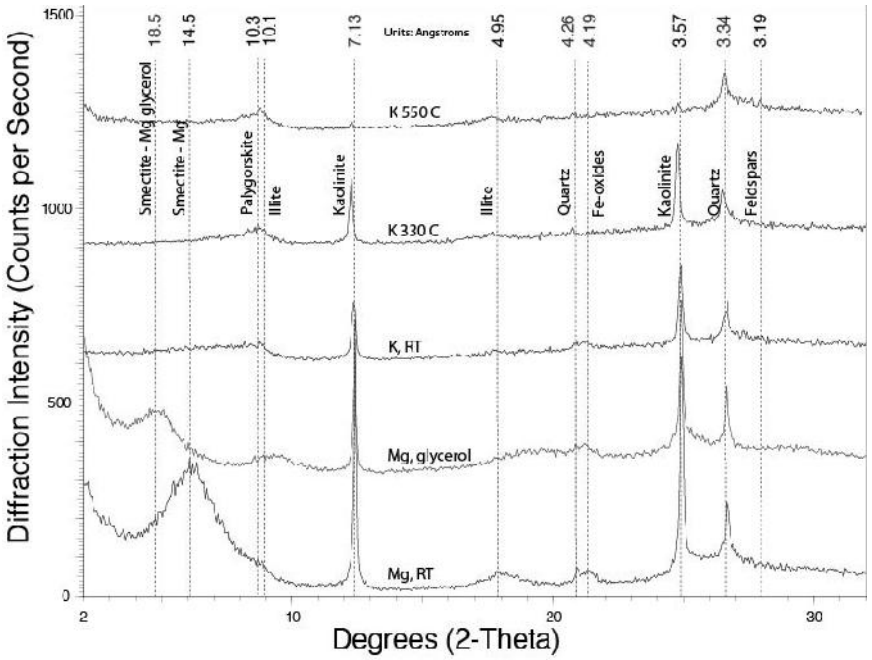

Fig. A.32. Texas Crushed Stone clay fraction mineral identification by X-ray diffraction analysis

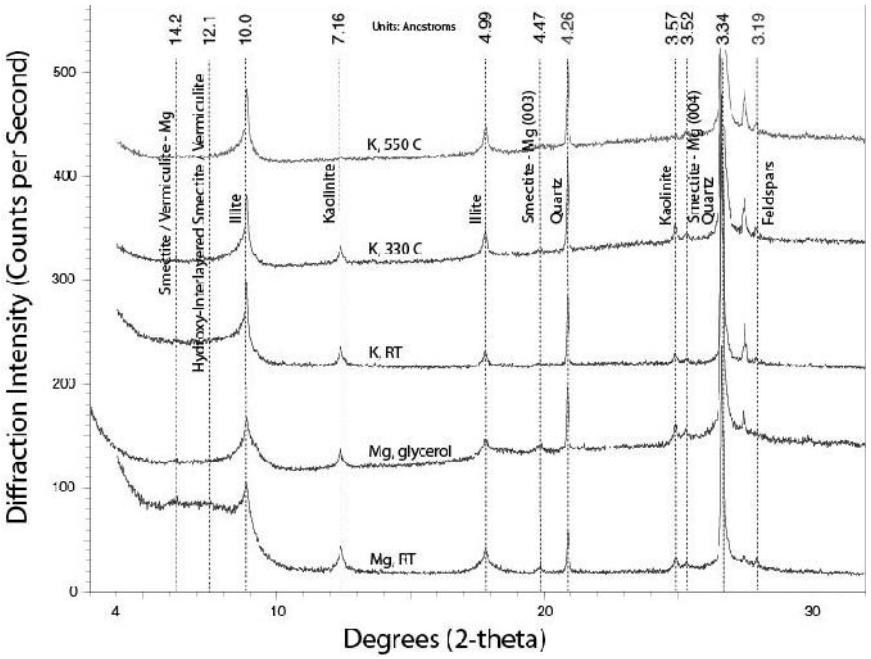

Fig. A.33. Tolar coarse clay fraction mineral identification by X-ray diffraction analysis

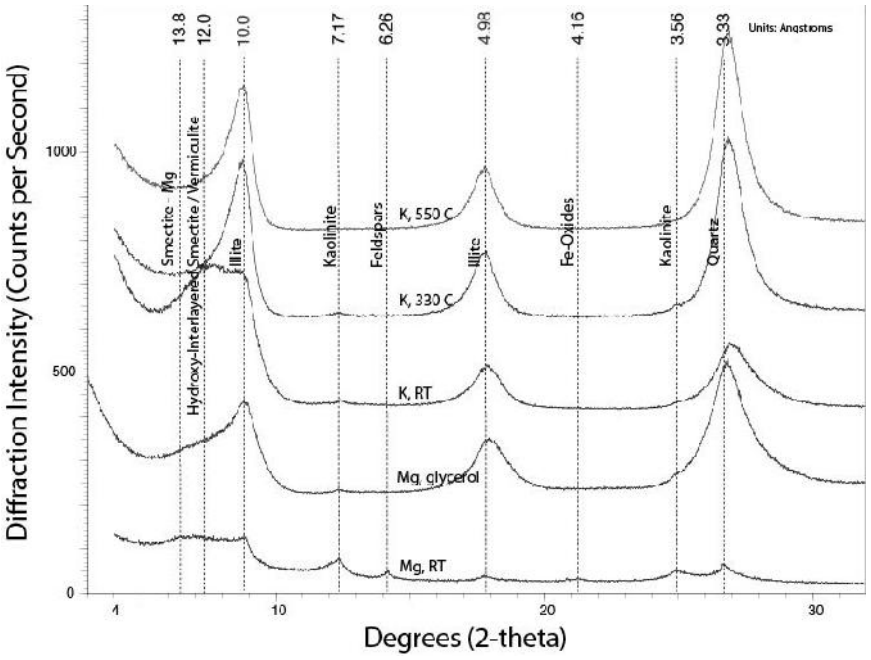

Fig. A.34. Tolar fine clay fraction mineral identification by X-ray diffraction analysis

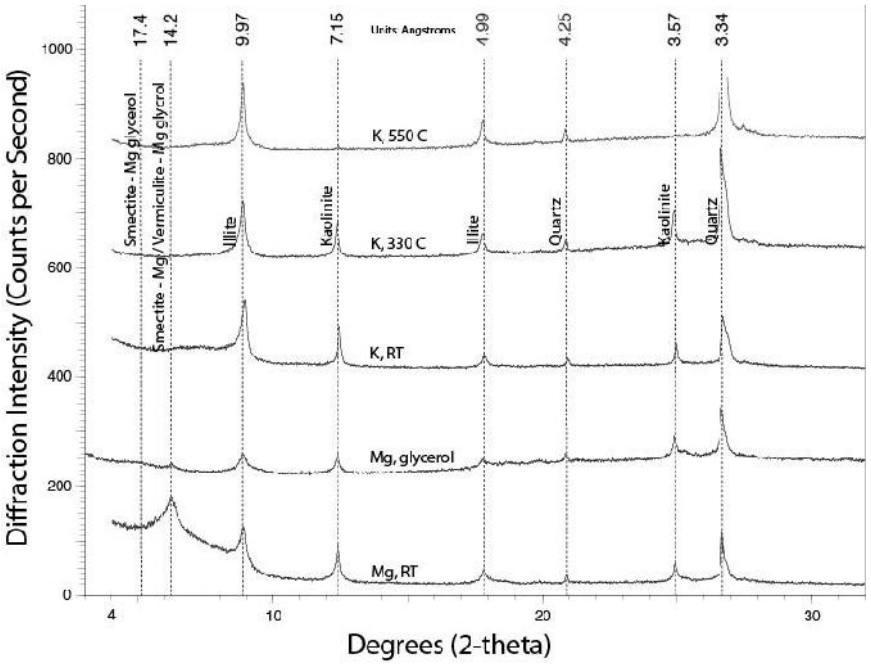

Fig. A.35. Whitney coarse clay fraction mineral identification by X-ray diffraction analysis

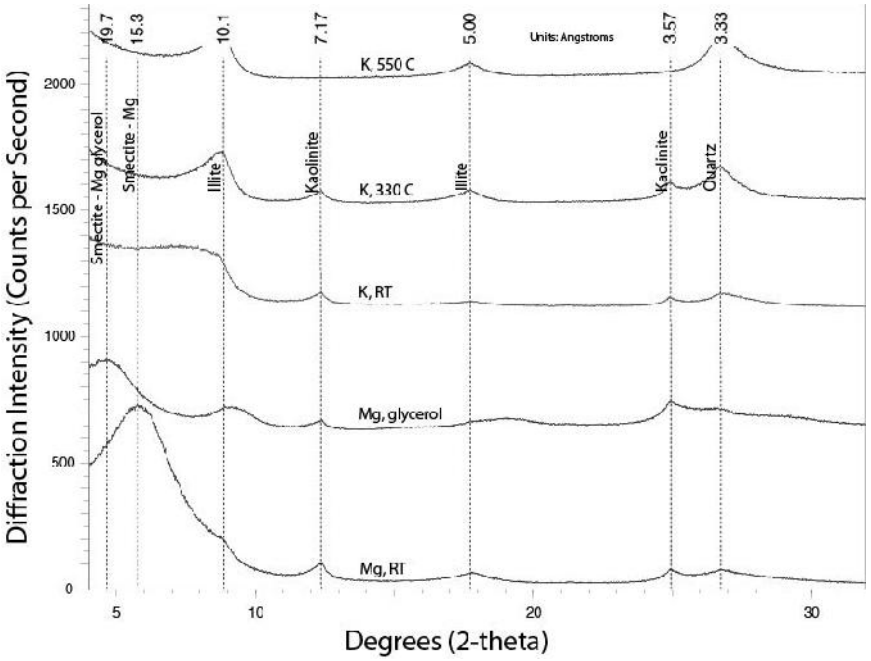

Fig. A.36. Whitney fine clay fraction mineral identification by X-ray diffraction analysis

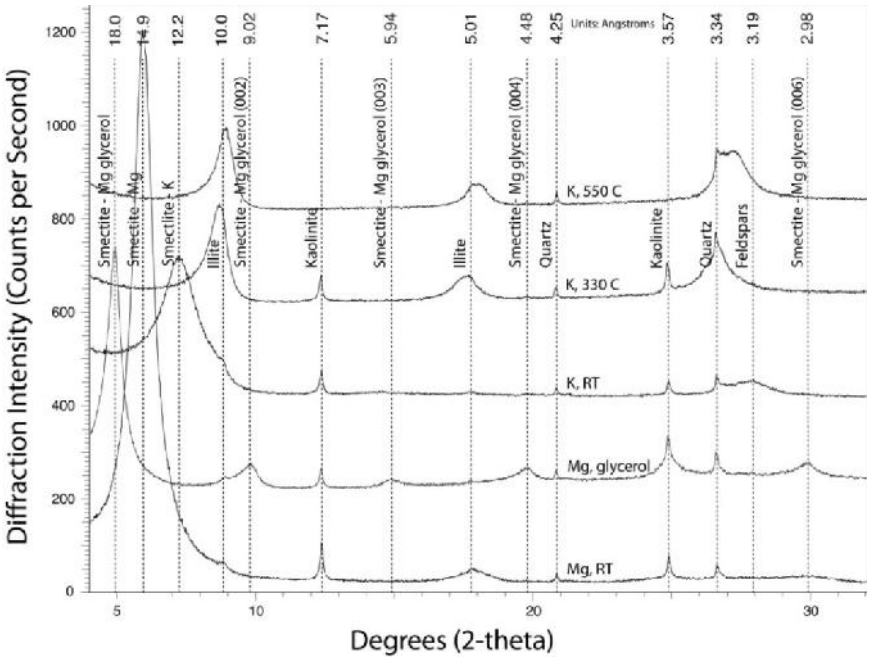

Fig. A.37. Woods coarse clay fraction mineral identification by X-ray diffraction analysis

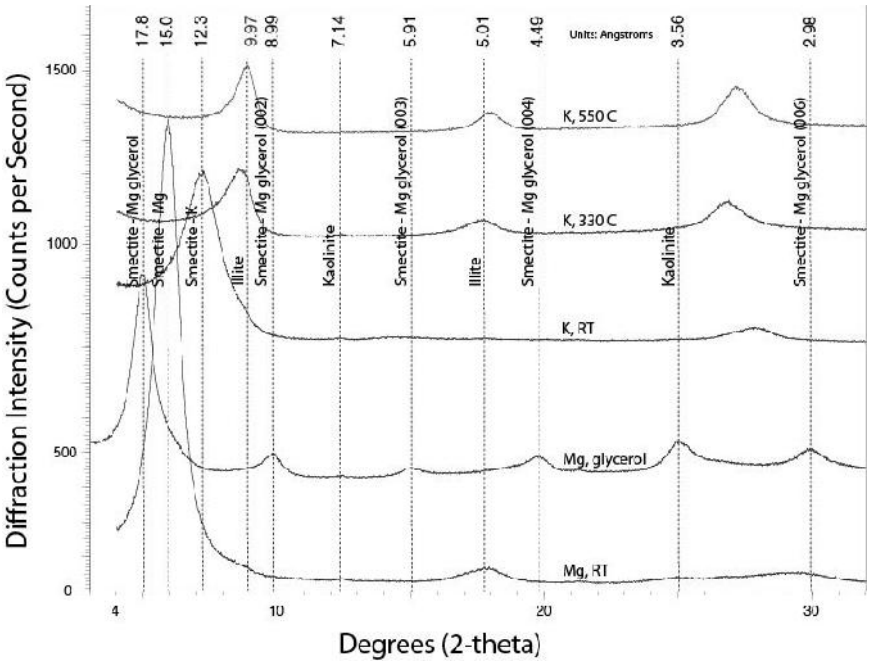

Fig. A.38. Woods fine clay fraction mineral identification by X-ray diffraction analysis

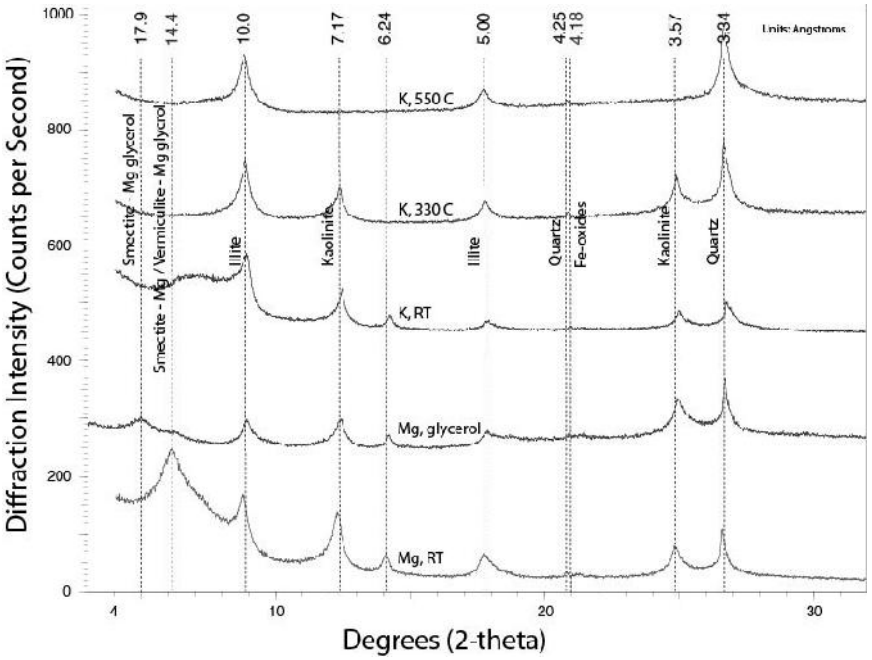

Fig. A.39. Yarrington coarse clay fraction mineral identification by X-ray diffraction analysis

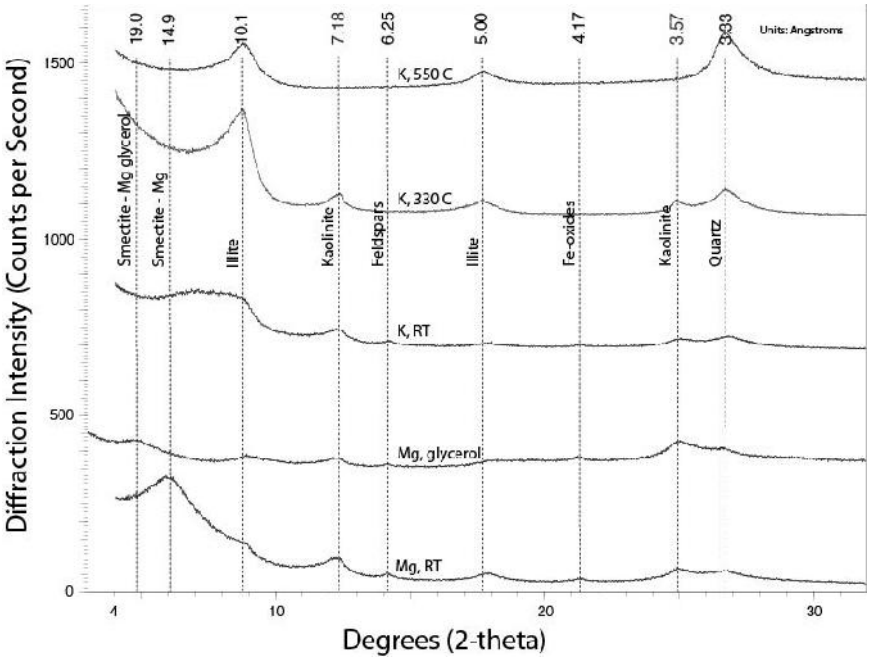

Fig. A.40. Yarrington fine clay fraction mineral identification by X-ray diffraction analysis

APPENDIX B

INFRARED ABSORPTION SPECTRA OF AGGREGATE CLAYS

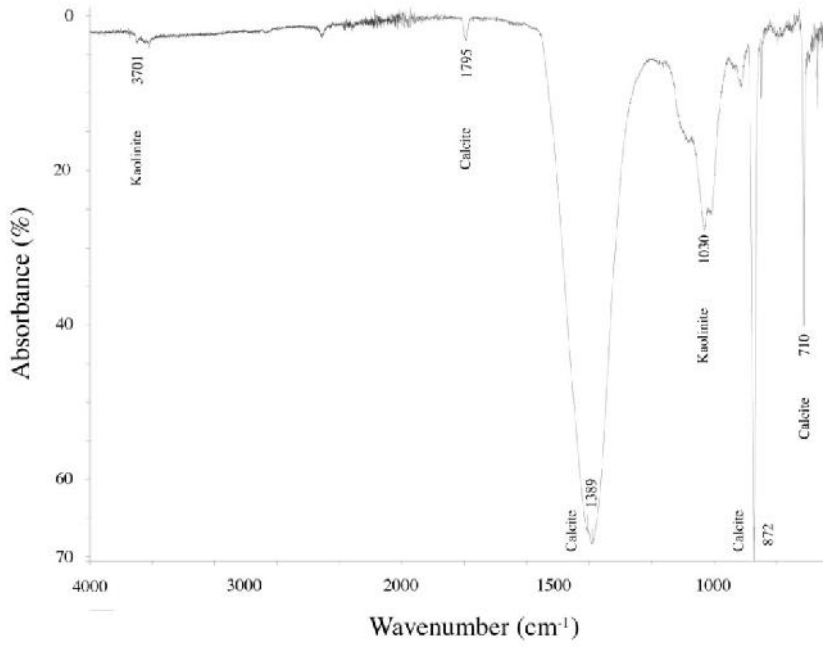

Fig. B.1. Blum clay infrared absorption spectrum (FTIR-ATR)

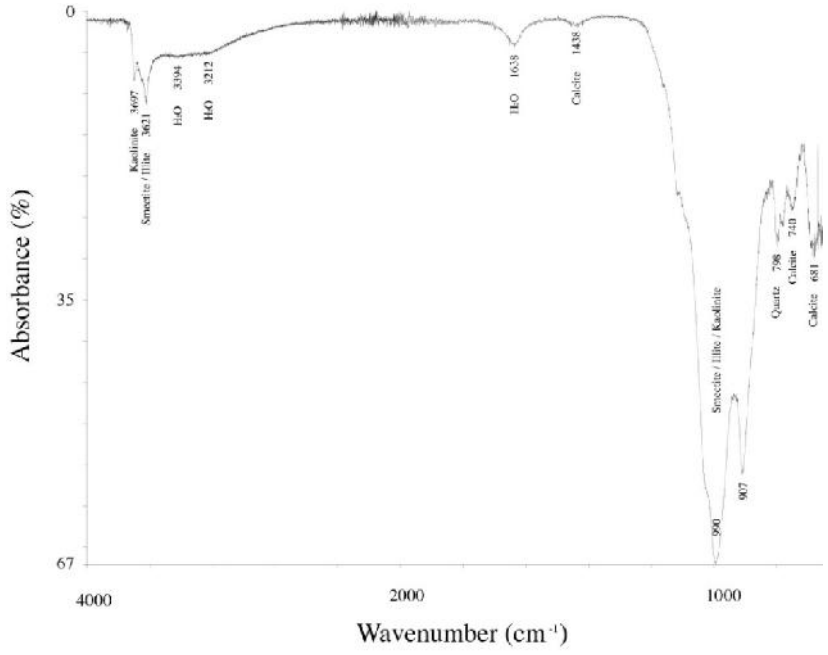

Fig. B.2. Hoot clay infrared absorption spectrum (FTIR-ATR)

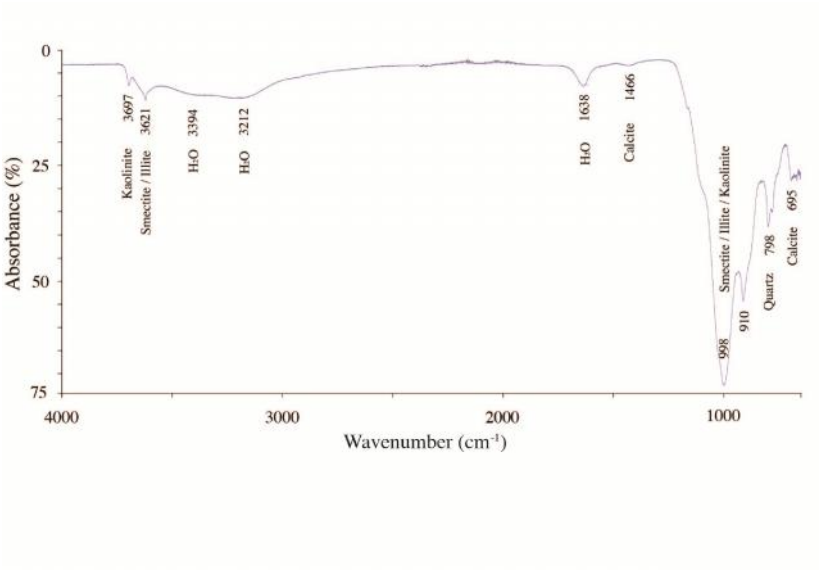

Fig. B.3. Jarrell 2 clay infrared absorption spectrum (FTIR-ATR)

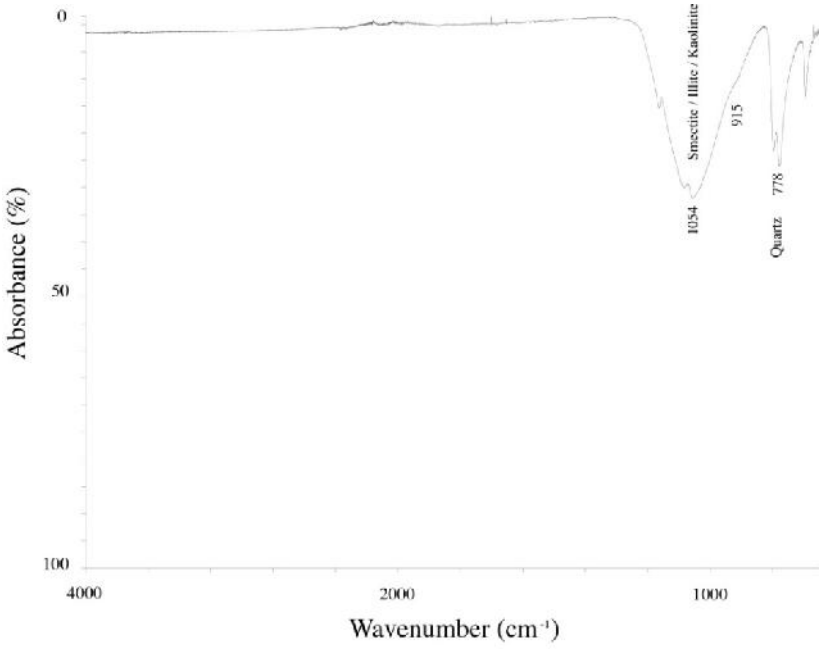

Fig. B.4. Little River clay infrared absorption spectrum (FTIR-ATR)

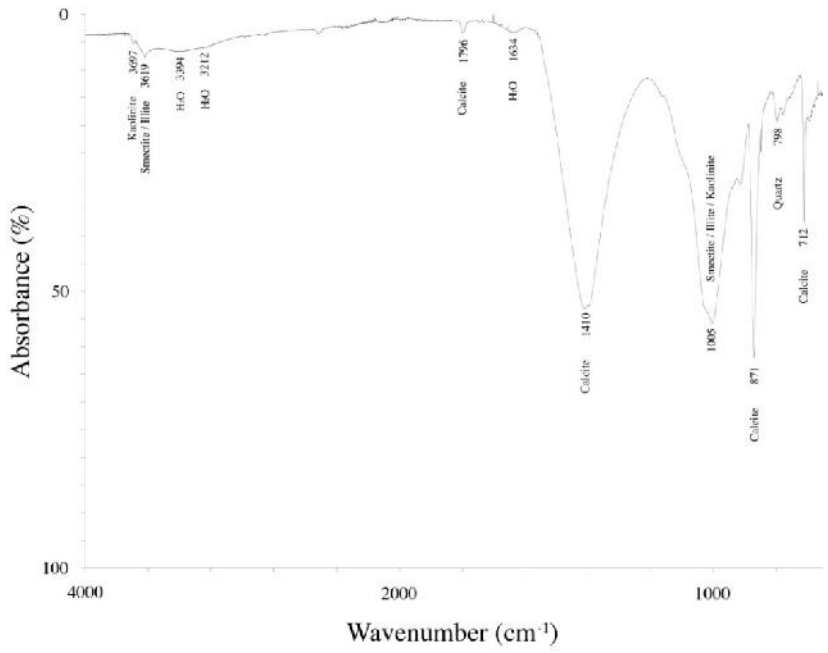

Fig. B.5. Pit 365 clay infrared absorption spectrum (FTIR-ATR)

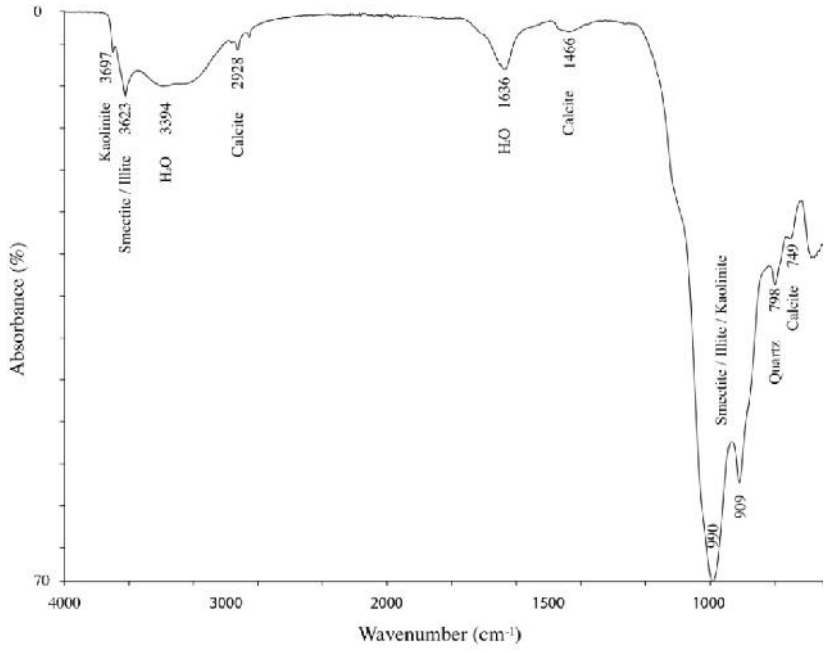

Fig. B.6. Scarmado clay infrared absorption spectrum (FTIR-ATR)

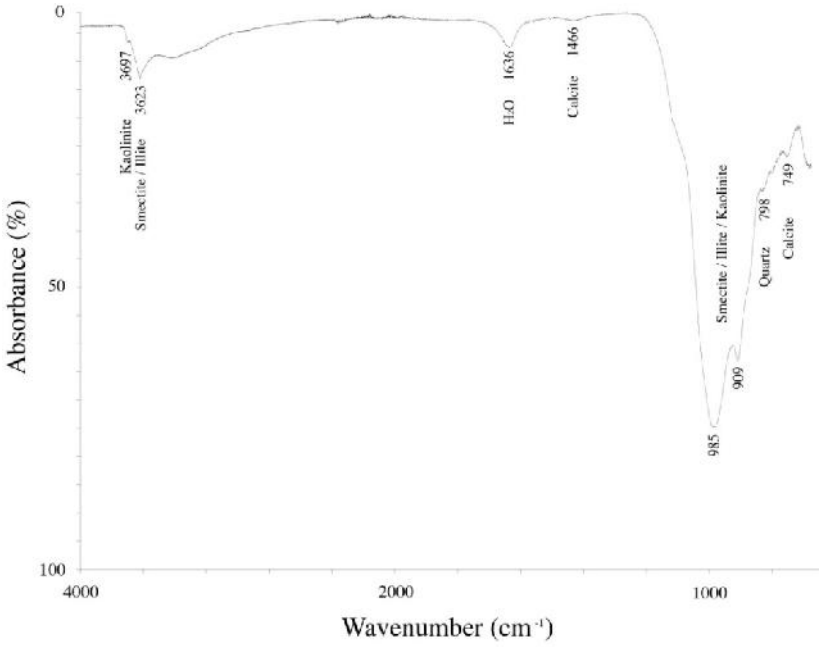

Fig. B.7. Whitney clay infrared absorption spectrum (FTIR-ATR)

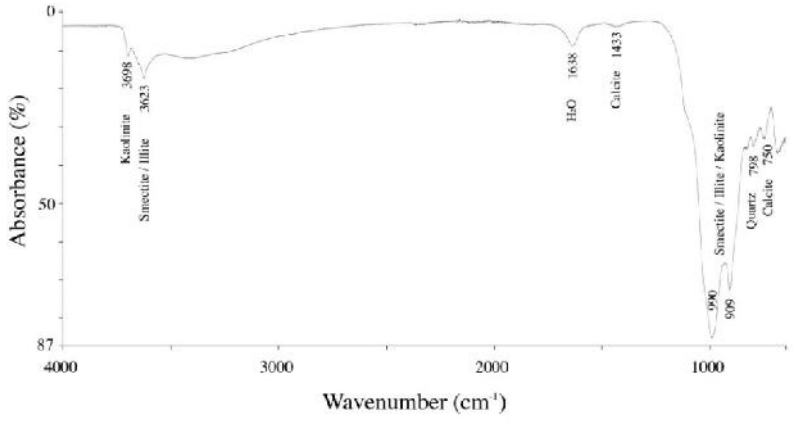

Fig. B.8. Yarrington clay infrared absorption spectrum (FTIR-ATR)

APPENDIX C

ELECTRON MICROGRAPHS

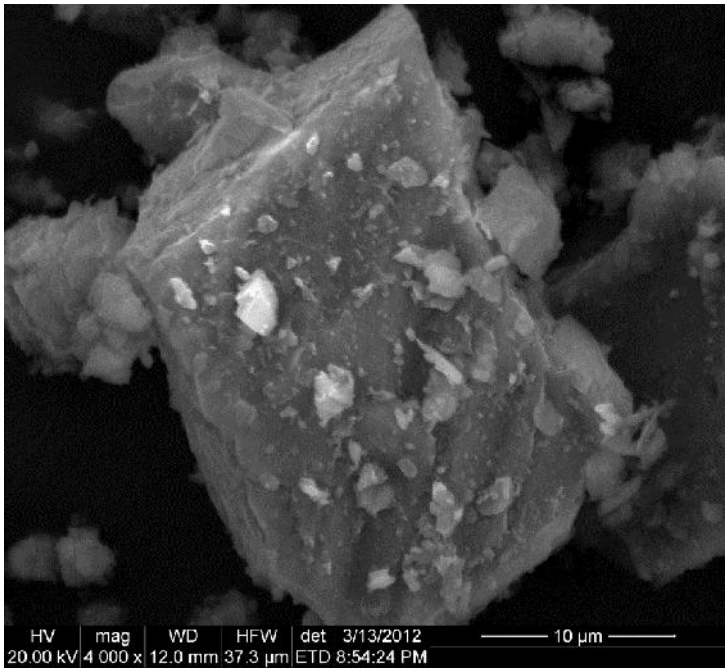

Fig. C.1. McKelligon Granite (SEM) - calcite particle with clay coatings

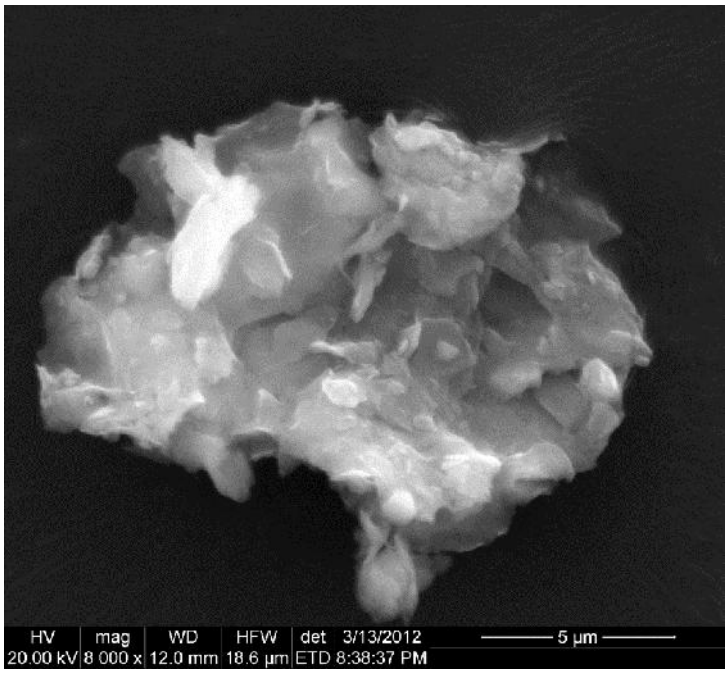

Fig. C.2. Whitney siliceous and limestone gravel (SEM) - aggregatation of clay particles

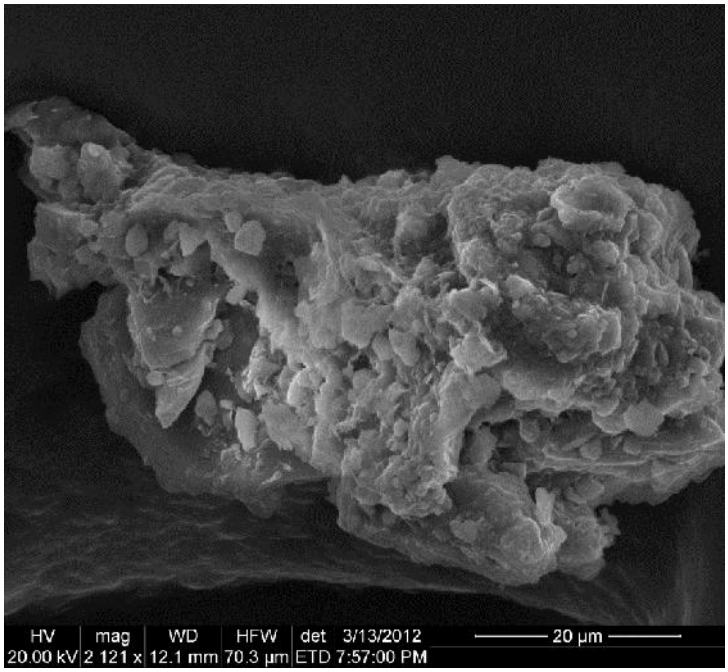

Fig. C.3. Woods smectite -rich river gravel (SEM) – clay particle coatings on calcite

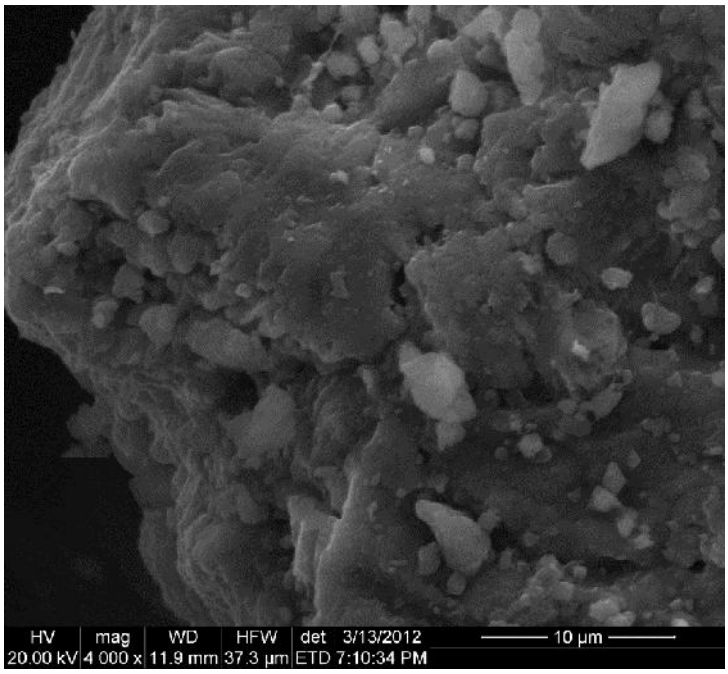

Fig. C.4. Yarrington smectite-rich crushed limestone (SEM) – clay particle coatings on calcite

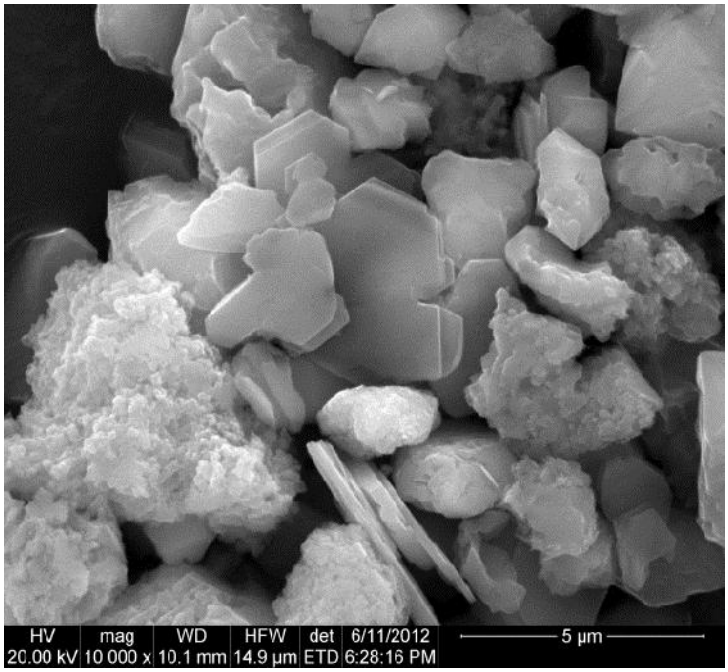

Fig. C.5. Helotes crushed limestone (SEM) – hexagonal kaolinite crystals

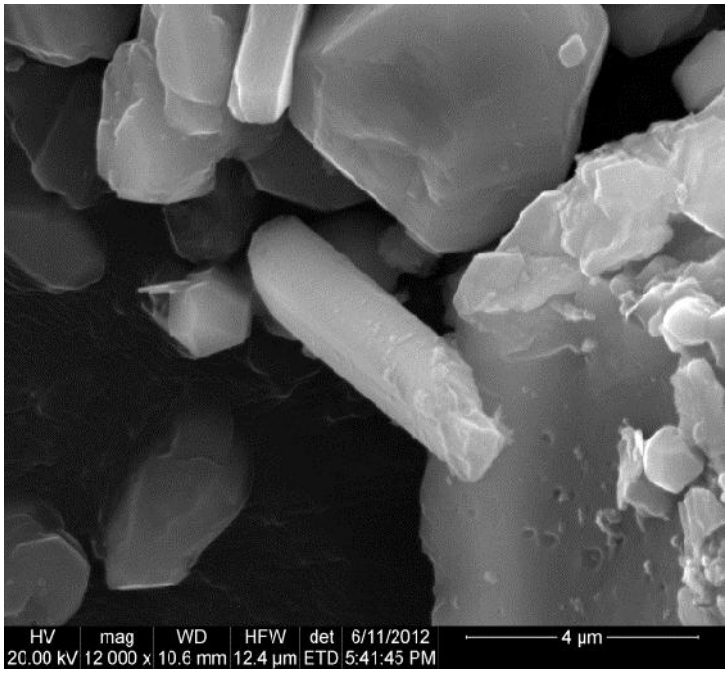

Fig. C.6. Rankin crushed limestone (SEM) – hexagonal kaolinite crystals

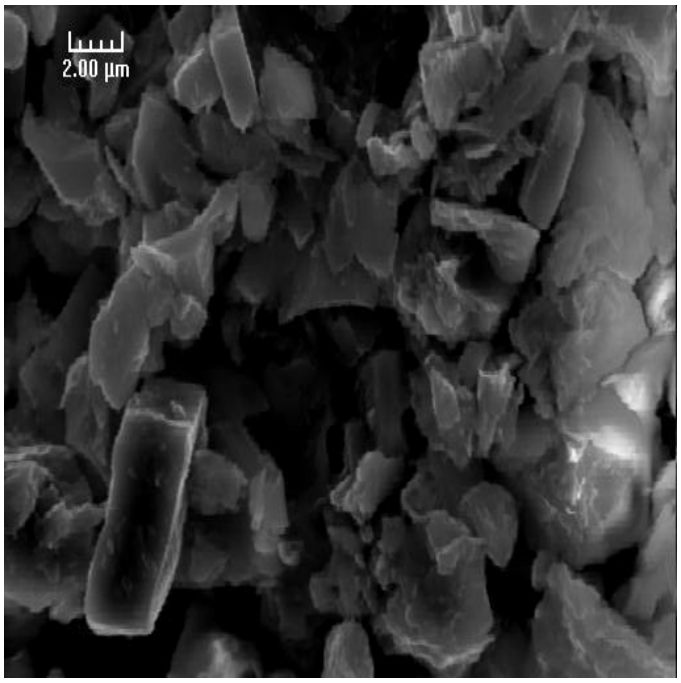

Fig. C.7. Jones Mill hornfels (SEM, 5000 X) – pyroxenes, quartz, and layer silicates

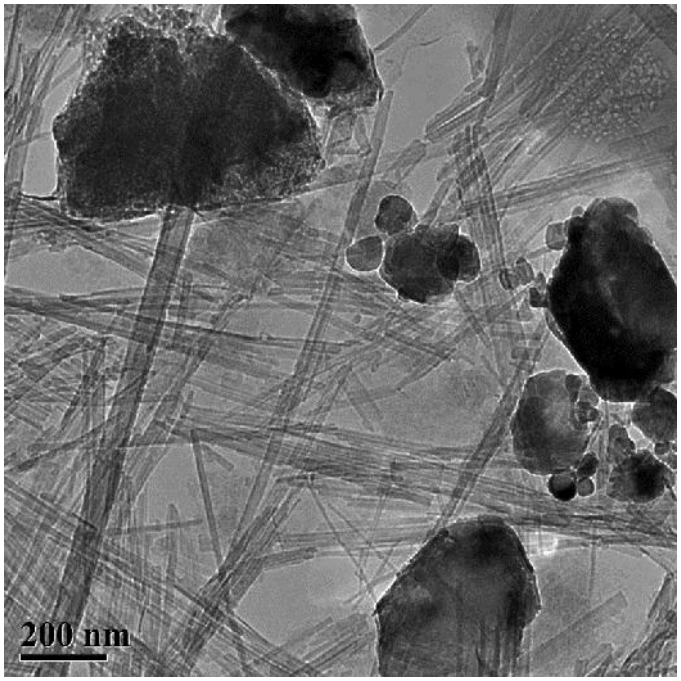

Fig. C.8. Armor clay fraction (TEM, 15000 X) – fibrous palygorskite/sepiolitE

APPENDIX D

RIETVELD QUANTIFICATION RESULTS

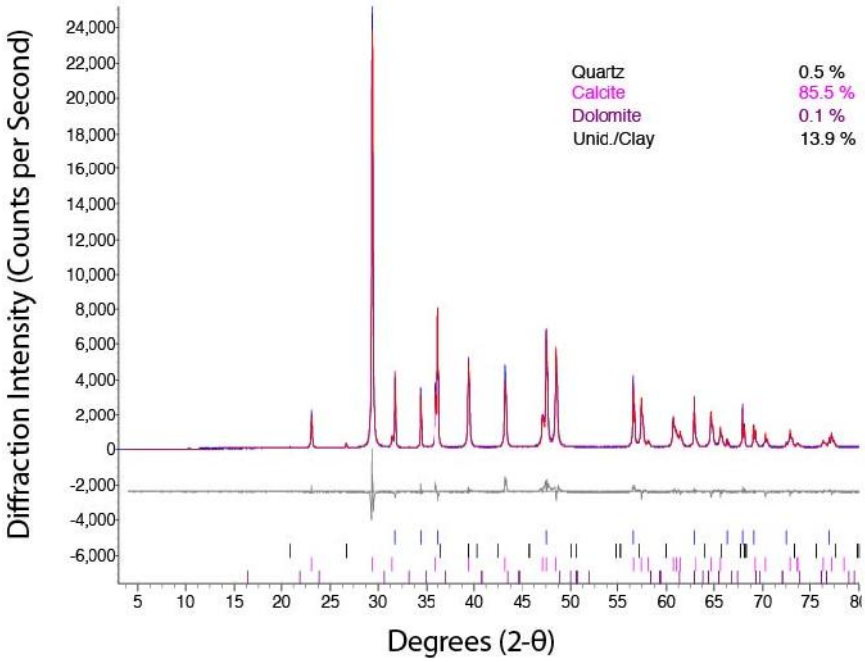

Fig. D.1. Blum total-sample quantification results from Rietveld method

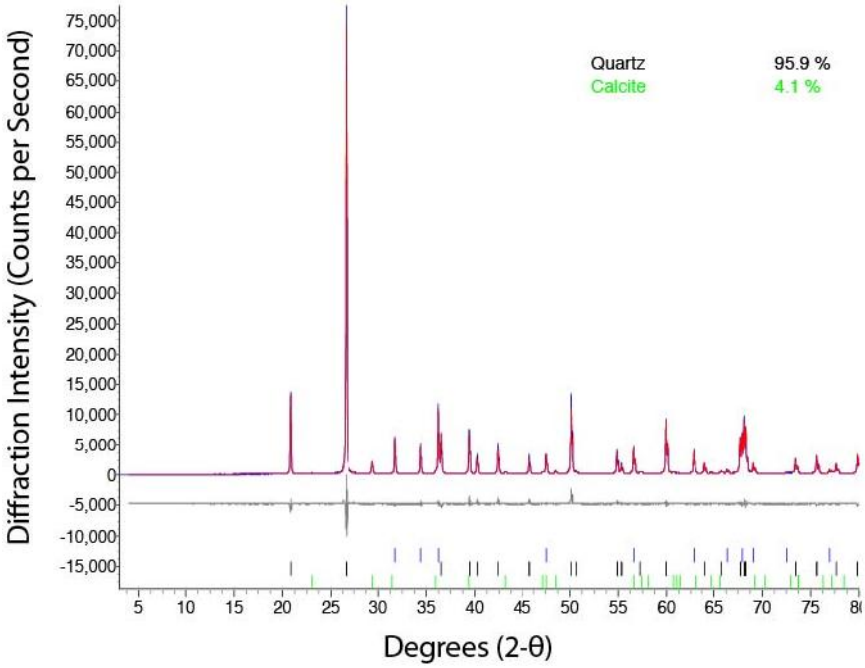

Fig. D.2. Fordyce Murphy total-sample quantification results from Rietveld method

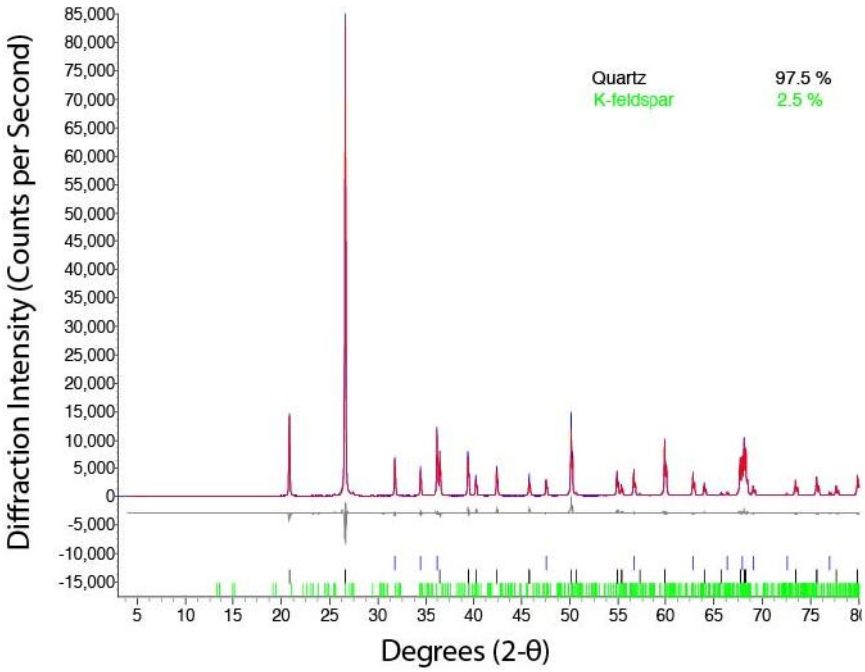

Fig. D.3. Hoot total-sample quantification results from Rietveld method

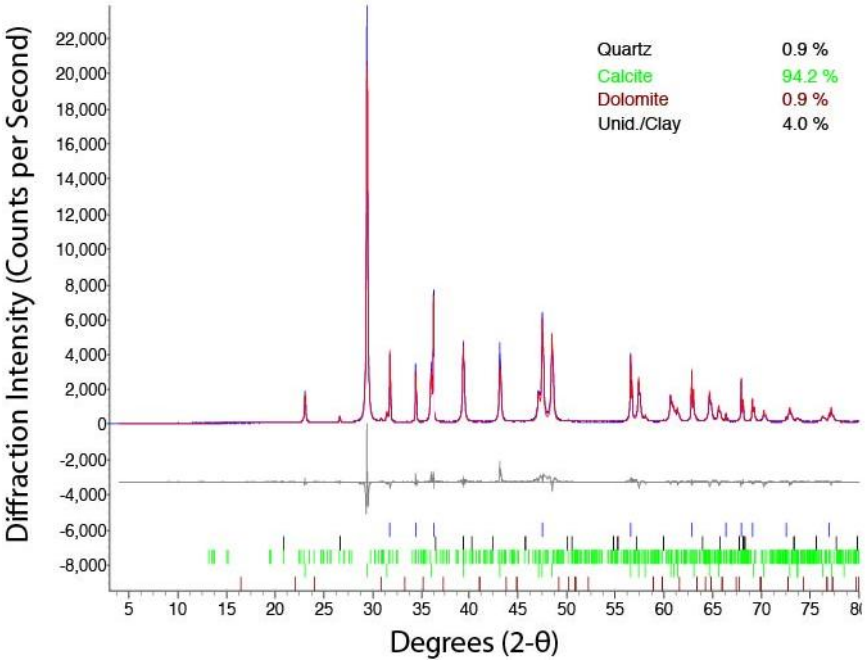

Fig. D.4. Jarrell 1 total-sample quantification results from Rietveld method

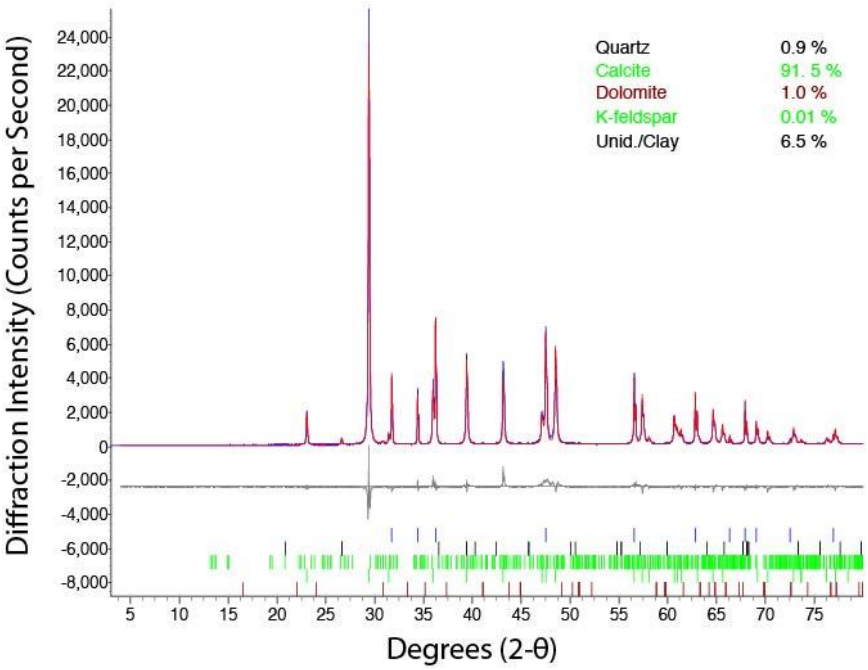

Fig. D.5. Jarrell 2 total-sample quantification results from Rietveld method

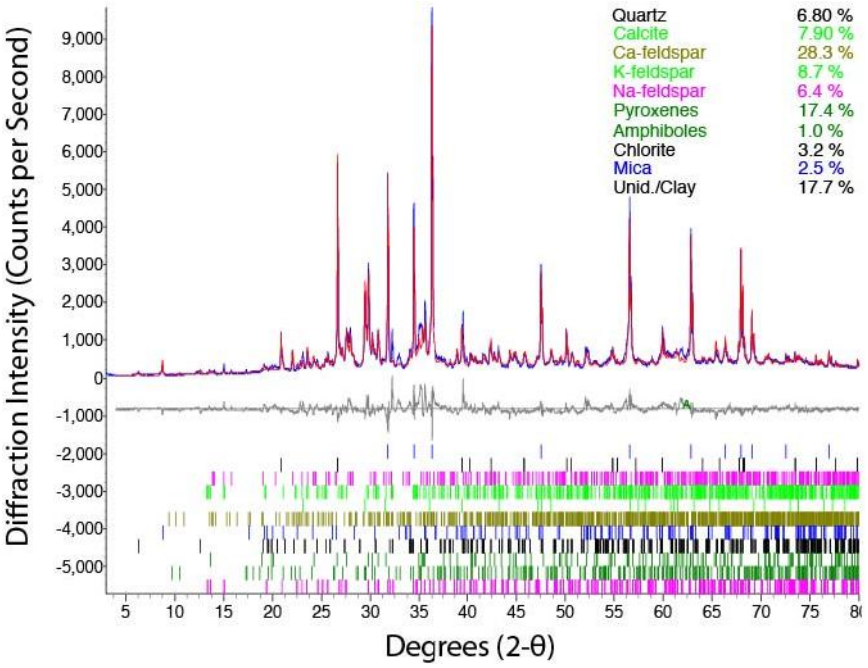

Fig. D.6. Jones Mill total-sample quantification results from Rietveld method

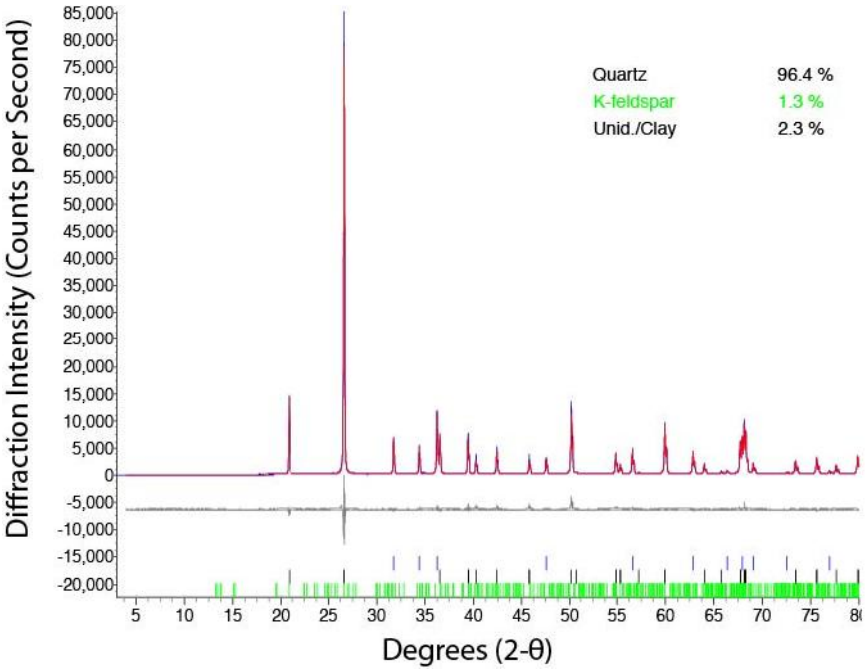

Fig. D.7. Little River total-sample quantification results from Rietveld method

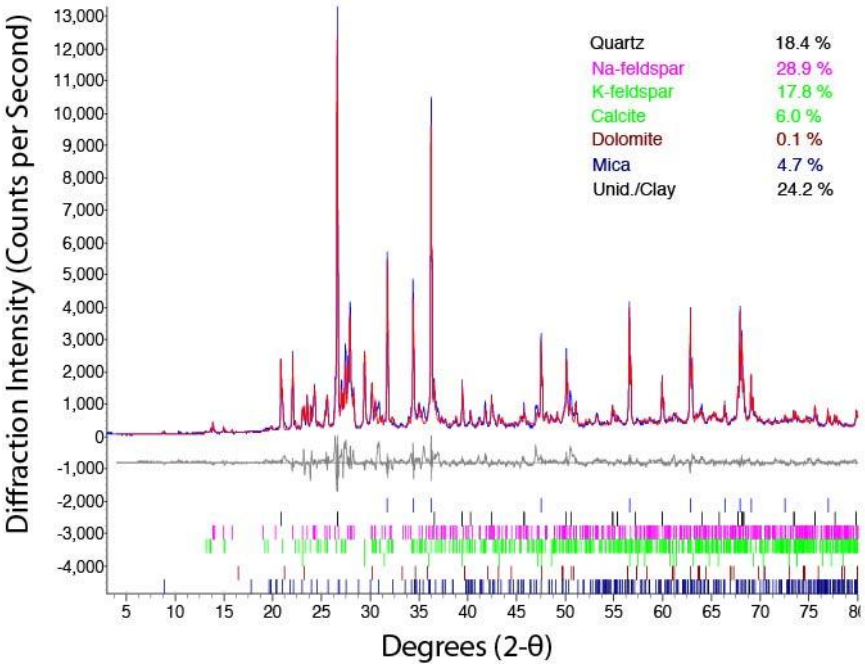

Fig. D.8. McKelligon Granite total-sample quantification results from Rietveld method

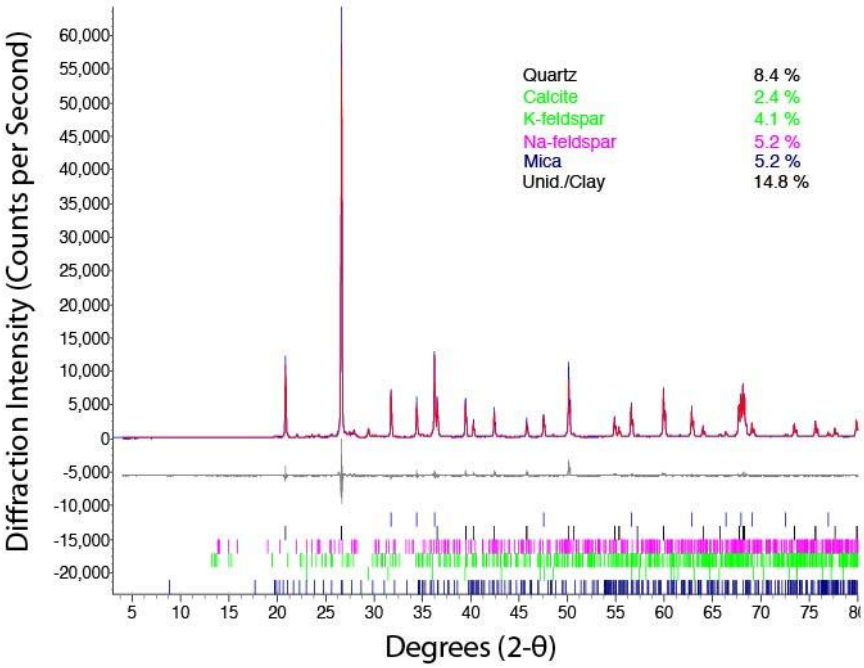

Fig. D.9. Pit 365 total-sample quantification results from Rietveld method

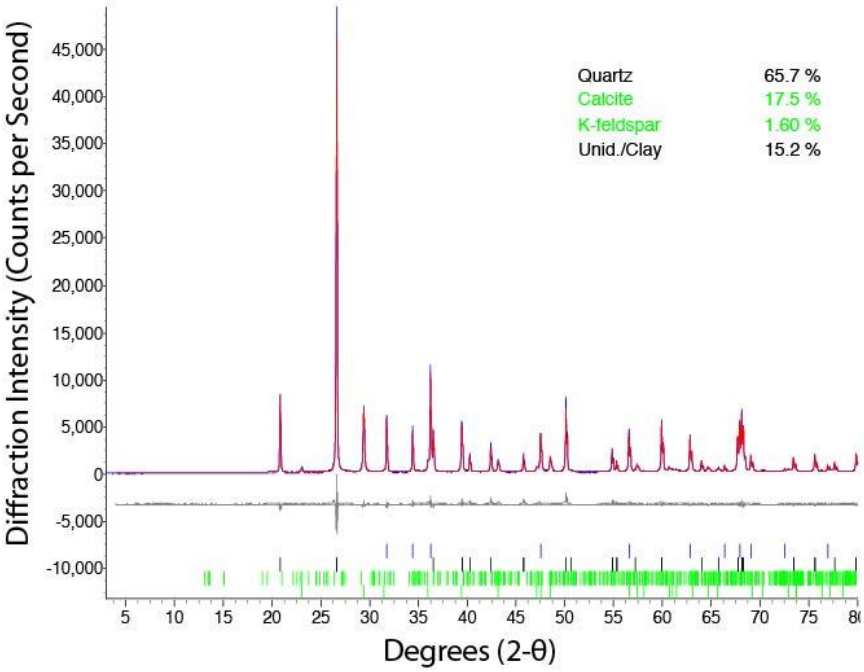

Fig. D.10. South Noodle total-sample quantification results from Rietveld method

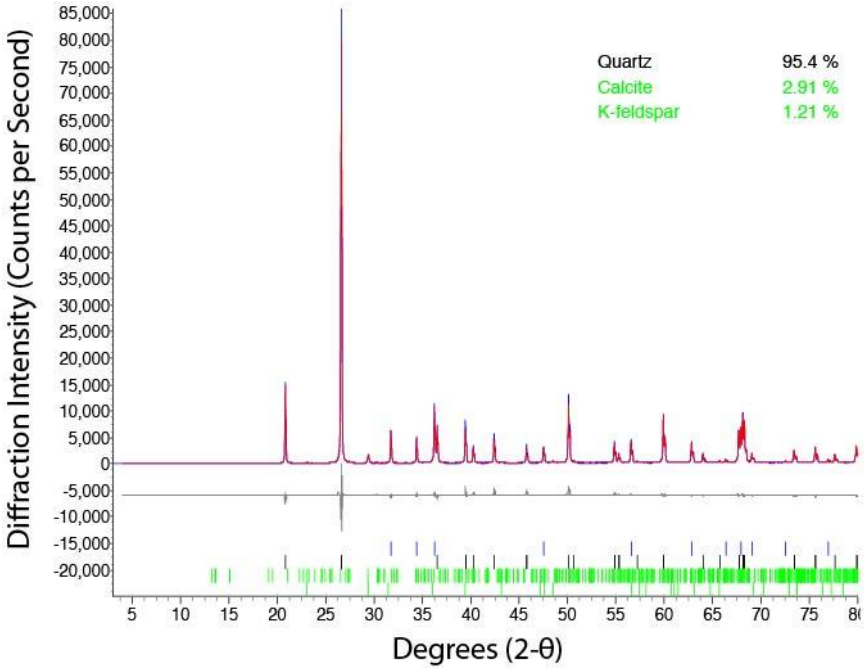

Fig. D.11. Scarmado total-sample quantification results from Rietveld method

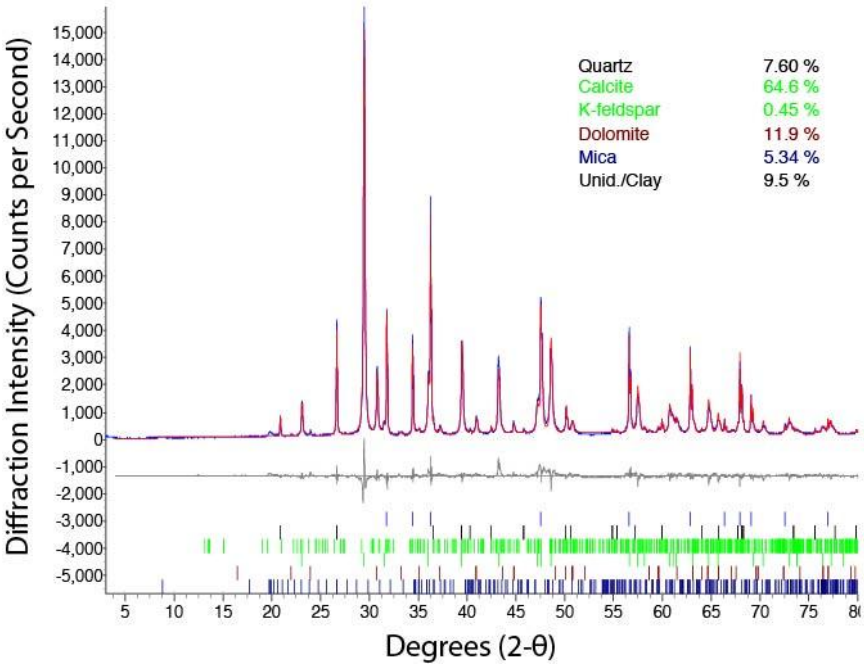

Fig. D.12. Tolar total-sample quantification results from Rietveld method

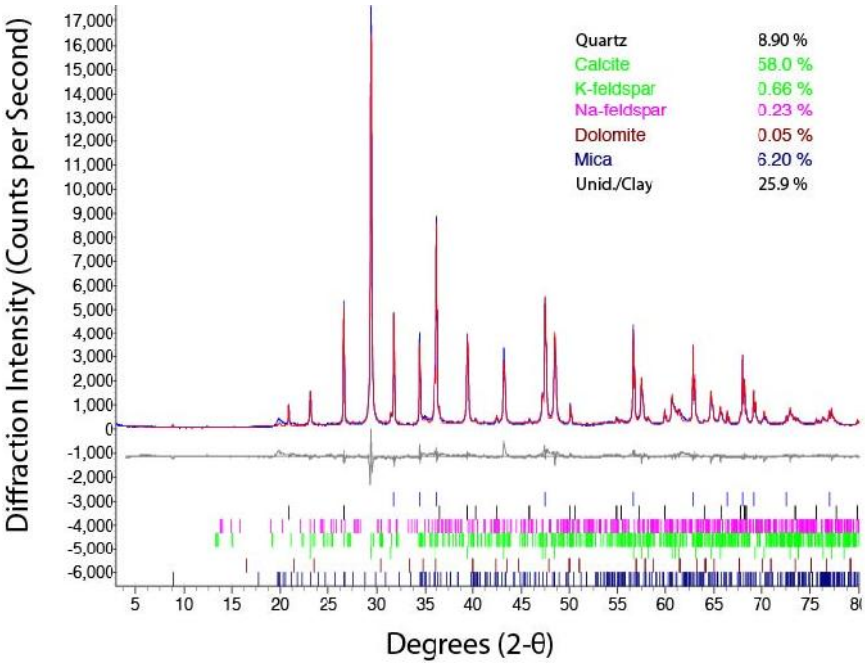

Fig. D.13. Whitney total-sample quantification results from Rietveld method

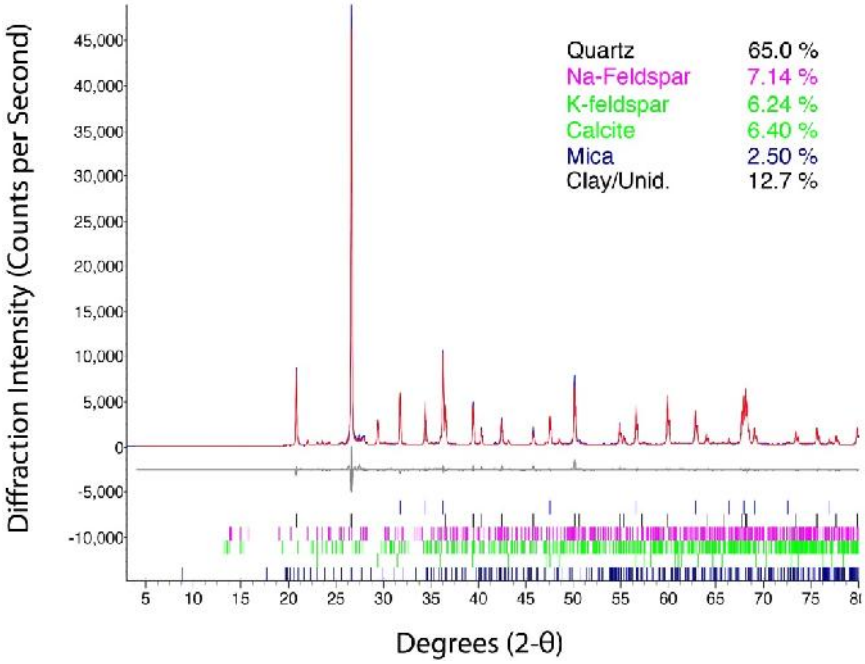

Fig. D.14. Woods total-sample quantification results from Rietveld method

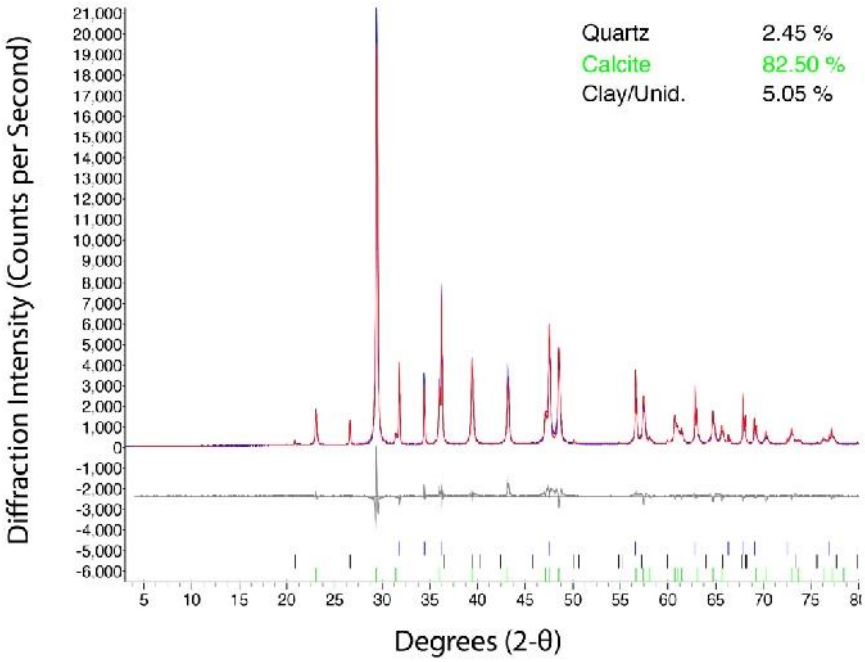

Fig. D.15. Yarrington total-sample quantification results from Rietveld method